SEL-64-007

95p.

N64-19309
CODE-1
(NASA CR-53820;
SEL-64-007)

Alouette Topside Soundings Monitored at Stanford University

OTS:

by

J. O. Thomas and A. Y. Sader

December 1963 95p ref

UNPUBLISHED PR

OTS PRICE

XEROX $ 8.60 ph

MICROFILM $ 3.05 mf.

Technical Report No. 6

Prepared under
National Aeronautics and Space Administration
(NASA Grant NsG 30-60)

RADIOSCIENCE LABORATORY

STANFORD ELECTRONICS LABORATORIES

STANFORD UNIVERSITY · STANFORD, CALIFORNIA

, Calif.

2281954

RC
#4

CASE FILE COPY

DDC AVAILABILITY NOTICE

Qualified requesters may obtain copies of this report from DDC. Foreign announcement and dissemination of this report by DDC is limited.

SEL 64-007

ALOUETTE TOPSIDE SOUNDINGS MONITORED AT STANFORD UNIVERSITY

by

J. O. Thomas and A. Y. Sader

December 1963

Technical Report No. 6

Prepared under

National Aeronautics and Space Administration
Grant NsG 30-60

Radioscience Laboratory
Stanford Electronics Laboratories
Stanford University Stanford, California

ACKNOWLEDGEMENTS

The authors wish to acknowledge gratefully the courtesy of scientists of the Canadian Defence Research Telecommunications Establishment, Ottawa, Canada, particularly Dr. J. H. Chapman and Dr. G. L. Nelms who made a number of topside ionograms available to the authors in the early stages of development of this work.

They wish also to thank Dr. J. H. Chapman of the Canadian Defence Research Telecommunications Establishment and Mr. J. E. Jackson of the Goddard Space Flight Center, National Aeronautics and Space Administration for permission to monitor signals from the Alouette satellite at Stanford. The telemetry receiving station at Stanford has been operated by Messrs. S. Hall, D. Annett, and K. Byram. It is a pleasure to acknowledge the efforts of all of these contributors to the program of work described in this report.

The interest of Professors O. G. Villard, Jr. and O. K. Garriott of the Radioscience Laboratory is gratefully acknowledged.

The work was financed by a grant, NsG 30-60 from the National Aeronautics and Space Administration.

— ABSTRACT —

19309

Alouette topside soundings recorded at the Stanford Satellite Monitoring Facility have been used to determine the diurnal, seasonal and latitudinal variations of electron density at the orbit of the satellite over a wide range of latitudes. The necessary data manipulations and calculations were carried out in a digital computer program which is described briefly. Examples of topside ionograms observed at Stanford under a wide variety of conditions are presented and their main features are described. Author

CONTENTS

	Page
Acknowledgements	ii
Abstract	iii
Contents	iv
Tables	v
Illustrations	vi
Nomenclature	xi
I. Introduction	1
II. The Alouette Satellite and its Orbit	3
III. The Program of Observations at Stanford and Associated Calculations	4
A. The Calculation of the Geographic Latitude and Geographic Longitude of the Satellite at a Given Time	5
B. Derivation of the Magnetic Parameters at the Satellite	9
C. Calculation of the Electron Density at the Satellite	14
D. Program of Observations and Description of Typical Ionograms	19
IV. Results of the Calculations	19
A. Latitudinal, Diurnal and Seasonal Variations	20
B. The Accuracy of the Observations	22
V. Conclusions	24
APPENDIX A. The Calculation of the Latitude and Longitude of the Sub-Satellite Point	25
APPENDIX B. Rectangular Approximation to the Trapezium ABCD, Figures 4 and 5	31
APPENDIX C. Interpolation in Curvilinear Coordinates - The Derivation of Equation (6)	33
APPENDIX D. The Digital Computer Program	36
References and Bibliography	37
Tables (Numbers 3, 4, 5, 6, 9 and 10)	40
Figures	49

TABLES

Table	Title	Page
1	Positional and Magnetic Coordinates of Receiving Site	2
2	Alouette Orbital Elements	4
3	Alouette Positional Data	40
4	Alouette Positional Data	41
5	Total Magnetic Field at the Ground	42
6	Dip Angle (Deg.)	44
7	Nomenclature	15
8	The Relevant Magneto-ionic Conditions	16
9	Description of Typical Topside Ionograms	46
10	The Magnitude of the Error in N_v	47
A1	The Error in the Calculation of Longitude	30

ILLUSTRATIONS

Figure	Title
1a	Map showing the position of the telemetry station operated by the Radioscience Laboratory, Stanford University. The dotted area indicates the location of the approximate zone in which line-of-sight signals from Alouette are detectable. The variation of the earth's total field is also shown.
1b	Map showing location of the telemetry station together with lines of constant magnetic dip angle.
2a	To illustrate, in perspective, the elevation of the tangent plane, CSB, through the location of Stanford, S, with a concentric sphere 1000 km above the earth.
2b	To illustrate the intersection of a tangent plane (LNPQ) through the location of Stanford, S, with a concentric sphere 1000 km above the earth. The equation of the plane LNPQ is $\cos\theta \cos\theta_o \cos(\phi - \phi_o) + \sin\theta \sin\theta_o = r/p$ where θ_o and ϕ_o are the geographic latitude and longitude of the point S, θ and ϕ are the geographic latitude and longitude west of a point on the plane distance p from the center of the earth and r is the radius of the earth. The equation of the cone is given by $r/p = \cos 30°$ so that $\cos\theta \cos\theta_o \cos(\phi - \phi_o) + \sin\theta \sin\theta_o = \cos 30°$ For Stanford, $\theta_o = 37.4°$ and $\phi_o = 122.2°$.
3a	To illustrate the determination of the position of the satellite for a north-south pass.
3b	To illustrate the determination of the position of the satellite for a south-north pass.

Figure	Title
4	To illustrate the convergence of the meridians AC, BD at latitudes between θ_1 and θ_2. The latitude-longitude grid ABCD is used for the determination of the magnetic field parameters at the vehicle.
5	The portion ABCD of the grid shown in Figure 4 on an enlarged scale. The dimensions of the trapezium ABCD are computed in Appendix B for a latitude-longitude grid corresponding to $\theta_1 = 43°$ and $\theta_2 = 45°$. The line DE lies in the plane ABCD.
6	To illustrate the calculation of the magnetic field parameters at the sub-satellite point, T. In this diagram, the points ABCD of Figures 4 and 5 are redrawn at the corners of a rectangle.
7	Schematic diagram to illustrate the nomenclature used to describe features observed on topside ionograms.
8	Alouette video format. (Courtesy NASA).
NOTE:	Figures 9 through 24 are examples of topside ionograms observed at Stanford under a wide variety of conditions. Details concerning the ionograms are given in Table 9.
9 10	Daytime topside ionograms. Note topside reflected rays and ground returns. The plasma resonances (or spikes) are also clearly visible, as are the cyclotron harmonics.
11	Daytime topside ionogram. F2 layer critical frequency not observed (> 10.5 Mc/s).
12	Day-night transition type ionogram. Note clear Z trace.
13	Day-night transition type ionogram. Note spread F echoes.
14 15	Examples of nighttime ionograms.
16	Topside ionogram showing spread F.

Figure	Title
17 18	Topside ionograms showing multiple traces.
19 20 21	Topside ionograms taken approximately two minutes apart on the same pass. Note serrated appearance of resonances and the apparent reception of signals at low frequencies.
22	On this nighttime record, the curvature of the Extraordinary trace just below the cusp is in the opposite direction to that usually observed.
23 24	Further examples of records showing the apparent reception of signals at low frequencies.
25a	The variation with dip latitude of the frequency, f_{xv}, at which the Extraordinary trace has zero range, for a series of days in summer and in winter near local noon at the vehicle (June 1963 and December 1962). The numbers following the month shown on the diagram give the Greenwich Mean Time at the point of closest approach of the Alouette satellite to Stanford.
25b	The variation with dip latitude of the mid-day electron density at 1000 kilometers deduced from the observational data plotted in the previous diagram (Fig. 25a) for a series of days in summer and in winter. The dates for each pass are shown together with the Greenwich Mean Time of the closest point of approach to Stanford of the Alouette satellite.
26a	The variation with dip latitude of the frequency, f_{xv}, at which the Extraordinary trace has zero range, for a series of nights in summer and in winter near local midnight at the vehicle. The numbers following the month as shown on the diagram correspond to the Greenwich Mean Time at the point of closest approach of the Alouette satellite to Stanford. The results are for May and June 1963 and December 1962.

Figure	Title
26b	The variation with dip latitude of the midnight electron density at 1000 kilometers deduced from the observational data plotted in the previous diagram (Fig. 26a) for a series of nights in summer and in winter. The dates for each pass are shown together with the Greenwich Mean Time of the point of closest approach to Stanford of the Alouette satellite.
27	The average variation with dip latitude of the electron density near noon at 1000 kilometers for International Quiet Days in summer and winter. The results are for quiet days in January, May, June and July 1963, and for December 1962.
28	The average variation with dip latitude of the electron density near midnight at 1000 kilometers for International Quiet Days in summer and winter. The results are for quiet days in January, May, June and July 1963, and December 1962.
29	The variation with local time at the vehicle near noon of the electron density at 1000 kilometers over the range of dip latitudes, 45° to 55° North for a series of days in summer (circles) and in winter (dots).
30	The variation with local time at the vehicle during the day of electron density at 1000 kilometers for a series of latitude ranges in summer (1963).
31	The variation with local time at the vehicle during the day of electron density at 1000 kilometers for a series of latitude ranges in winter (1962-3).
32	The nighttime electron density at 1000 kilometers over the range 45° to 75° North geomagnetic latitude in summer (circles) and in winter (dots). The electron density is shown as a function of local time at the vehicle. The results are for 1962-3.

APPENDICES:

Figure	Title
A.1	The trajectory of the Alouette satellite over a latitude range of 10° is assumed to be in the plane ATC.
A.2	Coordinate system for the calculation of the latitude and longitude of the sub-satellite point.
C.1	To illustrate the curvilinear coordinate system used in the derivation of equation (6).
D.1	Flow diagram to illustrate the arrangement of the digital computer program for the calculation of electron density at the Alouette orbit.

NOMENCLATURE

v	The suffix v is used to denote the value of a quantity measured at, or corresponding to, the location of the vehicle.
CPAZ	Greenwich Mean Time of the point of closest approach of the vehicle to the receiving station.
f	Frequency.
f_N	Plasma frequency.
f_{Nv}	Plasma frequency at the vehicle.
f_{ov}	Frequency at which Ordinary ray has zero range (X = 1). This is the same as the plasma frequency at the vehicle, f_{Nv}.
f_{xv}	Frequency at which Extraordinary ray has zero range (X = 1 - Y).
f_{zv}	Frequency at which Z ray has zero range (X = 1 + Y).
f_{Mv}	Plasma resonance ($X = 1 - Y^2$).
f_{Nv}	Plasma resonance (X = 1). This is the same as the frequency for the Ordinary trace zero range echoes.
$f_{z\infty}$	Frequency at which Z trace has infinite virtual depth $\left(X = \frac{1 - Y^2}{1 - Y^2 \cos^2 (\pi/2 - \theta_v)}\right)$
f_H	Electron gyro-frequency.
f_{Hv}	Electron gyro-frequency at the vehicle.
θ_v	Dip angle at the vehicle.
X	f_N^2/f^2
Y	f_H/f

ALOUETTE TOPSIDE SOUNDINGS MONITORED AT STANFORD UNIVERSITY

J. O. Thomas* and A. Y. Sader

Radioscience Laboratory
Stanford University
Stanford, California

I. INTRODUCTION

In accordance with a policy statement of the Topside Sounder Working Group (Appendices Q and R, 13th Working Group Meeting Minutes), concerning participation in the Canadian Topside Sounder S-27 program, the telemetry signals from the Canadian Satellite "Alouette" have been recorded whenever the vehicle is in the vicinity of the receiving station at Stanford. Both the topside soundings and the VLF telemetry signals are monitored. This activity at Stanford lies in the category of that of the "non-participating" agencies in the S-27 program. Under this arrangement, the telemetry signals are received whenever the satellite can be acquired by the Stanford monitoring facility although the specific experiments carried on the vehicle are not especially switched on for monitoring at Stanford. The observations themselves and the results of the calculations involving these observations are made available to the Canadian Defence Research Telecommunications Establishment. This report outlines those results which concern the first series of observations which have been made at Stanford of soundings of the topside of the ionosphere.

The telemetry station operated by the Radioscience Laboratory, Stanford University, for the monitoring of satellite signals has received the signals from the Canadian Topside Sounder "Alouette" on a routine basis since December 4, 1962. The precise location of the receiving site is indicated on the map in Fig. 1a, in which the dotted area indicates the location of the approximate zone in which line-of-sight signals from Alouette are detectable at sufficient strength to obtain good

* Now at NASA, Ames Research Center, Moffett Field, California.

observational recordings of the topside of the ionosphere. Positional coordinates and magnetic data relevant to the Stanford location are presented in Table 1. The maps (Figs. 1a, b) also show the magnitude

TABLE 1

POSITIONAL AND MAGNETIC COORDINATES OF RECEIVING SITE

Stanford University	Coordinate (degrees)
Geographic latitude	37.43 N
Geographic longitude	122.16 W
Geomagnetic latitude	43.7 N
Dip latitude	45.98 N
Dip angle	64.2 N
Total field (Gauss)	.515

of the earth's magnetic field in the Stanford area together with lines of constant magnetic dip angle: these quantities are required in the mathematical analysis for the conversion of the topside h'(f) data into electron density profiles as described by Thomas, Long and Westover (1963) and by Thomas and Westover (1963). Details of the Alouette experiments have been published by the Canadian Defence Research Telecommunications Establishment (CDRTE 1962) and in a paper by Warren (1962) and the first results have been described in a series of papers in the January issue of the Canadian Journal of Physics, Volume 41, page 188, 1963, in articles by Warren, Lockwood, Petrie, Hagg, Muldrew, and Nelms. A complete bibliography (to August 1963) of papers on the subject is included in the references.

In this report, details concerning the satellite and its orbit, the program of observations at Stanford, and the main features of the observed topside ionograms are described. Some derived topside electron density profiles were also computed. In addition, the diurnal, seasonal and latitudinal variations of electron density at the orbit of the satellite (~1000 km above the surface of the earth) have been deduced from observations of the extraordinary ray trace. The necessary

data manipulations and calculations are carried out in a digital computer program which is also described.

II. THE ALOUETTE SATELLITE AND ITS ORBIT

The following details reproduced from the publication CDRTE (1962) relate to the construction, design and orbital elements of the Alouette satellite which was launched by a Thor Agena B from the Pacific Missile Range on September 29, 1962.

Mechanical

Shape - oblate spheroid (of spun aluminum)
Diameter - 42 inches
Height - 34 inches
Overall Weight - 319 pounds
Sounding Antennas - two crossed dipoles, 150 feet from tip to tip, and 75 feet from tip to tip
Telemetry Antennas - four whips (turnstile configuration)
Number of Solar Cells - 6480 arranged in groups of 45
Batteries - 12 Ni-Cd

Electrical

Sounding Transmitter - completely transistorized
- Frequency Sweep - 0.45 to 11.8 Mc/s in approximately one megacycle per second
- Pulse Width - 100 microseconds
- Pulse Repetition Frequency - 67 cps
- Peak Pulse Power - 100 watts into 400 ohm load

Sounding Receiver - transistorized
- Frequency Sweep - 0.45 to 11.8 Mc/s
- Noise Figure - 8 db
- Minimum signal detection through antenna matching networks - 19 db above KTB
- Cosmic Noise data provided by AGC voltage.

Beacon Transmitter - Frequency 136.980 Mc/s at 0.25 watts power
Frequency 136.080 Mc/s at 2.0 watts power

Orbital Elements

The Alouette orbital elements as computed from Minitrack Observations at NASA Computation Center for September 29, 1962 are given in Table 2 below.

TABLE 2

ALOUETTE ORBITAL ELEMENTS

Anomalistic Period		105.4139	Minutes
Inclination		80.464	Degrees
Mean Anomaly		23.754	Degrees
Argument of Perigee		329.895	Degrees
/Motion	Minus	2.566	Degrees per day
Latitude of Perigee	Minus	29.65	Degrees
Right Ascension of Ascending Node		165.773	Degrees
/Motion	Minus	0.984	Degrees per day
Semi-Major Axis		1.15893	Earth Radii
Eccentricity		0.00245	
Perigee		618.7	Statute Miles
Apogee		641.1	Statute Miles
Velocity at Perigee		16467	Miles per hour
Velocity at Apogee		16387	Miles per hour

The telemetry signals which are received using standard equipment are recorded on Sanborn pen recorders and on magnetic tape. The observational data are also transcribed on to 35 mm film to provide a photographic record of the variation of the vertical depth of reflection beneath the satellite, h', as a function of the frequency, f, of the transmitted radio waves. The topside ionograms are of excellent quality and cover the range approximately 450 kc/s to 11.8 Mc/s in a time of about 18 seconds. Examples of topside ionograms recorded at Stanford are given in Section III.

III. THE PROGRAM OF OBSERVATIONS AT STANFORD AND ASSOCIATED CALCULATIONS

In order to derive information about the electron density in the upper F2 layer from the observed topside ionograms, it is necessary to know the position of the satellite accurately at the time when the sounding is made so that the strength and direction of the earth's field

at the location of the vehicle can be determined. The required calculations are described below.

III.A. THE CALCULATION OF THE GEOGRAPHIC LATITUDE AND GEOGRAPHIC LONGITUDE OF THE SATELLITE AT A GIVEN TIME.

Details concerning the predicted position of the Alouette satellite at any time are available on a routine basis. The predictions are provided regularly for the use of the Stanford satellite monitoring facility by the National Aeronautics and Space Administration and are of two kinds (references [1] and [2]). The predictions [1] give the time at which the satellite passes above the geographic equator and also the longitude at which it crosses the equator together with the date and pass number for south-north passes. The longitudes which are counted from the Greenwich meridian are given as longitudes west (longitude west = 360 degrees minus longitude east). This longitude corresponds to the projection of the radius vector from the center of the earth to the satellite, on to the equatorial plane. Orbital details for the satellite have been published by the Canadian Defence Research Telecommunications Establishment (CDRTE 1962) and were given in Section II. From time to time, a second set of predictions is available (reference [2]) which gives a set of satellite position data in the form of corrections to be applied to the equatorial crossing data. The predictions [1] and [2] may be used to determine the satellite's position within the area bounded by the horizon from Stanford. Examples of these predictions are shown in Tables 3* and 4*, and an example is presented later of how these predictions are used to derive the position of the satellite at any given time.

---

* These Tables are presented at the end of the Report (pages 40 and 41).

Let S (Fig. 2a) represent the position of Stanford and CSB be the tangent to the earth's surface at S, intersecting the almost circular Alouette orbit at C and B. The angle $\hat{BOS}$ at the center of the earth is given by

$$\hat{BOS} = \cos^{-1}\left(\frac{6370}{7370}\right) = 30°11'$$

For convenience, we assume this angle to be 30° so that direct line of sight signals cannot be received unless the satellite is at a distance corresponding to less than 30° latitude from Stanford University (geographic latitude 37.43° North, geographic longitude 122.16° West). From Fig. 2b, it is seen that $\hat{SOM} = 30°$. Thus

$$\tan \hat{S'OM'} = \frac{S'M'}{OS'} = \frac{S'M'/OS}{OS'/OS} = \frac{\tan \hat{SOM}}{\cos \hat{S'OS}} = \frac{\tan 30°}{\cos 37°}$$

so that

$$\hat{S'OM'} = 35°52' \simeq 36°.$$

From Figs. 2a, b, it is seen that the satellite must, if it is to be received at Stanford, (point S in Figs. 2a, b) lie in an area bounded by a circle of diameter 7370 km formed by the intersection of the tangent plane to the earth passing through Stanford with a sphere of radius 7370 km. Thus, if it is possible to receive line-of-sight signals from the satellite then the satellite telemetry signals can be received within the range 37° ± 30° of latitude and 122° ± 36° longitude about the position of Stanford, that is, from 7° to 67° north in latitude and from 86° to 158° west in longitude. These are the extreme values which the coordinates of the satellite could take and these extreme values of latitude and longitude could not, of course, be achieved simultaneously. Thus, if a square is plotted of side corresponding to distances of 122° ± 36°, 37° ± 30°, the longitude and latitude are so related that the satellite's position projected on the tangent plane by a conical projection from the center of the earth will lie inside

the circle inscribed in the square LNPQ (Fig. 2b) if its telemetry is to be received at Stanford.

In order to determine the position of the satellite at any given time, t_o, the following procedure is adopted. Let the horizontal lines in Fig. 3a,b represent the parallels of latitude drawn 10° apart. Let AB represent the direction (Fig. 3a) of a north-south pass and the point O represent the position of the satellite at the time t_o. Let GH and IJ represent the longitudes at which the satellite crosses the parallels EF and CD, respectively (Fig. 3a).

Suppose X = the west longitude of the satellite at the time, t_o, corresponding to the point O in Fig. 3a,b, and let

Y = the north latitude of the satellite at the time, t_o

X_1 = the west longitude of the line GH

X_2 = the west longitude of the line JI

Y_1 = the north latitude of the line, EF, crossed at time t_1 just before time, t_o

Y_2 = the north latitude of the line, CD, crossed at time t_2 just after the time, t_o

t_E = time of equatorial crossing

l_E = longitude of equatorial crossing

Then

$$Y = Y_1 + \frac{dt}{\Delta t}(Y_2 - Y_1) \qquad (1)$$

$$X = X_1 + \frac{dt}{\Delta t}(X_2 - X_1) \qquad (2)$$

where

$$dt = (t_o - t_E) - (t_1 - t_E) = t_o - t_1 \qquad (3)$$

$$\Delta t = t_2 - t_1 \qquad (4)$$

In (1) and (2), $(Y_2 - Y_1)$ and $(X_2 - X_1)$ are computed from the table of corrections to the predictions at the equator crossing (refs. [1] and [2]).

For a south-north pass $(Y_2 - Y_1)$ is positive, as are dt and Δt. The quantity $\frac{dt}{\Delta t}(Y_2 - Y_1)$ is added to Y_1 in Eq. (1). For a north-south pass, $(Y_2 - Y_1)$ is negative, whereas dt and Δt are still positive. In this case, the correction $\frac{dt}{\Delta t}(Y_2 - Y_1)$ is subtracted from Y_1.

Similar interpolation gives the value of the west longitude. The method is illustrated by the following example:

For pass number 977 recorded on the 9th of December 1962, the position of the satellite was required when the frequency f_{xv} (Sec. III.C) was recorded. This time, t_o, was observed to be 2016.40 GMT. Reference to Table 3* shows that for this particular pass number, the predictions give the equatorial crossing time t_E as 1941.40 GMT. Therefore, $t_o - t_E = 35$ minutes and this is the time difference from the equator to the actual position of the satellite at the time t_o. Reference to Table 4 indicates that for latitude 60° $(\equiv Y_1)$ the quantity $t_1 - t_E$ is 34.65 minutes. For latitude 50° $(\equiv Y_2)$ the quantity $t_2 - t_E$ is 37.70 minutes. Thus, the pass is known to be north-south. Hence, $\Delta t = 37.70 - 34.65 = 3.05$ minutes and $dt = 35 - 34.65 = .35$ minutes

$$Y = Y_1 + \frac{dt}{\Delta t}(Y_2 - Y_1) = 60 + \frac{.35}{3.05}(50 - 60) = 58.85°$$

By a similar procedure, X, the west longitude is determined as 122.93°.

The latitudes and longitudes (determined from tables similar to Table 4) for the crossing points of the 10° latitude-longitude network used for calculating the position of the sub-satellite point correspond to projections from the plane of the orbit on to the earth's equatorial plane and on to a meridian plane respectively. In the calculations described above, linear interpolation in time was used. If the interpolation had been made over the curved path of the Alouette orbit, slightly different and more accurate values of the longitude and latitude of the sub-satellite point would have been derived. The magnitude of the error is greater in the computed longitudes than it is for the computed latitudes because of the high inclination of the orbit. The magnitude of the error is computed in Appendix A and is shown to be negligibly small in both cases, so that the linear interpolation used in the calculations is justified.

* See p. 40.

Once the geographic coordinates of the position of the satellite at the time t_o are known, it is possible to deduce the magnetic field strength and the dip angle at the location of the satellite. The procedure for doing this is described below.

III.B. DERIVATION OF THE MAGNETIC PARAMETERS AT THE SATELLITE

The dip angle and gyro-frequency at the satellite may be computed directly from observations of the plasma resonances, gyro-resonances, and zero-range echoes which appear on the ionogram (Lockwood 1963, Calvert and Goe 1963), as described in III.C. Alternatively, the dip angle and gyro-frequency may be determined for the exact location of the satellite by extrapolation of ground based observations of the earth's magnetic field. These quantities may then be compared with those derived directly from the ionograms and hence used to provide an indication of the accuracy of the field model used for the extrapolation from ground based observations. In practice, it is found that both procedures produce the same result to a high degree of accuracy (III.C).

In order to determine the dip angle and gyro-frequency for electrons at the location of the sub-satellite point (determined by the procedure described in III.A), it is necessary to utilize the best known values for these quantities as measured on the ground. Extrapolations are then made in the manner described below to derive these quantities at the height of the satellite. The magnetic field parameters at the ground are obtained from refs. [3] and [4]. For computational purposes, a grid is constructed on the surface of the earth at intervals of 2° of longitude and latitude in the range 90° to 146° west longitude and 6° to 70° north latitude as shown in Fig. 4. The value of the earth's total field F (gauss) at each point of this grid is then represented as a matrix stored in the digital computer. This matrix of ground values of the earth's total field is shown in Table 5* and the dip matrix is shown in Table 6* The portion ABCD of the grid shown in Fig. 4 may be approximated to by a trapezium which, at latitudes 43° to 45° north has the dimensions computed in Appendix B and shown in Fig. 5. In practice, except for very high latitudes, it is sufficiently accurate to regard

* See pp. 42 through 45.

ABCD as a rectangle and linear interpolation may be used to determine the magnetic field parameters inside this rectangle. This approximation is justified in Appendix B where the magnitude of the trapezium sides are calculated for a typical example.

Basically the calculation relates to the derivation of the appropriate magnetic parameters for the exact location of the satellite by interpolation in the correct manner within the grid system on the surface of the earth. Once the value of the earth's total field at the appropriate sub-satellite point (T, Figs. 4 and 5) has been determined, an extrapolation involving an inverse cube law is then made to derive the corresponding quantity at the location of the vehicle. In the case of the dip angle it is assumed that at the location of the satellite, its value is the same as that at the point T on the surface of the earth (Fig. 4).

Let (x,y) be the coordinates of the point T on the grid system so that

$$x_1 < x < x_2; \quad y_1 < y < y_2$$

where x_1 and x_2 are consecutive values of the longitude grid lines and y_1 and y_2 are consecutive values of the latitude grid lines (Fig. 5).

In Fig. 6, the points ABCD of Fig. 5 are re-drawn at the corners of a rectangle instead of a trapezium and a simple expression, based on a rectangular-grid is first derived for the magnetic field at T. It is then shown (Appendix C) that a more accurate derivation, allowing for the curvature of the grid lines leads to a simple modification of this expression and it is shown that the rectangular approximation is, in practice, sufficiently accurate for observations made at Stanford.

Suppose that at the corners of the grid network ABCD, the magnetic field parameter concerned (i.e., the total field or the dip angle) has the values shown in Fig. 6 so that the total field (or dip angle as the case may be) takes the values z_1, z_2, and z_3 at the points D, C and B respectively.

For convenience we write

$$X = x - x_1; \quad Y = y - y_1$$

$$a = x_2 - x_1; \quad b = y_2 - y_1$$

$$p = z_2 - z_1; \quad q = z_3 - z_1$$

Thus a and b correspond to the grid spacing (2° in the computations described) and p and q correspond to tabular differences in the magnetic field matrices (Table 5 or 6).

From Fig. 6,

$$T\,T'' = T\,T' + T'\,T'' = N\,N' + M\,M'$$

Now

$$\frac{M\,M'}{C\,C'} = \frac{M\,D}{C\,D} \quad \therefore \quad M\,M' = \frac{X}{a}\,p$$

and

$$\frac{N\,N'}{B\,B'} = \frac{D\,N}{D\,B} \quad \therefore \quad N\,N' = \frac{Y}{b}\,q$$

Thus

$$T\,T'' = \frac{X}{a}p + \frac{Y}{b}q$$

So that the value of the magnetic field parameter at the sub-satellite point, T, is given by

$$z - z_1 = \frac{(x - x_1)}{(x_2 - x_1)}\,(z_2 - z_1) + \frac{(y - y_1)}{(y_2 - y_1)}\,(z_3 - z_1)$$

or

$$z = \frac{X}{a} p + \frac{Y}{b} q + z_1 \qquad (5)$$

In Appendix C it is shown that the expression (5) is modified when the curvature of the lines ABCD is allowed for so that z is given by

$$z = \left(\frac{\cos \theta}{\cos \theta_1}\right) \frac{X}{a} p + \frac{Y}{b} q + z_1 \qquad (6)$$

where θ and θ_1 are the angles shown in Fig. 4.

The tabular differences p and q (Table 5) do not exceed .015 gauss and θ never exceeds $\theta_1 + 2°$. Hence the error in the computed total field z at T calculated assuming $\cos \theta / \cos \theta_1 = 1$ in (6) does not exceed .001 gauss for values of θ up to 86°. In other words, the rectangular grid formula (5) can be used in practice for the analysis of topside ionograms received at Stanford. Indeed, for a grid of spacing 2°, an accuracy of .001 gauss in the computed value of z would be obtained even if the tabular differences (Table 5) were as great at .05 gauss. In practice, the accuracy limitation arises from the trapezoidal contraction of the longitude meridians as one proceeds from the equator towards the poles. The contraction of meridians is discussed in Appendix B in which it is shown that the latitude and longitude grid of spacing 2° is, in fact, satisfactory for determining the two magnetic field parameters at the actual location of the satellite provided the latitude does not exceed 86° (a latitude never reached by Alouette).

As an example, the value of the total field z at the sub-satellite point T is computed below for a topside ionogram recorded at Stanford at 2016.40 GMT on 9th December 1962, pass number 977 (Section III.A). We have, for the point T

x = longitude west = 122.93°; y = latitude north = 58.85°

From Table 5 we find

$x_1 = 122°$ $\quad y_1 = 58°$ $\quad z_1 = .593$ gauss

$X = 0.93°$ $\quad Y = 0.85°$ $\quad z_2 = .592$ gauss

$x_2 = 124°$ $\quad y_2 = 60°$ $\quad z_3 = .594$ gauss

Thus

$$a = x_2 - x_1 = 2°; \quad b = y_2 - y_1 = 2°$$

$$p = z_2 - z_1 = - .001 \text{ gauss}$$

$$q = z_3 - z_1 = + .001 \text{ gauss}$$

Hence

$$z = z_1 + \frac{p\,X}{a} + \frac{q\,Y}{b} \simeq .593 \text{ gauss}$$

Similarly, for the dip angle (Table 6)

$$z_1 = 81.2°$$

$$z_2 = 80.7°$$

$$z_3 = 82.4°$$

and x, x_1, x_2, y, y_1, y_2, are as given above.

Then

$$p = -0.5; \quad q = 1.2$$

Hence the dip angle, z, at the satellite is given by

$$z = z_1 + \frac{p\,X}{a} + \frac{q\,Y}{b} = 81.2° + .28° = 81.48°$$

In this section it has been shown how the magnetic parameters at the satellite may be derived from extrapolation of ground measured values provided the position of the satellite at a given time is known accurately. It is possible however to deduce the magnitude of the earth's field at the location of the vehicle and also to calculate the value of the dip angle at the satellite from measurements on some of the resonance phenomena which are observed on the ionogram itself. Before the procedures for doing so are outlined, the main features of topside ionograms observed at Stanford are presented and the nomenclature used in their analysis is given.

III.C. CALCULATION OF THE ELECTRON DENSITY AT THE SATELLITE

The main features of a typical daytime ionogram observed at Stanford are presented schematically in Fig. 7. In this diagram both the traces produced by the reflected rays and the resonance phenomena are indicated. The nomenclature used to describe the main features of these ionograms is shown on the diagram and detailed in Table 7. The plasma resonance phenomena observed on the Alouette ionograms are not discussed in detail in this report. However, the relevant magneto-ionic conditions which are satisfied by the main resonance phenomena and also by the zero range reflection conditions are summarized in Table 8. The equations (7) to (12) of Table 8 can be solved for the three unknowns X, Y and θ_v, and hence for f_{Nv}, the plasma frequency at the vehicle, for f_{Hv}, the electron gyro-frequency at the height of the vehicle, and for θ_v, the value of the dip angle at the vehicle (Lockwood 1963).

TABLE 7

NOMENCLATURE

v	The suffix v is used to denote the value of a quantity measured at, or corresponding to, the location of the vehicle.
CPAZ	Greenwich Mean Time of the point of closest approach of the vehicle to the receiving station.
f	Frequency.
f_N	Plasma frequency.
f_{Nv}	Plasma frequency at the vehicle.
f_{ov}	Frequency at which Ordinary ray has zero range (X = 1). This is the same as the plasma frequency at the vehicle, f_{Nv}.
f_{xv}	Frequency at which Extraordinary ray has zero range (X = 1 - Y).
f_{zv}	Frequency at which Z ray has zero range (X = 1 + Y).
f_{Mv}	Plasma resonance ($X = 1 - Y^2$).
f_{Nv}	Plasma resonance (X = 1). This is the same as the frequency for the Ordinary trace zero range echoes.
$f_{z\infty}$	Frequency at which Z trace has infinite virtual depth $\left(X = \frac{1 - Y^2}{1 - Y^2 \cos^2 (\pi/2 - \theta_v)}\right)$
f_H	Electron gyro-frequency.
f_{Hv}	Electron gyro-frequency at the vehicle.
θ_v	Dip angle at the vehicle.
X	f_N^2/f^2
Y	f_H/f

Magneto-ionic Condition	Remarks	Frequency		
$Y = \frac{1}{n}$, n = 1,2, . . .	Cyclotron harmonics	nf_{Hv}	- - - - -	(7)
X = 1 + Y	Z trace zero range echoes.	f_{zv}	$f_{zv}^2 = f_{Nv}^2 - f_{zv}f_{Hv}$	(8)
X = 1	Ordinary trace zero range echoes.	f_{ov}	$f_{ov}^2 = f_{Nv}^2$	(9)
X = 1	Plasma resonance.	f_{Nv}		
$X = \frac{1 - Y^2}{1 - Y^2\cos^2(\pi/2 - \theta_v)}$	Z trace infinite range echoes.	$f_{z\infty}$	- - - - -	(10)
$X = 1 - Y^2$	Magnetic plasma resonance.	f_{Mv}	$f_{Mv}^2 = f_{Nv}^2 + f_{Hv}^2$	(11)
X = 1 - Y	Extraordinary trace zero range echoes.	f_{xv}	$f_{xv}^2 = f_{Nv}^2 + f_{xv}f_{Hv}$	(12)

TABLE 8

THE RELEVANT MAGNETO-IONIC CONDITIONS

In this table, $X = f_N^2/f^2$, $Y = f_H/f$.

Thus, for example, equation (9), giving the condition X = 1 for the plasma resonance (or 0 spike) can be used immediately to give the plasma frequency at the vehicle since this is simply the frequency at which the plasma resonance (or 0 spike) is observed (Fig. 7). Similarly, the equation (7) can be used to give the value of the gyro-frequency at the vehicle from a direct measurement of the frequency at which the cyclotron harmonics are observed. These values of f_{Hv} and f_{Nv} may then be substituted into equation (10) to give the dip angle at the vehicle θ_v. The magnitudes of the dip angle and the gyro-frequency at the vehicle deduced as above may then be compared with the values computed by the method described in the previous section and an estimate may be obtained in this way of the reliability of the model used for extrapolating the observed values of the field parameters measured at the ground. In practice, either technique is sufficiently accurate for the calculation of electron densities using the procedures described below.

An inspection of the ionograms received at Stanford indicates that the Extraordinary ray trace is usually the most clearly visible on the ionogram and, unlike the case of the Ordinary ray trace, the frequency at which the Extraordinary ray has zero range is usually easily recognized. This frequency, f_{xv}, (Fig. 7) has accordingly been measured and equation (12), corresponding to the condition X = 1 - Y has been used to determine the value of the electron density at the vehicle. Thus,

$$f_{Nv}^2 = f_{xv}^2 - f_{xv} f_{Hv} \qquad (12)$$

In the results which are described in Section IV, the magnetic field parameters were deduced from the extrapolated ground values rather than from direct measurements on the ionograms. In this case, the electron gyro-frequency f_{Hv} was derived from the value of the total field F_v computed at the vehicle from the equation $f_{Hv} = 2.84\ F_v$ where f_{Hv} is given in megacycles per second and F_v is in gauss. F_v was calculated from F, the value of the earth's total field at the ground using an inverse cube relation. The use of a more accurate model for the extrapolation from the value of the total field at the ground to the value at

the vehicle indicates that the inverse cube extrapolation leads to errors of about 27 kc/s (i. e., about 2.5%) in the value of f_{Hv} (E. L. Hagg and G. L. Nelms private communication).

For example for pass number 977 considered previously, the satellite was at geographic latitude 58.85° N and geographic longitude 122.93° W at 2016.40 GMT when the frequency f_{xv} was observed to be 1.5 Mc/s. The total intensity of the earth's magnetic field at the ground is determined as .593 gauss for this location. Hence the gyro-frequency for electrons at the vehicle, f_{Hv}, is calculated as 1.09 Mc/s which agrees with the value obtained by direct measurement of the gyro resonances. Substitution in (12) gives the plasma frequency N_v at the vehicle

$$N_v = 1.24 \times 10^4 (f_{Nv}^2) = 1.24 \times 10^4 (2.25 - 1.5 \times 1.09)$$

$$N_v = 9000 \text{ electrons per c.c.}$$

The actual calculation of the electron density at the vehicle from equation (12) is performed using a digital computer program which is discussed briefly in Appendix D. The program requires as input the frequency at which the Extraordinary ray trace has zero range, f_{xv}, together with the time at which f_{xv} was observed, t_o, the pass number and the time and longitude of the equatorial crossing for the pass concerned. The printed output from the computer gives the electron density at the vehicle, N_v, together with data about the location of the vehicle, the time of observation, the magnetic dip angle and the electron gyro-frequency at the location of the vehicle at the time concerned (See Appendix D). The output data are obtained on magnetic tape which can be further processed so that the electron density at the vehicle, for a given pass, is automatically plotted against dip latitude* or local time at the vehicle as desired.

---

* The nomenclature used is that recommended by Chapman (1963).

The result of carrying out calculations of the kind outlined above using data from a large number of topside ionograms is presented in Section IV where the accuracy of the derived electron densities is also considered in detail.

III.D. PROGRAM OF OBSERVATIONS AND DESCRIPTION OF TYPICAL IONOGRAMS

Ionograms from the Alouette topside sounder were recorded whenever the vehicle could be acquired by the satellite monitoring facility. Two passes per day were recorded, the telemetry signals being received over a period of approximately twelve minutes per pass so that under favorable circumstances approximately 40 ionograms could be obtained covering a range of latitudes which, under the best circumstances, could extend from about 7° N to 67° N geographic for each pass. In Fig. 8 the video format used for the display of the virtual depth data is illustrated.

From the Alouette ionograms which were recorded, some typical examples have been picked to show some of the main features which were observed and these are illustrated in the sequence of figures labelled 9 - 24. Table 9*summarizes information concerning these ionograms and presents a brief account of the main features which the particular examples are meant to illustrate.

IV. RESULTS OF THE CALCULATIONS

In a companion paper (Thomas and Westover 1963), a detailed description is given of a digital computer program for converting the information contained in the reflected ray traces observed on topside ionograms into electron density profiles for the upper part of the F region and examples were given in that report of some derived topside N(h) profiles. The present report is concerned with the calculation of the electron density at the vehicle and in particular with the determination of the diurnal, seasonal and latitudinal variations of this quantity at the Alouette orbit. Some of the main results of the calculations are described below.

* See end of report, page 46.

A number of passes were selected for detailed study from the regular sequence of twice daily sets of ionograms monitored as a routine by the Radioscience Laboratory. The data examined were for a series of days and nights selected to correspond to summer and winter conditions in the northern hemisphere and include results for January, May, June and July 1963 and December 1962.

IV.A. LATITUDINAL, DIURNAL AND SEASONAL VARIATIONS.

In Fig. 25a the observed mid-day values of the quantity f_{xv} are plotted for a series of days selected to represent summer and winter conditions as a function of dip latitude: each point corresponds to one ionogram. In Fig. 25b the data of Fig. 25a have been converted into electron densities at the satellite using equation (12). It is clear from Fig. 25b that during the daytime the electron density falls uniformly from low to high latitudes and it is clear also that the electron density in winter at a given latitude is lower than that in summer. These observations were made when the Greenwich Mean Times of the point of closest approach of the vehicle to Stanford were as shown on the diagrams so that the results of Figs. 25a,b correspond roughly to local noon conditions at the vehicle. In Fig. 26a,b the corresponding quantities are shown for a series of summer and winter nights. Reference to Fig. 26b indicates that during the summer night the electron density reaches a minimum at a dip latitude of approximately 65° N and an examination of the curves for the 12th, 13th and 14th of June also indicates the existence of a sharp local increase of electron density at approximately a dip latitude of 74° N on each night. The results for winter nights show a steady but small decrease of electron density with increasing latitude. Again, the results of Fig. 26b correspond to Greenwich Mean Times at the vehicle which are as indicated so that the observations correspond to local midnight at the vehicle approximately. Altogether 105 passes were studied and the results shown in Figs. 25a,b and 26a,b are typical of the data examined. It is quite clear that the observations repeat themselves consistently and

that the Alouette experiment provides an extremely reliable and accurate technique for obtaining the electron density at 1000 kilometers in a very simple way. The data of Figs. 25 and 26 give a sample, selected at random from the 105 passes examined. In Figs. 27 and 28 a mean curve has been drawn through the observations for a number of International Quiet Days so that a representative variation of N_v with dip latitude is obtained for summer and winter daytime and nighttime conditions. Due to the precession of the orbit, it is possible by taking results over a long period of time, to determine the diurnal variation of the electron density at the satellite. Typical results are shown in Fig. 29 in which the variation in electron density at 1000 kilometers is given as a function of local time at the vehicle for the daytime period near noon. The electron density is plotted both for summer (circles) and for winter (dots). The results shown in Fig. 29 correspond to the dip latitude range 45° to 55° North and the individual points correspond to different days so that the spread in these observations may arise from day-to-day variations at the location of the vehicle. In Fig. 29 a smooth line has been drawn through the plotted points. Similar results were derived for a whole series of dip latitude ranges and smooth lines were drawn through the plotted points. These curves are drawn for the summer observations in Fig. 30 and for the winter observations in Fig. 31. It is interesting to compare the results illustrated in these two figures. An examination of Fig. 30 indicates that the diurnal variation is not the same at different latitudes and that the time at which the maximum electron density at 1000 kilometers is reached depends on the dip latitude. At high latitudes the peak occurs about half an hour after noon whereas at low latitudes it occurs about one and a half hours after noon.

The decrease in electron density at a given time with increasing latitude is also illustrated in Figs. 30 and 31. A comparison of the results of Fig. 30 corresponding to summer observations with those of Fig. 31 corresponding to winter observations, indicates that the general level of electron density over a given geomagnetic latitude range is lower in winter than it is in summer and that in a given geomagnetic

latitude range the electron density in summer can be approximately twice that in winter at a given time. The winter observations do not show the marked increase in electron density which occurs after noon in the summer observations, although there is again evidence that the maximum is reached later in the afternoon in low latitudes than it is at high latitudes. Typical daytime electron densities in summer at 1000 kilometers at noon during 1963 are of the order of 15,000 to 20,000 electrons per cubic centimeter with perhaps as many as 30,000 electrons per cubic centimeter at very low latitudes. In winter at noon the number of electrons varied from about 8,000 to 10,000/cm^3. The electron density in the nighttime ionosphere at about 1000 kilometers is illustrated in Fig. 32 in which observations for both summer and winter are shown. An examination of the nighttime electron densities observed over a series of latitude ranges indicates that after midnight there is no strong dependence of the nocturnal N_v variation on latitude and it is therefore convenient to present all the results over the latitude range 45° to 75° North magnetic in one diagram, Fig. 32. An examination of Fig. 32 indicates that the electron density at 1000 kilometers shows considerable variation from night to night with electron densities at midnight ranging from 1,000 per cm^3 to 10,000 per cm^3 with 5,000 per cm^3 as a mean figure.

IV.B. THE ACCURACY OF THE OBSERVATIONS

The absolute error ΔN_v in N_v, the electron density at the vehicle computed from (12) is given by

$$\Delta N_v = 1.24 \times 10^4 \Delta (f_{Nv}^2) = 1.24 \times 10^4 \Delta f_{xv} (2f_{xv} - f_H) \qquad (13)$$

where Δf_{xv} is the error in measurement of the quantity f_{xv}. The relative error is

$$\frac{\Delta N_v}{N_v} = \Delta f_{xv} \left[\frac{1}{(f_{xv} - f_H)} + \frac{1}{f_{xv}} \right] \qquad (14)$$

It is clear that the magnitude of the error in f_{Nv} and hence in N_v depends on the magnitude of the observed quantity f_{xv} and on the accuracy to which it can be measured ($\pm$ .05 Mc/s). During the daytime when f_{xv} is relatively large the error in electron density derived using equation (12) is negligibly small. However, as the electron density at the vehicle falls from its daytime to its nighttime value and as f_{xv} approaches the electron gyro-frequency f_H, it is clear that the electron density at the vehicle will then be computed from the difference of two small and almost equal quantities, namely, f_{xv}^2 and $f_{Hv}f_{xv}$ and the absolute and relative errors in N_v become large. Under these circumstances, it is best for the nighttime observations to compute the electron density at the vehicle not from the quantity f_{xv} corresponding to the frequency at which Extraordinary traces zero range but from the plasma resonance corresponding to the condition X = 1. The magnitude of the error in N_v resulting from the use of equation (12) has been computed from (13) and (14) and is shown in Table 10 for different assumed values of f_{Hv} for Δf_{xv} = .05 Mc/s. It is clear that the technique using the Extraordinary trace becomes unreliable for very low values of f_{xv} and is probably not safe to use when $f_{xv} - f_{Hv}$ is less than 0.8 Mc/s. Thus it is likely that nighttime electron densities deduced from the Extraordinary trace corresponding to values of less than 2,000 electrons per cubic centimeter are somewhat unreliable and for these occasions, the X = 1 resonance provides a better measurement. However, as can be seen from Table 10,* except under the circumstances just outlined, the electron density at the vehicle can be determined from (12) to an accuracy of better than $\pm$ 10%. Thus, apart from the need indicated above for caution when using the Extraordinary trace when the electron density at the vehicle is low, the technique described in this report offers a very simple and accurate way of determining the electron density at the Alouette orbit and its variations with time.

* See pp. 47 and 48.

V. CONCLUSIONS

It has been shown that a measurement of the frequency at which the Extraordinary ray trace observed on topside ionograms has zero range provides a rapid and accurate technique for determining the electron density at the location of the Alouette satellite. The calculation requires a knowledge of the dip angle and the gyro-frequency for electrons at the location of the vehicle. These can be derived from extrapolated values of the earth's field as measured at the ground (provided the position of the satellite at a given time is known accurately) or from observations on the ionograms themselves. Techniques for calculating the position of the satellite from accurate positional data determined from the Alouette orbital elements were described.

Using these techniques, the latitudinal, diurnal and seasonal variations of the electron density at the Alouette orbit have been determined for conditions representative of summer and winter daytime and nighttime periods. It is observed that the electron density at 1000 kilometers varies from nighttime minimum values of approximately 2,000 electrons per cc to daytime maximum values likely to be reached near the magnetic equator of about 40,000 electrons per cc. The electron density falls steadily from low latitudes to high latitudes and is greater in summer than in winter by a factor of the order of two. The summer daytime variations in electron density at the vehicle are interesting in that they show that the maximum value of electron density at this level is reached much later in the afternoon at low latitudes than it is at high latitudes.

APPENDIX A. THE CALCULATION OF THE LATITUDE AND LONGITUDE OF THE SUB-SATELLITE POINT

It is assumed that the orbital trajectory of the Alouette satellite is planar over the latitude range of 10° considered below. Since the orbit is almost circular so that the distance from the center of the earth is almost constant, the trajectory in this plane could be defined as a function $\psi = f(w)$, where w is the azimuth in the orbital plane ATC (Fig. A.1) and ψ is the angle (measured clockwise) from the equatorial crossing point to the point corresponding to the projection of the satellite on to the plane of the equator. T in this figure corresponds to the sub-satellite point and may be represented by the coordinates (w, θ) or (ψ, θ). In accordance with Kepler's laws, the area swept out by the radius vector to the satellite during unit time is proportional to the azimuth w defined above. The longitudes (determined from tables similar to Table 4) for the crossing points of the 10° latitude-longitude network used for calculating the position of the sub-satellite point (Section III.A) correspond to projections from the plane of the orbit on to the equatorial plane. In the calculations described, linear interpolation in time using these longitudes are made. If the interpolation had been carried out over the curved path of the Alouette orbit, a slightly different and more accurate longitude would have been derived for the sub-satellite point. The magnitude of this error is evaluated below.

From the orbital elements, the inclination of the plane orbit is known to be 80.464° so that the complement β of this angle (Fig. A.1) is 9.534°. Consider the rectangular coordinate system OXYZ defined in the plane of the equator with OY corresponding to the direction of a south-north equatorial crossing of the satellite. The equation of the orbital plane in this coordinate system (Fig. A.1) is

$$\frac{X}{Z} = - \tan \beta \qquad (A.1)$$

For the same system in spherical coordinates a unit vector, $\vec{U}$, will have the components

where

$$\vec{U} = \frac{X}{\rho}\vec{i} + \frac{Y}{\rho}\vec{j} + \frac{Z}{\rho}\vec{k}$$

$$\vec{R} = X\vec{i} + Y\vec{j} + Z\vec{k} = \rho\ \vec{U}$$

and $\vec{i}$, $\vec{j}$, and $\vec{k}$ are unit vectors along OX, OY, and OZ respectively, ρ is the distance from the origin to the point concerned (OP), and θ is the angle between the plane OXY and the line OP (Fig. A.2).
Thus

$$\vec{U} = \cos\theta \sin\psi\, \vec{i} + \cos\theta \cos\psi\, \vec{j} + \sin\theta\, \vec{k} \qquad (A.2)$$

If the coordinates of the unit vector $\vec{U}$ are to satisfy equation (A.1) then

$$\vec{U}_o = -\sin\theta \tan\beta\, \vec{i} + \cos\theta \cos\psi\, \vec{j} + \sin\theta\, \vec{k} \qquad (A.3)$$

and $\vec{U}_o$ now lies in the orbital plane.

Comparing (A.2) and (A.3)

$$\cos\theta \sin\psi = -\sin\theta \tan\beta \qquad (A.4)$$

so that

$$\sin\psi = -\tan\theta \tan\beta$$

The vector product $\vec{U}_o \cdot \vec{j}$ may be written

$$\vec{U}_o \cdot \vec{j} = \left\{-\sin\theta \tan\beta\, \vec{i} + \cos\theta \cos\psi\, \vec{j} + \sin\theta\, \vec{k}\right\} \cdot \left\{\vec{j}\right\}$$

$$\vec{U}_o \cdot \vec{j} = \cos\theta \cos\psi\, (\vec{j})^2 = \cos\theta \cos\psi$$

Also since the two vectors lie in the orbital plane we have

$$\vec{U}_o \cdot \vec{j} = |\vec{U}_o| \; |\vec{j}| \cos w = \cos w$$

Hence

$$\cos w = \cos \theta \cos \psi \tag{A.5}$$

For the cross product we may write Fig. A.1

$$\vec{U}_o \times \vec{j} = - |\vec{U}_o| \; |\vec{j}| (\sin w) \; \vec{n}$$

$$\vec{n} = \cos \beta \; \vec{i} + \sin \beta \; \vec{k}$$

Thus

$$\vec{U}_o \times \vec{j} = - \sin w \; (\cos \beta \; \vec{i} + \sin \beta \; \vec{k})$$

Also

$$\vec{U}_o \times \vec{j} = \begin{vmatrix} \vec{i} & \vec{j} & \vec{k} \\ -\sin \theta \tan \beta & \cos \theta \cos \psi & \sin \theta \\ 0 & 1 & 0 \end{vmatrix} \tag{A.6}$$

$$= - \sin \theta \; \vec{i} - \sin \theta \tan \beta \; \vec{k}$$

$$= - (\sin \theta \; \vec{i} - \cos \theta \sin \psi \; \vec{k}) \qquad \text{from (A.4)}$$

Equating the $\vec{k}$ components

$$-\sin w \sin \beta = \cos \theta \sin \psi \tag{A.7}$$

Dividing (A.7) by (A.5) gives

$$\psi = 2\pi - \arctan(\sin\beta \tan w) = f(w) \qquad (A.8)$$

The function f (w) is continuous for all values of w so that:

$$\frac{f(w+h) - f(w)}{h} = f'(w + K_1 h)$$

where K_1 lies between 0 and 1. The assumption that $\psi = f(w)$ is linear corresponds to taking the first term of the Taylor series for the interval h and neglecting the remaining terms. The remainder may be expressed, for the middle of the interval $h' = h/2$

$$\frac{h'^2}{2!} f''(w + K_2 h')$$

where K_2 lies between 0 and 1. This expression may be approximated by

$$(f'(w + h') - f'(w)) \frac{h'}{2!} = \Delta, \text{ say.}$$

The relative error in ψ in the interval h is given by

$$(f'(w + h') - f'(w)) \frac{1}{4} = \frac{\Delta}{h} = E \text{ say,} \qquad (A.9)$$

and this is the neglected term over the interval concerned.

Differentiating equation (A.8) gives

$$f'(w) = \frac{-2 \sin\beta}{1 + \sin^2\beta + \cos 2w \cos^2\beta}$$

Substituting in (A.9)

$$E = h' \sin\beta \left[\frac{-1}{1 + \sin^2\beta + \cos 2(w + h')\cos^2\beta} + \frac{1}{1 + \sin^2\beta + \cos 2w \cos^2\beta} \right] \qquad (A.10)$$

where E is the relative error Δ/h.

In order to find a relation between θ and w we eliminate ψ between equations (A.4) and (A.5) using the identity

$$\sin^2\psi + \cos^2\psi = 1$$

Thus

$$\tan^2\theta \tan^2\beta + \frac{\cos^2 w}{\cos^2\theta} = 1$$

$$\cos^2 w = \cos^2\theta - \sin^2\theta \tan^2\beta$$

$$\cos 2w = \frac{\cos 2\theta}{\cos^2\beta} - \tan^2\beta \qquad \text{(A.11)}$$

Since the latitude interval is 10°,

$$\cos 2(w + h') = \frac{\cos 2(\theta + 5)}{\cos^2\beta} - \tan^2\beta \qquad \text{(A.12)}$$

From (A.11) and (A.12), the quantities w and h' may be calculated. These values of w and h', together with the value of β for the Alouette orbit are then substituted in (A.10) to give the relative error E.

The error in longitude has been computed for Alouette ($\beta = 9.536°$) for a series of ranges of latitudes. The results are shown in Table A1.

It is also possible to compute ψ for steps of one degree in θ from (A.8) using the relation

$$\sin w = \sin\theta/\cos\beta$$

given immediately above. This is given in Table A1 in the column labelled ψ (computed). In addition, linear interpolation has been made in these computed values of ψ at integral multiples of 10°. The resulting values of ψ (interpolated) for the middle of each latitude range are also shown in this table. The difference ψ (computed) - ψ (interpolated) is always positive and gives the maximum error in longitude which can arise over the particular interval of latitude concerned. This quantity is shown in the

last column of Table A1 and agrees with the approximate values, Δ, of the calculated error from the Taylor expansion shown in the third column of Table A1.

TABLE A1

THE ERROR IN THE CALCULATION OF LONGITUDE

Geographic Latitude (Degrees)	Latitude at Mid-interval, h. (Degrees)	Δ (Degrees)	ψ(Computed) (Degrees)	ψ (Interpolated) (Degrees)	Maximum Error (Degrees)
0 - 30	25	.07	355.51	355.46	0.05
30 - 40	35	.12	353.24	353.17	0.07
40 - 50	45	.24	350.33	350.17	0.16
50 - 60	55	.51	346.12	345.77	0.35
60 - 70	65	1.3	338.88	337.80	1.08

The interpolated longitudes are too small by an amount which does not exceed the value shown in the last column of Table A1 and it is clear that except for very high latitudes, the error due to using a linear interpolation in the determination of longitude is small.

Reference to Tables 5 and 6 indicates that the differences at the end points of the 2° grid network of the values of total field and dip angle near 70° latitude are of the order of .001 gauss and 0.5 degrees respectively.

Thus for the range of latitudes relevant to the observations described in this report, even if the maximum possible error in the computed longitude were to occur, the resulting change in the values of f_{Hv} and θ_v (required in the computation of the electron density at the vehicle) would be negligible.

A similar error arises in the calculation of the latitude of the vehicle. This error may be calculated by a similar procedure using

$$\theta = f(w) = \frac{1}{2} \arccos \left\{ \cos 2w \cos^2\beta + \sin^2\beta \right\} = \arcsin (\sin w \cos \beta)$$

where the angles are, as before, given in Figs. A.1 and A.2, (c.f. (A.8)).

An evaluation of the magnitude of this error in latitude shows that it is even smaller than that computed above for longitudes since the plane of the orbit is highly inclined to the equatorial plane.

APPENDIX B. RECTANGULAR APPROXIMATION TO THE TRAPEZIUM ABCD, FIGURES 4 and 5.

The difference in lengths between AB and CD, Figs. 4 and 5, can be expressed relatively to the shorter parallel AB.
We have

$$AB = 2kR_2$$

where $k = \pi/180$ and R_2 is the distance from A or B to the axis of the earth (line passing through the geographic poles. Thus, if R is the earth's radius

$$AB = 2kR\cos\theta_2$$

$$CD = 2kR\cos\theta_1$$

So that

$$(CD - AB) = .0349R\,(\cos\theta_1 - \cos\theta_2)$$

Writing

$$\cos\theta_1 - \cos\theta_2 = 2\sin\left(\frac{\theta_1 + \theta_2}{2}\right)\sin\left(\frac{\theta_2 - \theta_1}{2}\right)$$

And noting that

$$\theta_2 = \theta_1 + 2^\circ$$

Then

$$(CD - AB) = .0698R\sin(\theta_1 + 1)^\circ \sin 1^\circ$$

And

$$AB = .0349R\cos\theta_2$$

APPENDIX B. (continued)

For $\theta_2 = 45°$ and $\theta_1 = 43°$ we find AB $\simeq$ 157.2 km, CD $\simeq$ 162.6 km

From Figure 4 it is seen that

$$2 \tan \delta/2 = a/c \text{ and } b = c \sin \theta'$$

Thus for $\theta = 44°$

$$\tan \delta/2 = \frac{a}{2b} \sin \theta' = \sin \theta' \tan (1°) = .012$$

From Figure 4

$$CD - AB = 2\ BD \tan \delta/2 = 5.39 \text{ km}$$

Thus for the calculation of the field parameters, the difference in the lengths of the parallels AB and CD may be neglected for the location of Stanford and for all latitudes below approximately 86°.

APPENDIX C. INTERPOLATION IN CURVILINEAR COORDINATES - THE DERIVATION OF EQUATION (6).

Let z be a scalar parameter defining the magnetic field at the sub-satellite point T (Fig. C.1). Let L and M be the curvilinear coordinates of the point T on the sphere representing the earth. The origin for this coordinate system is taken as the point D in the grid network ABCD of spacing 2°. L is thus the length measured along the parallel at the latitude through T from the meridian through BD having a west longitude ϕ. M is the length measured along the meridian through T from the parallel at latitude θ. The corresponding coordinates referred to the intersection of the Greenwich meridian and the plane of the equator as origin are denoted by l and m respectively.

Let l_1 and l_2 be consecutive values of the longitude grid lines and m_1 and m_2 consecutive values of the latitude grid lines (Fig. C.1). It should be noted that l_1, l_2, m_1, m_2, l, and m, refer to lengths along the sphere and not to the corresponding angles which are ϕ_1, ϕ_2, θ_1 and θ_2 respectively (Fig. C.1).

Thus

$$l_1 < l < l_2; \quad m_1 < m < m_2.$$

We write

$$dl = l - l_1; \quad dm = m - m_1$$

We define

$$G(l, m) = z$$

so that a set of curves G (l,m) = constant would correspond to a set of lines on the sphere along which the magnetic parameter concerned (dip or total field) is constant.

Suppose that at the corners of the grid network ABCD (Figs. C.1 and 6), the magnetic field parameter z has the values z_1 at D, z_2 at C and z_3 at B. Developing the function G around the point D (Fig. C.1), the total differential of z is given by

$$dz = \frac{\delta z}{\delta l} \, dl + \frac{\delta z}{\delta m} \, dm \qquad (C.1)$$

We have

$$L = \delta l = l_2 - l_1 = Rk \, (\phi_2 - \phi_1) \cos \theta_1$$

where $k = \pi/180$ and R is the radius of the earth.

Thus

$$\frac{\delta z}{\delta l} = \frac{z_3 - z_1}{Rk \, (\phi_2 - \phi_1) \cos \theta_1} = \frac{q}{Rk \, (x_2 - x_1) \cos \theta_1} \qquad (C.2)$$

$$M = \delta m = m_2 - m_1 = Rk \, (\theta_2 - \theta_1)$$

So that

$$\frac{\delta z}{\delta m} = \frac{z_2 - z_1}{Rk \, (\theta_2 - \theta_1)} = \frac{p}{Rk \, (y_2 - y_1)} \qquad (C.3)$$

where p, q, x_1, x_2, y_1 and y_2 are as previously defined (Section III.B).

We have

$$dl = l - l_1 = Rk \, (x - x_1) \cos \theta$$

$$dm = m - m_1 = Rk \, (y - y_1)$$

where θ is the latitude of the point T.

Substituting (C.2) and (C.3) in (C.1), the value of the magnetic field parameter at the sub-satellite point T is given by

$$z - z_1 = p \frac{(x - x_1) \cos \theta}{(x_2 - x_1) \cos \theta_1} + q \frac{(y - y_1)}{(y_2 - y_1)}$$

$$z = \left(\frac{\cos \theta}{\cos \theta_1}\right) \frac{X}{a} p + \frac{Y}{b} q + z_1$$

which is the previously quoted equation (6) of Section III.B.

APPENDIX D. THE DIGITAL COMPUTER PROGRAM.

A flow chart of the computer program for the calculation of the electron density at the vehicle appears in Figure D.1.

The program makes use of three matrices, namely

A) Tables of positional data of which Table 4 is a typical example.

B) Total intensity of the earth's magnetic field (Table 5).

C) Dip Angles (Table 6).

The program is written in SUBALGOL, a compiler language in use on Stanford University's IBM 7090 computer. In order to allow a more universal usage of the program, a version in machine language using FORTRAN II is also available.

The calculation of the electron density at the vehicle from the data on a single ionogram takes about 1/10th of a second.

INPUT-OUTPUT DATA

The program requires as input data:

1. One two-digit number giving the number of ionograms in one pass.
2. The pass number, date, and the time at which the closest approach of the vehicle to Stanford occurred.
3. The time, (t_o), at which f_{xv}, the frequency at which the Extraordinary ray has zero range, was observed.
4. The equatorial crossing data, t_E and l_E.
5. The frequency, f_{xv}.

The output from the program consists of:

1. Ionogram identification data, pass number, date, CPAZ, local time at the vehicle, GMT at the vehicle as required.
2. The geographic latitude and longitude at the satellite.
3. The gyro-frequency f_{Hv} at the satellite.
4. The plasma frequency f_{Nv} at the satellite.
5. The dip latitude at the location of the vehicle.
6. The electron density at the vehicle.

REFERENCES

[1] Alouette positional data, Parts I and II, published by NASA Goddard Space Flight Center.

[2] Alouette positional data, Part III, published by NASA Goddard Space Flight Center.

[3] The total intensity of the earth's magnetic field for the year 1955, published by the Hydrographic Office, Washington, D. C.

[4] The magnetic inclination or dip angle for the year 1955, published by the Hydrographic Office, Washington, D. C.

BIBLIOGRAPHY

Calvert, W. and Goe, G. B., "Plasma resonances in the upper ionosphere," Journal of Geophysical Research (in press).

C.D.R.T.E., "Alouette, Satellite 1962 Beta Alpha One," published by the Canadian Defence Research Board, Ottawa, 1962.

Chapman, S., "Geomagnetic nomenclature," Journal of Geophysical Research, 68, 1174, 1963.

Hagg, E. L., "A preliminary study of the electron density at 1000 kilometers," Canadian Journal of Physics, 41, 195, 1963.

Hartz, T. R., "A study of interference on the Alouette topside sounder records," Technical Memorandum No. 415, Canadian Defence Research Telecommunications Establishment, Ottawa, 1963.

Jackson, J. E., "NASA investigation of the topside ionosphere," NASA Goddard Space Flight Center Report NASA X-615-63-105, 1963.

Jackson, J. E., Blumle, L. J., and Fitzenreiter, R. J., "The NASA topside sounder program," NASA Goddard Space Flight Center Report NASA X-615-63-9, 1963.

King, J. W., "Investigations of the upper ionosphere deduced from topside sounder data," Nature, 197, 636, 1963.

King, J. W., Smith, P. A., Eccles, D., and Helm, H., "The structure of the upper ionosphere as observed by the topside sounder satellite, Alouette," D.S.I.R. Report, Radio Research Station, Slough, England, 1963.

Knecht, R. W., and Russell, S., "Pulsed radio soundings of the topside of the ionosphere in the presence of spread F," Journal of Geophysical Research, 67, 1178, 1962.

Knecht, R. W., van Zandt, T. E., "Some early results from the ionospheric topside sounder satellite," Nature, Feb. 16, 1963.

Knecht, R. W., van Zandt, T. E., and Russell, S., "First pulsed radio soundings of the topside of the ionosphere," Journal of Geophysical Research, 66, 3078, 1961.

Knecht, R. W., van Zandt, T. E., and Watts, J. M., "The NASA fixed frequency topside sounder program," paper in Electron Density Profiles in the Ionosphere and Exosphere, edited by B. Maehlum, Pergamon Press, 246, 1962.

Lockwood, G. E. K., "Plasma and cyclotron spike phenomena observed in topside ionograms," Canadian Journal of Physics, 41, 190, 1963.

Lockwood, G. E. K., Petrie, L. E., "Low latitude field aligned ionization observed by the Alouette topside sounder," Planetary and Space Science, 11, 327, 1963.

Molozzi, A. R., "Instrumentation of the ionospheric sounder contained in the Satellite 1962 Beta Alpha One (Alouette)," presented at the Fourth Space Science Symposium in June 1963.

Muldrew, D. B., "The relationship of F-layer critical frequencies to the intensity of the outer Van Allen belt," Canadian Journal of Physics, 41, 199, 1963.

Muldrew, D. B., "Radio propagation along magnetic field-aligned sheets of ionization observed by the Alouette topside sounder," Journal of Geophysical Research (in press), 1963.

Nelms, G. L., "Scale heights of the upper ionosphere from topside soundings," Canadian Journal of Physics, 41, 202, 1963.

Petrie, L. E., "Topside spread echoes," Canadian Journal of Physics, 41, 194, 1963.

Thomas, J. O., Long, A. R., and Westover, D. E., "The calculation of electron density profiles from topside sounder records," Journal of Geophysical Research, 68, 3237, 1963.

Thomas, J. O., and Westover, D. E., "The calculation of electron density profiles from topside ionograms using a digital computer," Technical Report No. 5, Stanford Electronics Laboratories, Stanford University, 1963.

Thomas, J. O., "Canadian Satellite: The Topside Sounder Alouette," Science, 139, 229, 1963.

Warren, E. S., "Sweep frequency radio soundings of the topside of the ionosphere," Canadian Journal of Physics, 40, 1692, 1962.

Warren, E. S., "Perturbation of the local electron density by Alouette satellite," Canadian Journal of Physics, 41, 188, 1963.

Warren, E. S., "Some preliminary results of sounding of the topside of the ionosphere by radio pulses from a satellite," Nature, 197, 636, 1963.

TABLE 3

ALOUETTE POSITIONAL DATA

From NASA Goddard Space Flight Center. Data source NORAD.
Issue Date 6 Dec 1962.

Bulletin 6 62B-Alpha 1 424 In four parts. Part I.

922	339.78987	.073243	.90532-10	0	1.15893	.00214
99.470	-.982	0	125.203	-2.565	0	99.67	80.48

Part II S-N Equator Crossings

REV	Time Z	Long W	REV	Time Z	Long W	REV	Time Z	Long W
7 Dec 62								
945	1124.54	149.07	946	1310.06	175.60	947	1455.59	202.13
948	1641.12	228.65	949	1826.64	255.18	950	2012.17	281.70
951	2157.70	308.23	952	2343.23	334.76			
8 Dec 62								
953	128.75	1.28	954	314.28	27.81	955	459.81	54.33
956	645.33	80.86	957	830.86	107.39	958	1016.39	133.91
959	1201.91	160.44	960	1347.44	186.96	961	1532.97	213.49
962	1718.49	240.02	963	1904.02	266.54	964	2049.55	293.07
965	2235.08	319.59						
9 Dec 62								
966	20.60	346.12	967	206.13	12.65	968	351.66	39.17
969	537.18	65.70	970	722.71	92.22	971	908.24	118.75
972	1053.76	145.27	973	1239.29	171.80	974	1424.82	198.33
975	1610.34	224.85	976	1755.87	251.38	977	1941.40	277.90

TABLE 4

ALOUETTE POSITIONAL DATA

Part III. Reduction to other latitudes and heights for REV 1171

LAT N	MINUTES PLUS	LONG CORR	HEIGHT KILOM	LAT S	MINUTES PLUS	LONG CORR	HEIGHT KILOM
SN 00	.00	.00	1010.4	NS 00	52.56	193.24	1016.8
SN 10	2.94	359.05	1008.4	NS 10	55.51	192.30	1020.1
SN 20	5.89	358.00	1007.8	NS 20	58.47	191.26	1024.4
SN 30	8.84	356.71	1008.3	NS 30	61.44	189.97	1029.5
SN 40	11.82	354.94	1009.9	NS 40	64.43	188.23	1034.9
SN 50	14.82S	352.29	1012.1	NS 50	67.46	185.60	1040.1
SN 60	17.87	347.76	1014.5	NS 60	70.54	181.13	1044.7
SN 70	21.06	338.17	1016.7	NS 70	73.76	171.68	1048.2
SN 80	25.30	296.02	1018.7V	NS 80	78.03	130.31	1050.1V
BULLETIN 000		62B-ALPHA 1 424					
N PT	26.26	277.18	1018.9V	S PT	78.99	111.60	1050.0V
NS 80	27.22	258.22	1019.0V	SN 80	79.96	92.53	1049.8V
NS 70	31.45	215.30	1018.7V	SN 70	84.23	48.84	1046.4V
NS 60	34.65	205.56	1017.6V	SN 60	8745	38.96	1041.9V
NS 50	37.70	200.98	1016.2V	SN 50	90.52	34.33	1036.3V
NS 40	40.71	198.31	1014.8V	SN 40	93.54	31.64	1030.3V
NS 30	43.69	196.53	1013.9	SN 30	96.53	29.86	1024.2
NS 20	46.65	195.23	1013.8	SN 20	99.50	28.55	1018.6
NS 10	49.60	194.18	1014.7	SN 10	102.45	27.50	1013.9
NS 00	52.56	193.24	1016.8	SN 00	105.52	26.52	1010.4

TABLE 5

TOTAL MAGNETIC FIELD AT THE GROUND (GAUSS)

LATITUDE NORTH (DEG.)	LONGITUDE WEST (DEG.)														
	90	92	94	96	98	100	102	104	106	108	110	112	114	116	118
6	0.365	0.364	0.362	0.361	0.360	0.359	0.358	0.356	0.354	0.353	0.352	0.351	0.350	0.350	0.349
8	0.376	0.375	0.373	0.372	0.370	0.368	0.367	0.365	0.363	0.362	0.361	0.360	0.359	0.358	0.356
10	0.388	0.387	0.382	0.381	0.380	0.379	0.378	0.374	0.372	0.371	0.370	0.369	0.368	0.367	0.364
12	0.402	0.400	0.398	0.398	0.395	0.392	0.390	0.389	0.387	0.382	0.381	0.380	0.379	0.376	0.372
14	0.416	0.413	0.411	0.410	0.410	0.409	0.406	0.402	0.400	0.398	0.393	0.391	0.390	0.387	0.383
16	0.430	0.429	0.427	0.424	0.422	0.420	0.419	0.416	0.411	0.409	0.405	0.401	0.399	0.397	0.392
18	0.443	0.441	0.440	0.438	0.433	0.430	0.429	0.428	0.422	0.420	0.417	0.412	0.410	0.408	0.404
20	0.459	0.456	0.453	0.450	0.448	0.443	0.441	0.438	0.435	0.431	0.429	0.425	0.420	0.419	0.416
22	0.470	0.469	0.467	0.462	0.460	0.459	0.454	0.451	0.449	0.445	0.441	0.438	0.435	0.431	0.429
24	0.483	0.482	0.480	0.478	0.473	0.471	0.469	0.465	0.461	0.459	0.455	0.451	0.449	0.444	0.440
26	0.497	0.494	0.492	0.490	0.489	0.487	0.482	0.480	0.477	0.472	0.469	0.464	0.461	0.458	0.454
28	0.510	0.509	0.508	0.505	0.502	0.500	0.498	0.495	0.491	0.488	0.482	0.480	0.475	0.471	0.469
30	0.422	0.520	0.520	0.519	0.517	0.515	0.511	0.509	0.504	0.501	0.495	0.491	0.488	0.483	0.480
32	0.534	0.533	0.532	0.531	0.530	0.528	0.522	0.520	0.517	0.511	0.509	0.505	0.501	0.496	0.491
34	0.548	0.547	0.546	0.543	0.542	0.539	0.535	0.531	0.528	0.522	0.520	0.516	0.512	0.509	0.504
36	0.558	0.558	0.558	0.557	0.553	0.551	0.548	0.542	0.539	0.535	0.531	0.527	0.522	0.519	0.515
38	0.569	0.569	0.568	0.567	0.564	0.560	0.559	0.556	0.551	0.547	0.542	0.539	0.534	0.530	0.526
40	0.478	0.478	0.478	0.576	0.574	0.571	0.569	0.566	0.562	0.559	0.555	0.550	0.545	0.540	0.537
42	0.586	0.585	0.584	0.582	0.580	0.578	0.575	0.573	0.570	0.568	0.563	0.560	0.556	0.552	0.547
44	0.592	0.591	0.591	0.590	0.587	0.585	0.582	0.580	0.578	0.574	0.572	0.569	0.565	0.562	0.557
46	0.597	0.596	0.595	0.594	0.592	0.590	0.588	0.586	0.584	0.582	0.580	0.578	0.574	0.570	0.567
48	0.601	0.600	0.600	0.600	0.598	0.595	0.593	0.591	0.590	0.589	0.588	0.586	0.583	0.580	0.574
50	0.602	0.601	0.602	0.601	0.601	0.600	0.598	0.596	0.594	0.593	0.592	0.591	0.591	0.590	0.584
52	0.601	0.602	0.603	0.603	0.602	0.601	0.600	0.598	0.597	0.596	0.595	0.594	0.593	0.592	0.591
54	0.599	0.601	0.602	0.603	0.604	0.602	0.600	0.599	0.598	0.597	0.596	0.596	0.594	0.593	0.592
56	0.597	0.598	0.600	0.601	0.604	0.605	0.602	0.600	0.599	0.599	0.598	0.597	0.596	0.595	0.594
58	0.594	0.596	0.598	0.600	0.602	0.605	0.605	0.604	0.602	0.601	0.600	0.600	0.599	0.597	0.596
60	0.593	0.595	0.598	0.600	0.602	0.604	0.605	0.605	0.604	0.603	0.602	0.601	0.600	0.599	0.598
62	0.593	0.596	0.599	0.600	0.602	0.603	0.606	0.606	0.605	0.604	0.603	0.602	0.601	0.600	0.598
64	0.595	0.598	0.600	0.601	0.603	0.604	0.606	0.606	0.605	0.604	0.603	0.602	0.601	0.599	0.598
66	0.597	0.600	0.601	0.603	0.604	0.605	0.607	0.606	0.604	0.603	0.602	0.601	0.600	0.598	0.597
68	0.599	0.601	0.603	0.605	0.606	0.608	0.607	0.605	0.603	0.602	0.601	0.599	0.598	0.597	0.595
70	0.602	0.604	0.605	0.606	0.607	0.609	0.608	0.606	0.603	0.601	0.599	0.598	0.597	0.596	0.594

TABLE 5 (Continued)

TOTAL MAGNETIC FIELD AT THE GROUND (GAUSS)

LATITUDE NORTH (DEG.) \ LONGITUDE WEST (DEG.)	120	122	124	126	128	130	132	134	136	138	140	142	144	146
6	0.348	0.346	0.345	0.344	0.343	0.342	0.340	0.340	0.339	0.338	0.339	0.338	0.338	0.337
8	0.353	0.352	0.351	0.349	0.348	0.347	0.346	0.345	0.343	0.343	0.342	0.342	0.341	0.340
10	0.361	0.359	0.358	0.357	0.354	0.353	0.351	0.350	0.350	0.349	0.348	0.347	0.356	0.344
12	0.370	0.368	0.366	0.364	0.362	0.361	0.359	0.358	0.356	0.355	0.353	0.352	0.350	0.348
14	0.380	0.378	0.375	0.372	0.371	0.370	0.368	0.366	0.363	0.361	0.359	0.357	0.356	0.354
16	0.390	0.388	0.384	0.382	0.380	0.378	0.376	0.373	0.371	0.369	0.367	0.364	0.362	0.360
18	0.401	0.398	0.394	0.392	0.391	0.389	0.386	0.383	0.380	0.378	0.376	0.372	0.369	0.367
20	0.413	0.410	0.408	0.402	0.400	0.399	0.396	0.392	0.390	0.387	0.383	0.380	0.377	0.373
22	0.425	0.420	0.418	0.414	0.411	0.409	0.405	0.401	0.398	0.395	0.392	0.388	0.384	0.381
24	0.438	0.432	0.430	0.426	0.421	0.419	0.414	0.410	0.408	0.402	0.399	0.397	0.392	0.389
26	0.450	0.447	0.441	0.438	0.434	0.430	0.425	0.420	0.417	0.412	0.410	0.407	0.401	0.398
28	0.463	0.460	0.457	0.451	0.449	0.442	0.438	0.433	0.429	0.423	0.420	0.416	0.411	0.409
30	0.476	0.472	0.469	0.463	0.460	0.455	0.450	0.445	0.440	0.435	0.430	0.427	0.421	0.418
32	0.487	0.483	0.479	0.475	0.471	0.467	0.460	0.456	0.451	0.446	0.440	0.436	0.431	0.427
34	0.500	0.495	0.490	0.486	0.481	0.478	0.471	0.467	0.461	0.457	0.450	0.446	0.441	0.437
36	0.511	0.507	0.502	0.498	0.492	0.490	0.482	0.477	0.471	0.466	0.462	0.458	0.452	0.448
38	0.521	0.518	0.511	0.508	0.503	0.500	0.495	0.490	0.482	0.479	0.472	0.469	0.463	0.459
40	0.532	0.529	0.523	0.519	0.513	0.510	0.505	0.500	0.495	0.490	0.485	0.479	0.474	0.470
42	0.542	0.538	0.533	0.530	0.525	0.520	0.518	0.512	0.508	0.500	0.495	0.489	0.483	0.480
44	0.552	0.548	0.544	0.540	0.537	0.523	0.529	0.522	0.519	0.512	0.507	0.500	0.494	0.490
46	0.562	0.558	0.553	0.549	0.545	0.542	0.537	0.533	0.529	0.522	0.518	0.511	0.504	0.499
48	0.570	0.566	0.560	0.556	0.551	0.548	0.543	0.540	0.536	0.531	0.526	0.519	0.514	0.509
50	0.580	0.574	0.570	0.565	0.560	0.555	0.551	0.548	0.542	0.539	0.532	0.529	0.522	0.519
52	0.587	0.581	0.576	0.571	0.567	0.562	0.558	0.554	0.550	0.547	0.542	0.537	0.530	0.527
54	0.591	0.588	0.582	0.579	0.574	0.570	0.565	0.561	0.557	0.554	0.550	0.544	0.539	0.534
56	0.592	0.591	0.588	0.584	0.582	0.577	0.572	0.570	0.564	0.560	0.556	0.551	0.546	0.541
58	0.594	0.593	0.592	0.588	0.584	0.582	0.578	0.573	0.570	0.566	0.561	0.555	0.549	0.546
60	0.596	0.594	0.593	0.591	0.588	0.584	0.581	0.578	0.574	0.571	0.567	0.561	0.555	0.550
62	0.597	0.595	0.594	0.592	0.590	0.587	0.584	0.581	0.577	0.573	0.570	0.566	0.560	0.556
64	0.597	0.595	0.594	0.592	0.591	0.588	0.584	0.582	0.580	0.577	0.573	0.569	0.565	0.561
66	0.596	0.594	0.593	0.591	0.590	0.588	0.585	0.583	0.581	0.578	0.575	0.572	0.569	0.566
68	0.594	0.593	0.591	0.590	0.589	0.587	0.585	0.584	0.582	0.580	0.576	0.574	0.573	0.571
70	0.592	0.592	0.589	0.588	0.587	0.586	0.584	0.583	0.582	0.580	0.578	0.576	0.575	0.574

TABLE 6

DIP ANGLE (DEG.)

LATITUDE NORTH (DEG.)	LONGITUDE WEST (DEG.)																								
	90	92	94	96	98	100	102	104	106	108	110	112	114	116	118
6	34.0	33.7	32.5	32.0	31.8	30.4	29.8	28.4	27.9	26.8	26.0	25.8	24.3	24.0	23.0
8	37.0	36.3	36.0	35.5	34.3	33.8	32.9	32.0	31.0	30.4	29.8	28.7	27.9	27.4	26.4
10	40.2	39.9	39.5	38.3	38.0	37.2	36.0	35.3	34.3	34.0	33.2	32.0	31.8	30.8	30.0
12	42.6	42.4	42.0	41.5	40.9	40.0	39.7	38.7	38.0	37.3	36.4	36.0	35.7	34.8	34.1
14	45.8	45.3	45.0	44.3	44.0	43.5	42.3	41.9	41.2	40.7	40.4	40.0	39.5	38.4	38.0
16	48.3	48.1	47.9	47.5	46.4	45.8	45.3	44.4	44.0	43.7	43.0	42.4	42.0	41.7	41.2
18	50.8	50.5	50.3	50.0	49.5	48.6	48.0	47.5	46.5	46.0	45.8	45.0	44.4	44.0	43.7
20	53.2	52.8	52.7	52.2	51.8	51.3	50.8	50.2	49.3	48.5	48.3	47.8	47.2	46.5	46.0
22	55.6	55.2	55.0	54.7	54.2	53.7	53.0	52.3	52.0	51.6	50.3	50.0	49.7	49.3	48.3
24	57.7	57.3	57.0	56.7	56.2	55.8	55.4	54.9	54.2	53.8	53.2	52.7	52.3	52.0	51.3
26	59.7	59.5	59.2	59.0	58.6	58.2	57.8	57.3	56.8	56.2	55.8	55.3	55.0	54.4	53.9
28	61.8	61.5	61.2	61.0	60.9	60.5	60.0	59.5	59.0	58.6	58.2	57.8	57.2	56.8	56.3
30	63.3	63.2	63.0	62.7	62.5	62.3	62.0	61.7	61.3	60.8	60.3	59.8	59.5	59.0	58.5
32	65.2	65.0	64.8	64.5	64.3	65.2	63.9	63.7	63.3	63.0	62.4	62.0	61.7	61.2	60.8
34	66.8	66.7	66.7	66.6	66.5	66.3	66.0	65.8	65.3	65.0	64.3	64.0	63.5	63.0	62.7
36	68.5	68.4	68.3	68.2	68.1	68.0	67.8	67.7	67.3	67.0	66.7	66.2	65.7	65.2	64.7
38	70.2	70.3	70.3	70.2	70.1	70.0	69.8	69.6	69.2	68.7	68.3	68.0	67.3	67.0	66.6
40	71.8	71.9	71.8	71.8	71.7	71.6	71.5	71.2	70.8	70.6	70.3	70.0	69.5	69.0	68.5
42	73.0	73.1	73.2	73.2	73.2	73.1	73.0	72.8	72.5	72.1	71.7	71.3	70.9	70.6	70.2
44	74.3	74.6	74.8	74.8	74.7	74.6	74.5	74.3	74.1	73.8	73.6	73.0	72.8	72.3	71.8
46	75.8	76.1	76.3	76.3	76.2	76.1	75.8	75.7	75.4	75.3	75.0	74.6	74.3	73.8	73.4
48	76.8	77.0	77.2	77.3	77.2	77.1	77.1	76.9	76.8	76.6	76.4	76.1	75.8	75.4	75.0
50	77.7	77.9	78.1	78.3	78.4	78.5	78.6	78.5	78.3	78.2	78.0	77.7	77.3	77.0	76.6
52	78.7	79.0	79.2	79.5	79.7	79.8	79.9	79.9	79.8	79.6	79.2	78.9	78.6	78.4	78.0
54	79.9	80.1	80.4	80.7	80.7	80.8	81.0	81.0	80.9	80.8	80.7	80.4	80.2	79.7	79.3
56	80.7	81.0	81.3	81.6	81.7	82.0	82.2	82.3	82.2	82.0	81.8	81.6	81.3	81.0	80.7
58	81.5	81.9	82.2	82.5	82.7	82.8	83.1	83.3	83.3	83.2	83.0	82.8	82.6	82.3	81.9
60	82.3	82.7	83.0	83.3	83.6	83.8	84.0	84.2	84.3	84.2	84.1	84.0	83.8	83.6	83.2
62	83.1	83.5	83.8	84.1	84.5	84.8	85.0	85.1	85.2	85.2	85.2	85.1	84.8	84.6	84.3
64	83.9	84.3	84.7	85.1	85.4	85.7	86.0	86.2	86.3	86.3	86.2	86.1	85.9	85.6	85.3
66	84.5	85.0	85.4	85.8	86.1	86.4	86.7	86.9	87.0	87.1	87.1	87.0	86.8	86.6	86.3
68	85.2	85.5	85.9	86.3	86.6	87.0	87.3	87.5	87.7	87.8	87.8	87.7	87.6	87.4	87.2
70	85.5	86.0	86.3	86.7	87.0	87.4	87.7	88.0	88.3	88.5	88.6	88.7	88.6	88.4	88.1

TABLE 6 (Continued)
DIP ANGLE (DEG.)

LATITUDE NORTH (DEG.) \ LONGITUDE WEST (DEG.)	120	122	124	126	128	130	132	134	136	138	140	142	144	146
6	22.4	21.9	21.8	21.0	20.5	20.3	20.2	20.0	19.8	19.0	18.2	18.0	17.8	17.4
8	26.2	26.0	25.3	24.3	24.2	24.0	23.8	23.5	22.8	22.4	22.1	21.9	21.8	21.5
10	29.8	29.6	28.6	28.0	27.9	27.8	27.0	26.3	26.0	25.8	25.4	25.2	24.8	24.5
12	33.6	32.5	32.0	31.7	31.3	30.8	30.5	30.2	30.0	29.6	29.2	28.8	28.2	28.0
14	37.2	36.2	35.9	35.3	34.6	34.2	34.0	33.7	32.8	32.2	32.0	31.8	31.7	31.6
16	40.7	40.0	39.4	38.8	38.1	37.7	37.0	36.6	36.2	35.9	35.5	35.0	34.6	34.2
18	43.4	42.7	42.0	41.8	41.6	40.8	40.4	40.0	39.6	38.9	38.5	38.2	37.9	37.6
20	45.8	45.3	44.5	44.2	43.9	43.6	43.2	42.8	42.4	42.0	41.6	41.2	40.8	40.4
22	48.0	47.8	47.3	46.6	46.3	46.0	45.6	45.2	44.8	44.4	44.0	43.7	43.4	43.1
24	51.0	50.6	50.0	49.7	49.2	48.8	48.5	48.1	47.5	47.1	46.7	46.4	46.1	45.8
26	53.3	53.0	52.6	52.1	51.9	51.5	51.0	50.6	50.2	49.8	49.4	49.0	48.6	48.2
28	55.8	55.4	55.0	54.3	54.0	53.7	53.3	53.0	52.7	52.3	52.0	51.6	51.2	50.8
30	58.0	57.6	57.0	56.6	56.3	55.9	55.5	55.1	54.7	54.3	53.9	53.6	53.3	53.0
32	60.2	59.8	59.2	58.8	58.3	58.0	57.7	57.4	57.1	56.7	56.3	55.9	55.5	55.0
34	62.3	61.8	61.3	61.0	60.5	60.0	59.7	59.3	59.0	58.6	58.2	57.8	57.4	57.0
36	64.2	63.8	63.3	62.8	62.3	61.8	61.5	61.2	60.8	60.5	60.1	59.6	59.2	58.8
38	65.2	65.8	65.3	64.8	64.2	63.7	63.3	62.7	62.3	62.0	61.7	61.3	60.9	60.5
40	68.0	67.6	67.2	66.8	66.2	65.7	65.2	64.8	64.3	63.8	63.4	63.0	62.6	62.2
42	69.8	69.4	69.0	68.5	68.0	67.4	66.9	66.5	66.0	65.6	65.2	64.8	64.4	64.0
44	71.4	71.0	70.6	70.0	69.7	69.3	68.9	68.4	67.9	67.4	66.9	66.5	66.0	65.6
46	73.0	72.5	72.0	71.6	71.2	70.8	70.3	69.8	69.3	68.9	68.4	68.0	67.6	67.2
48	74.6	74.2	73.7	73.2	72.7	72.2	71.8	71.3	70.9	70.4	70.0	69.5	69.1	68.6
50	76.3	75.7	75.5	75.0	74.5	74.0	73.5	73.0	72.5	72.0	71.5	71.0	70.5	70.0
52	77.7	77.2	76.8	76.3	76.0	75.6	75.1	74.7	74.2	73.6	73.0	72.4	71.8	71.4
54	79.0	78.6	78.2	77.7	77.4	77.0	76.5	76.0	75.6	75.1	74.7	74.1	73.6	73.1
56	80.3	80.0	79.6	79.2	78.8	78.3	77.8	77.4	76.9	76.5	76.0	75.6	75.1	74.6
58	81.6	81.2	80.7	80.3	80.0	79.6	79.1	78.6	78.1	77.7	77.2	76.8	76.3	75.9
60	82.7	82.4	82.0	81.6	81.2	80.7	80.3	79.9	79.4	79.0	78.5	78.0	77.6	77.2
62	84.0	83.6	83.1	82.7	82.3	81.8	81.4	81.0	80.5	80.1	79.7	79.2	78.8	78.3
64	84.9	84.5	84.1	83.7	83.3	82.8	82.4	82.1	81.7	81.2	80.8	80.3	79.9	79.4
66	86.0	85.5	85.1	84.7	84.3	83.8	83.4	83.0	82.7	82.3	81.9	81.5	81.1	80.7
68	86.8	86.5	86.1	85.7	85.3	84.8	84.5	84.1	83.8	83.4	83.0	82.7	82.3	81.9
70	87.7	87.5	87.0	86.6	86.2	85.8	85.4	85.1	84.8	84.5	84.1	83.8	83.4	83.1

TABLE 9

DESCRIPTION OF TYPICAL TOPSIDE IONOGRAMS

Fig.	Date (1963)	Time (t_o) GMT H	M	S	Pass Number	Remarks
9	June 22	18	43	32	3637	Summer, daytime near noon.
10	March 15	21	40	03	2288	Equinox, near noon.
11	May 16	23	52	59	3135	Afternoon, summer.
12	May 11	01	16	38	3054	Evening conditions. Note Z trace.
13	July 16	15	55	34	3963	Early morning conditions.
14	April 5	05	23	53	2565	Nighttime ionogram. Note cusp near 1.8 Mc/s.
15	June 29	06	44	35	3726	Nighttime ionogram. Note cusp near 1.4 Mc/s.
16	July 20	14	53	40	4017	Early morning. Note spread F.
17	March 22	20	51	39	2383	Mid-day multiple traces.
18	March 22	07	12	29	2375	Midnight multiple traces.
19	May 23	22	45	30	3230	Early afternoon. Note low frequency signals.
20	May 23	22	47	15	3230	Early afternoon. Note low frequency signals.
21	May 23	22	50	10	3230	Early afternoon. Note low frequency signals.
22	June 14	08	02	24	3522	Midnight. Note curvature of Extraordinary ray.
23	July 1	17	08	50	3759	Note low frequency signals.
24	July 1	17	08	32	3759	Note low frequency signals.

TABLE 10

THE MAGNITUDE OF THE ERROR IN N_v

f_{Hv} (Mc/s)	N_v (electrons/cm^3)	f_{xv} (Mc/s)	ΔN_v	$\Delta N_v/N_v$ (%)
.5	40000.0	2.063	2248.6	5.6
	35000.0	1.949	2106.2	6.0
	30000.0	1.825	1953.5	6.5
	25000.0	1.692	1787.8	7.2
	20000.0	1.544	1605.0	8.0
	15000.0	1.378	1398.6	9.3
	10000.0	1.182	1155.9	11.6
	5000.0	.932	846.2	16.9
.6	40000.0	2.121	2258.0	5.6
	35000.0	2.007	2116.2	6.0
	30000.0	1.884	1964.3	6.5
	25000.0	1.751	1799.6	7.2
	20000.0	1.605	1618.1	8.1
	15000.0	1.440	1413.6	9.4
	10000.0	1.247	1174.0	11.7
	5000.0	1.002	870.9	17.4
.7	40000.0	2.180	2269.0	5.7
	35000.0	2.066	2128.0	6.1
	30000.0	1.944	1977.0	6.6
	25000.0	1.812	1813.4	7.3
	20000.0	1.667	1633.5	8.2
	15000.0	1.504	1431.2	9.5
	10000.0	1.314	1195.1	12.0
	5000.0	1.075	899.1	18.0
.8	40000.0	2.240	2281.7	5.7
	35000.0	2.127	2141.5	6.1
	30000.0	2.006	1991.5	6.6
	25000.0	1.875	1829.2	7.3
	20000.0	1.732	1651.1	8.3
	15000.0	1.570	1451.2	9.7
	10000.0	1.383	1219.0	12.2
	5000.0	1.150	930.6	18.6

TABLE 10 (continued)

THE MAGNITUDE OF THE ERROR IN N_v

f_{Hv} (Mc/s)	N_v (electrons/cm^3)	f_{xv} (Mc/s)	ΔN_v	$\Delta N_v/N_v$ (%)
	40000.0	2.302	2295.9	5.7
	35000.0	2.189	2156.7	6.2
	30000.0	2.069	2007.8	6.7
.9	25000.0	1.940	1847.0	7.4
	20000.0	1.797	1670.7	8.4
	15000.0	1.638	1473.6	9.8
	10000.0	1.454	1245.5	12.5
	5000.0	1.228	965.1	19.3
	40000.0	2.364	2311.8	5.8
	35000.0	2.253	2173.6	6.2
	30000.0	2.134	2025.9	6.8
1.0	25000.0	2.005	1866.7	7.5
	20000.0	1.865	1692.5	8.5
	15000.0	1.708	1498.1	10.0
	10000.0	1.528	1274.5	12.7
	5000.0	1.308	1002.2	20.0
	40000.0	2.428	2329.2	5.8
	35000.0	2.318	2192.1	6.3
	30000.0	2.200	2045.8	6.8
1.1	25000.0	2.073	1888.2	7.6
	20000.0	1.934	1716.1	8.6
	15000.0	1.780	1524.8	10.2
	10000.0	1.603	1305.8	13.1
	5000.0	1.390	1041.7	20.8
	40000.0	2.494	2348.1	5.9
	35000.0	2.384	2212.1	6.3
	30000.0	2.267	2067.3	6.9
1.2	25000.0	2.141	1911.4	7.6
	20000.0	2.005	1741.7	8.7
	15000.0	1.853	1553.6	10.4
	10000.0	1.680	1339.2	13.4
	5000.0	1.474	1083.3	21.7

FIGURES

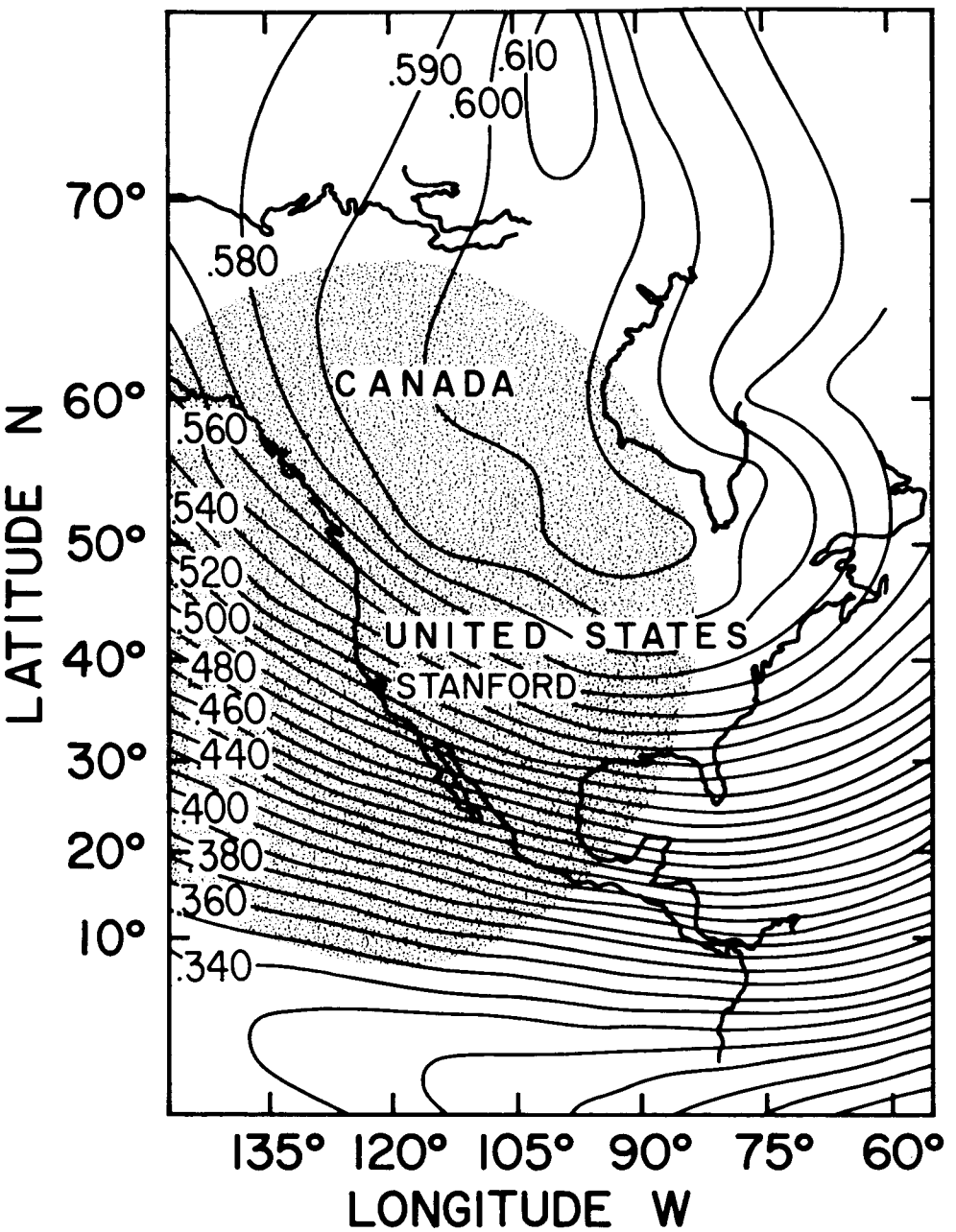

1a Map showing the position of the telemetry station operated by the Radioscience Laboratory, Stanford University. The dotted area indicates the location of the approximate zone in which line-of-sight signals from Alouette are detectable. The variation of the earth's total field is also shown.

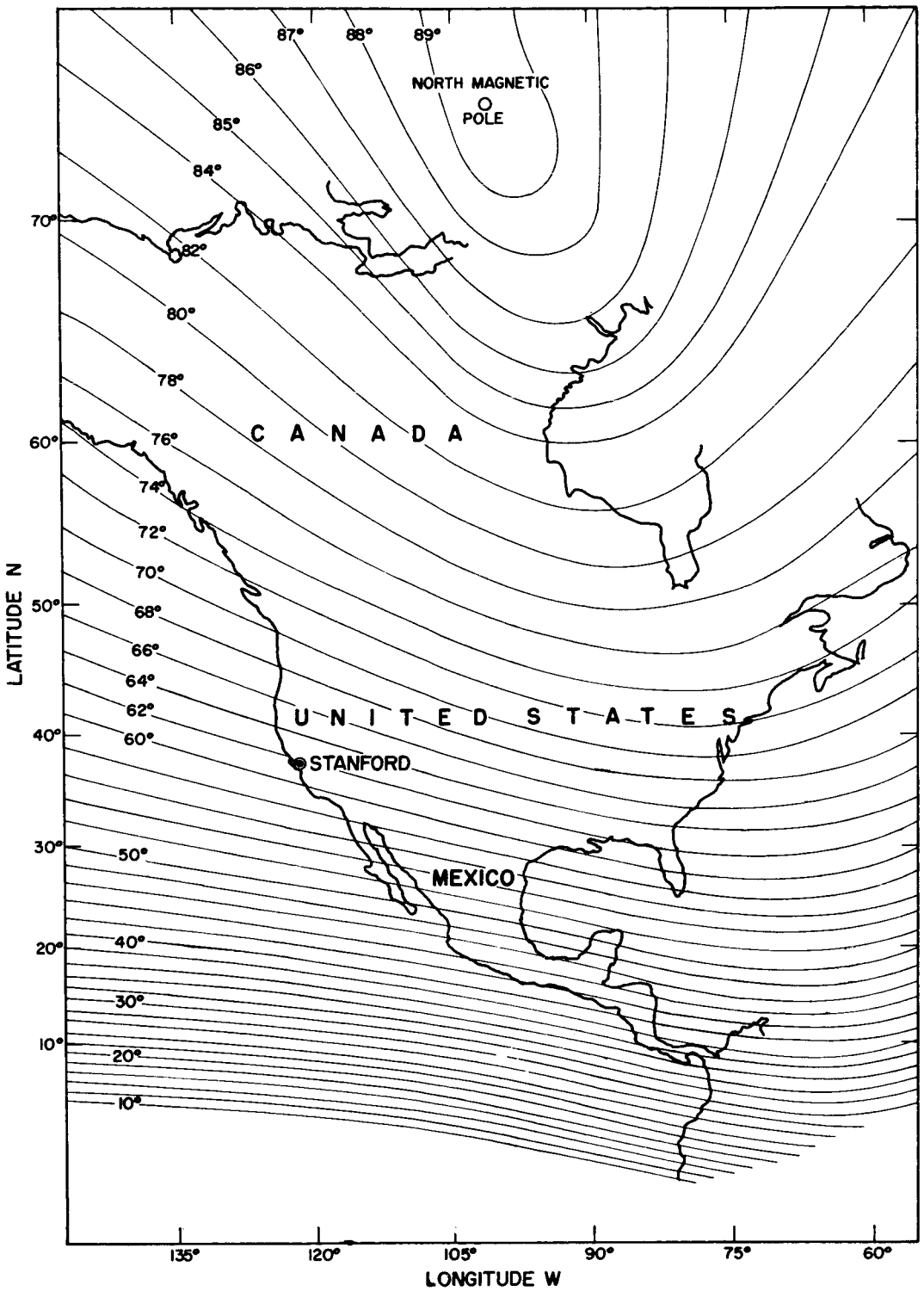

1b Map showing location of the telemetry station together with lines of constant magnetic dip angle.

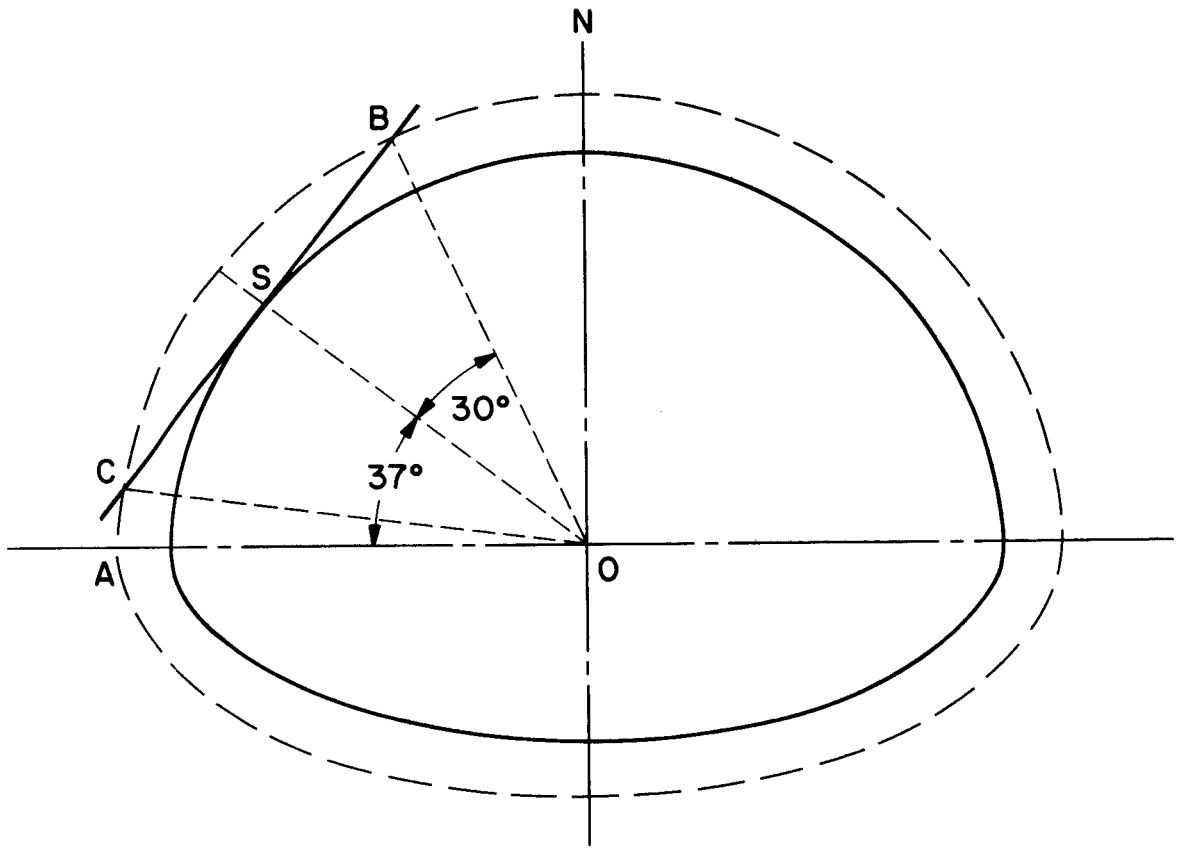

2a To illustrate, in perspective, the elevation of the tangent plane, CSB, through the location of Stanford, S, with a concentric sphere 1000 km above the earth.

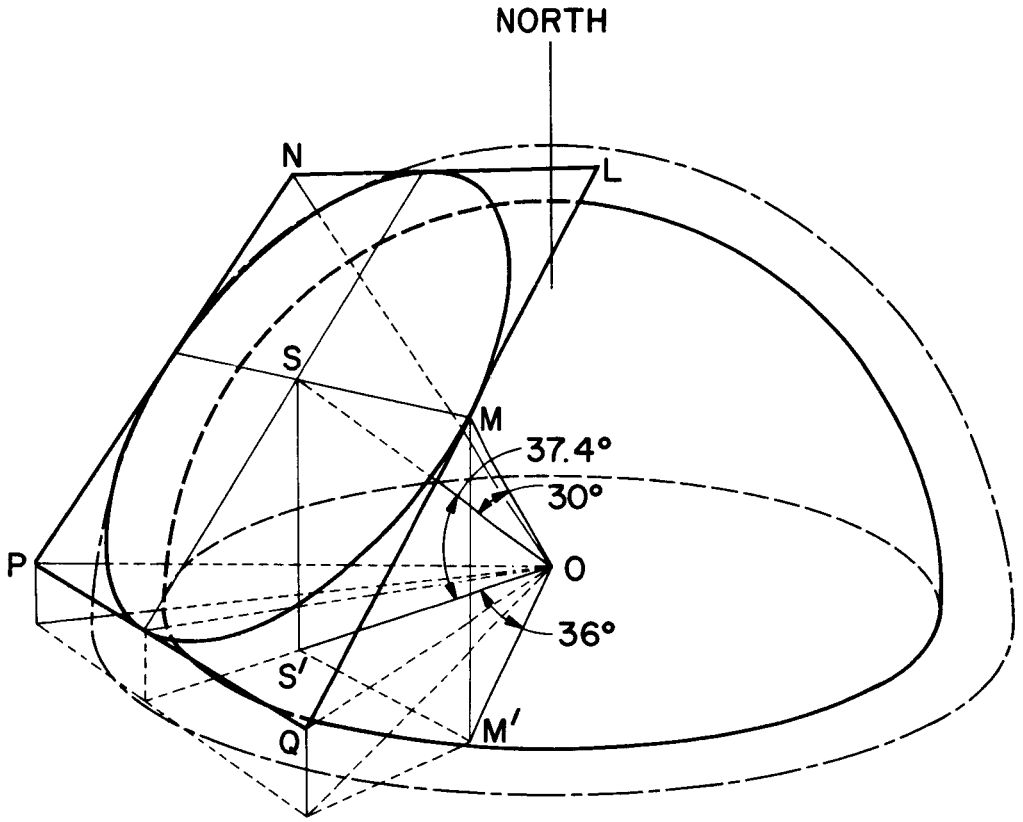

2b To illustrate the intersection of a tangent plane (LNPQ) through the location of Stanford, S, with a concentric sphere 1000 km above the earth. The equation of the plane LNPQ is

$$\cos\theta \cos\theta_o \cos(\phi - \phi_o) + \sin\theta \sin\theta_o = r/p$$

where

θ_o and ϕ_o are the geographic latitude and longitude of the point S, θ and ϕ are the geographic latitude and longitude west of a point on the plane distance p from the center of the earth and r is the radius of the earth. The equation of the cone is given by $r/p = \cos 30°$

so that

$$\cos\theta \cos\theta_o \cos(\phi - \phi_o) + \sin\theta \sin\theta_o = \cos 30°$$

For Stanford, $\theta_o = 37.4°$ and $\phi_o = 122.2°$.

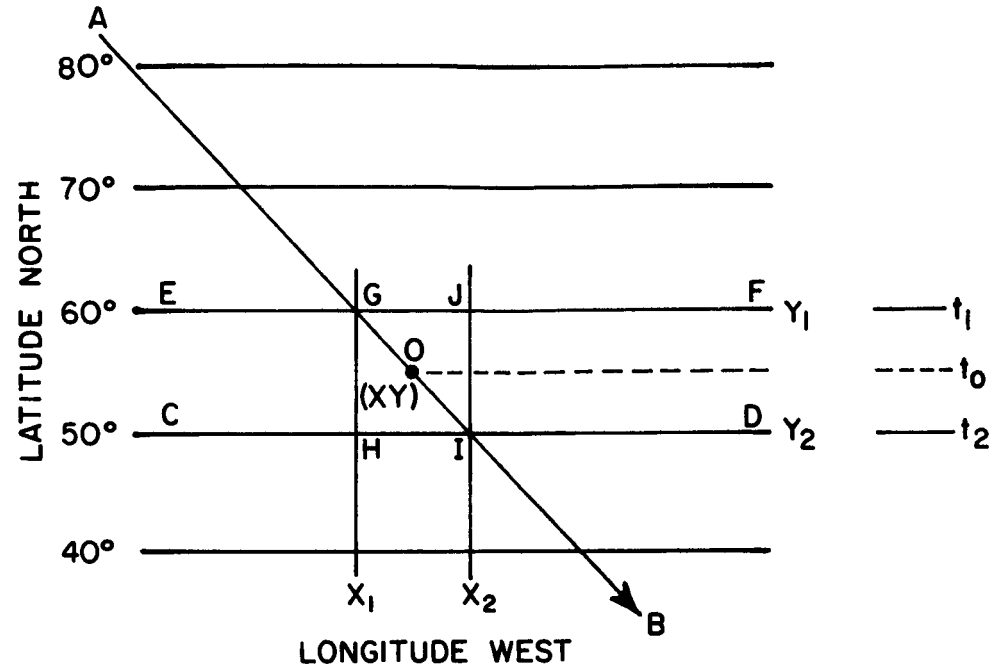

3a To illustrate the determination of the position of the satellite for a north-south pass.

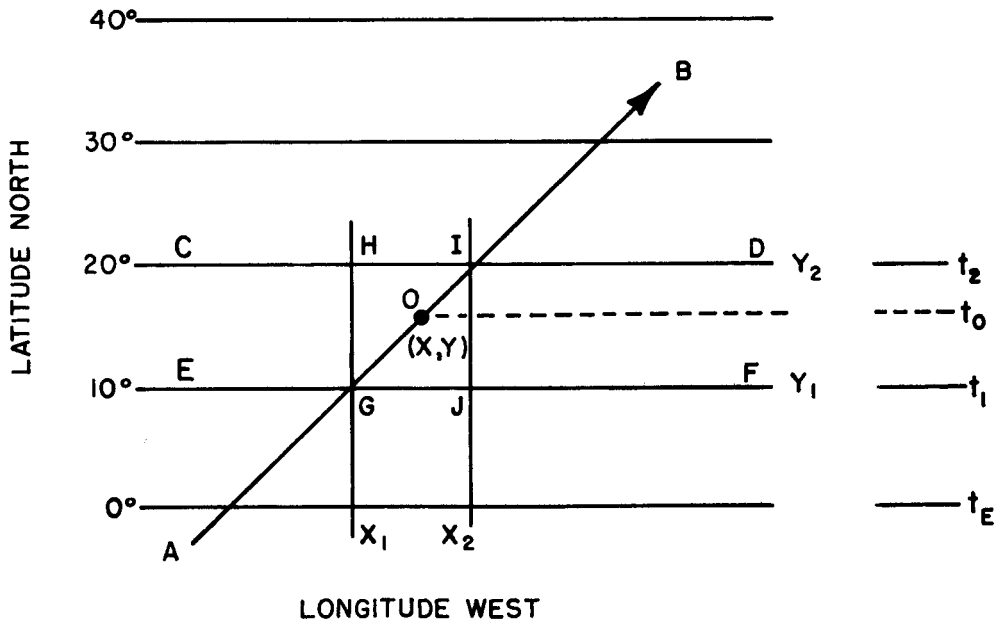

3b To illustrate the determination of the position of the satellite for a south-north pass.

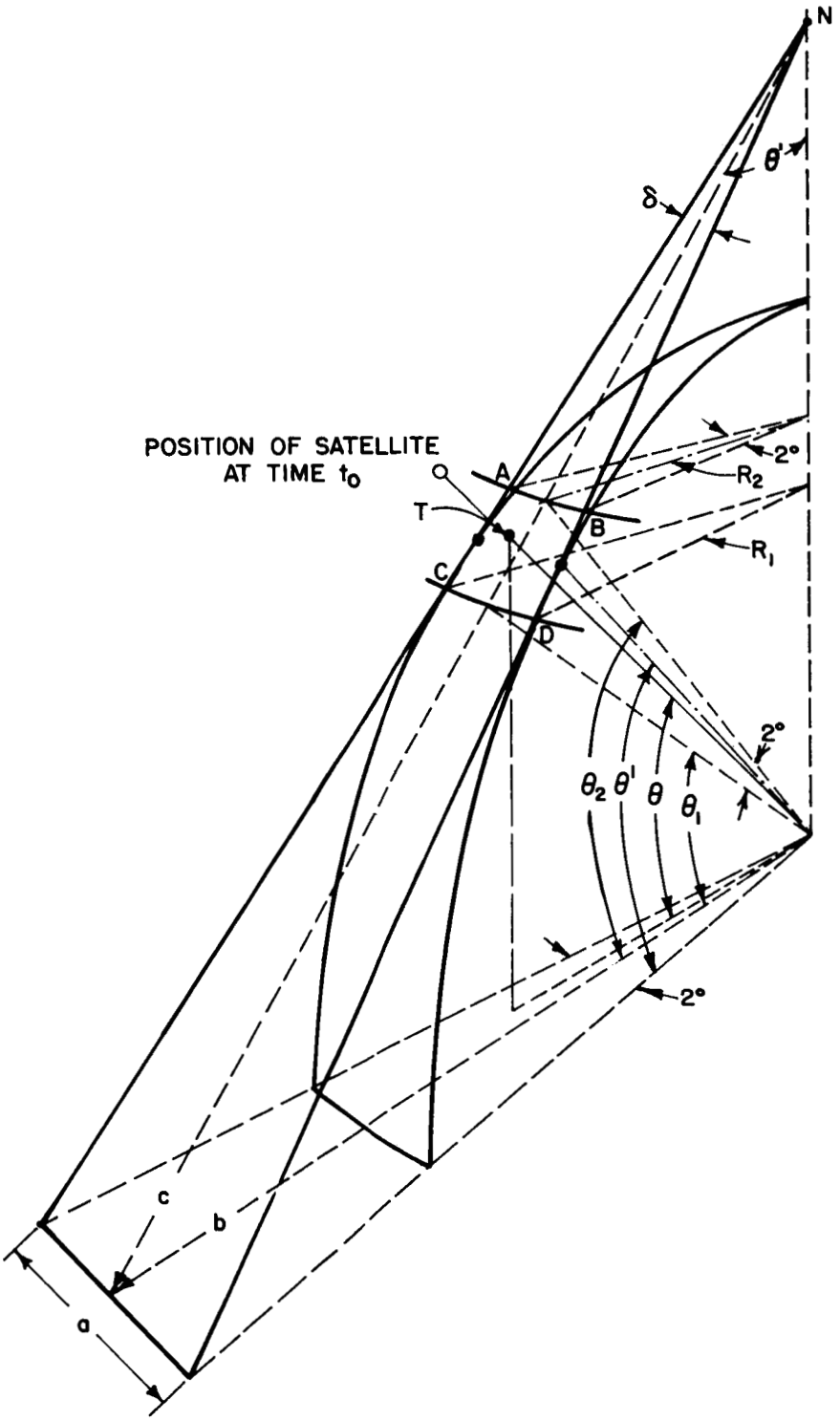

4 To illustrate the convergence of the meridians AC, BD at latitudes between θ_1 and θ_2. The latitude-longitude grid ABCD is used for the determination of the magnetic field parameters at the vehicle.

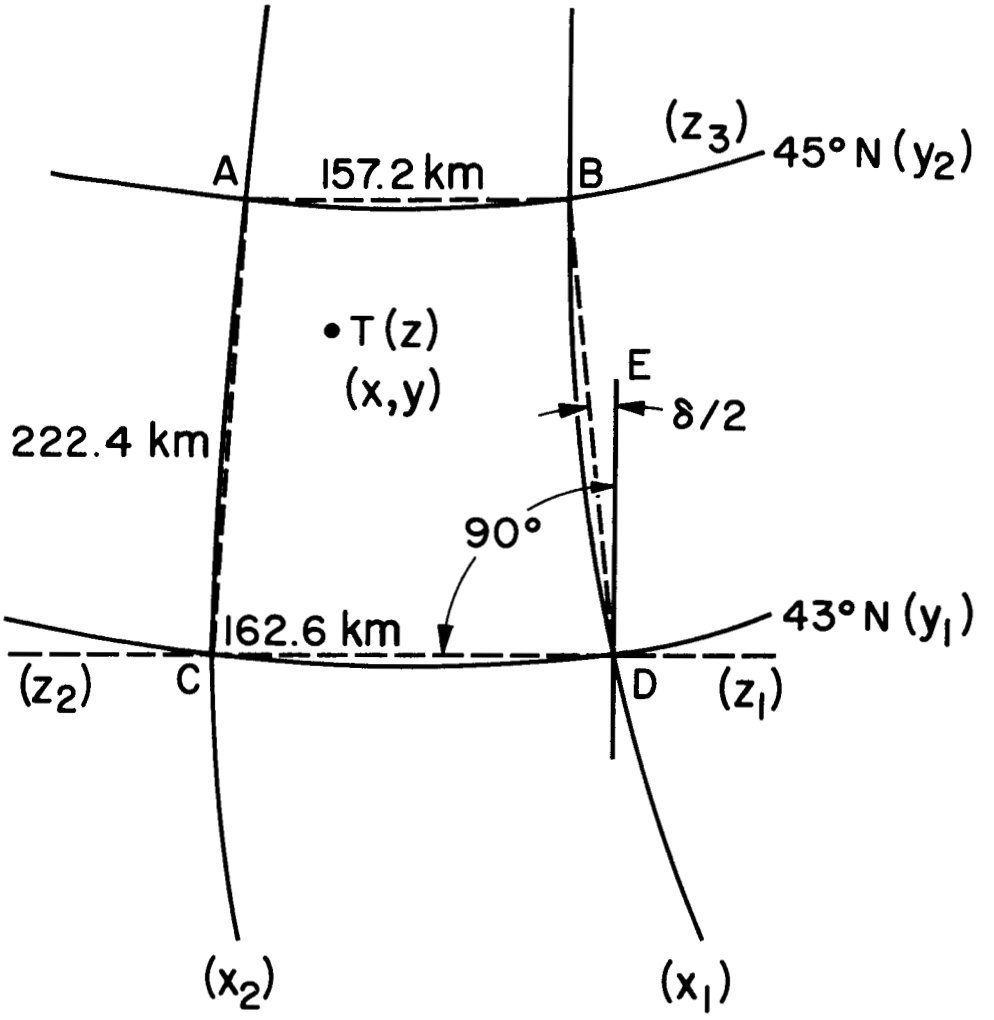

5 The portion ABCD of the grid shown in Figure 4 on an enlarged scale. The dimensions of the trapezium ABCD are computed in Appendix B for a latitude-longitude grid corresponding to $\theta_1 = 43°$ and $\theta_2 = 45°$. The line DE lies in the plane ABCD.

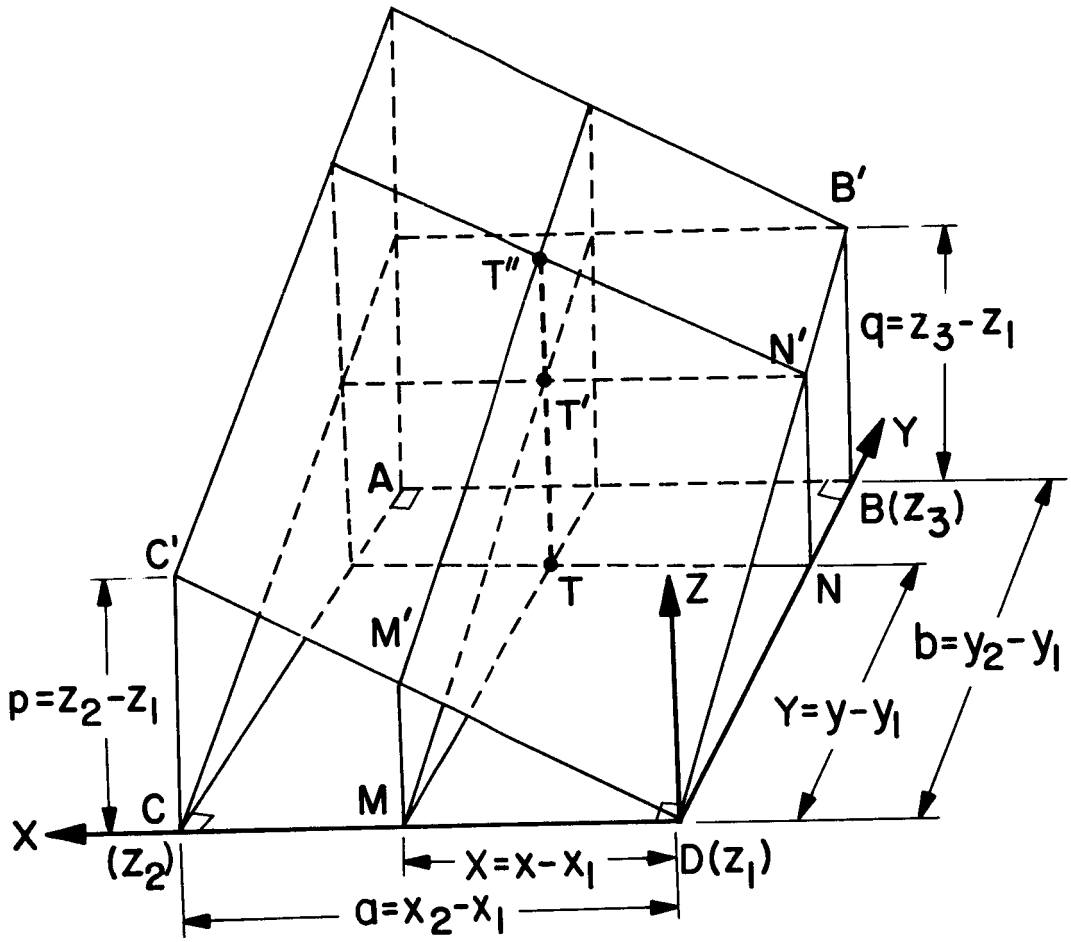

6 To illustrate the calculation of the magnetic field parameters at the sub-satellite point, T. In this diagram, the points ABCD of Figures 4 and 5 are redrawn at the corners of a rectangle.

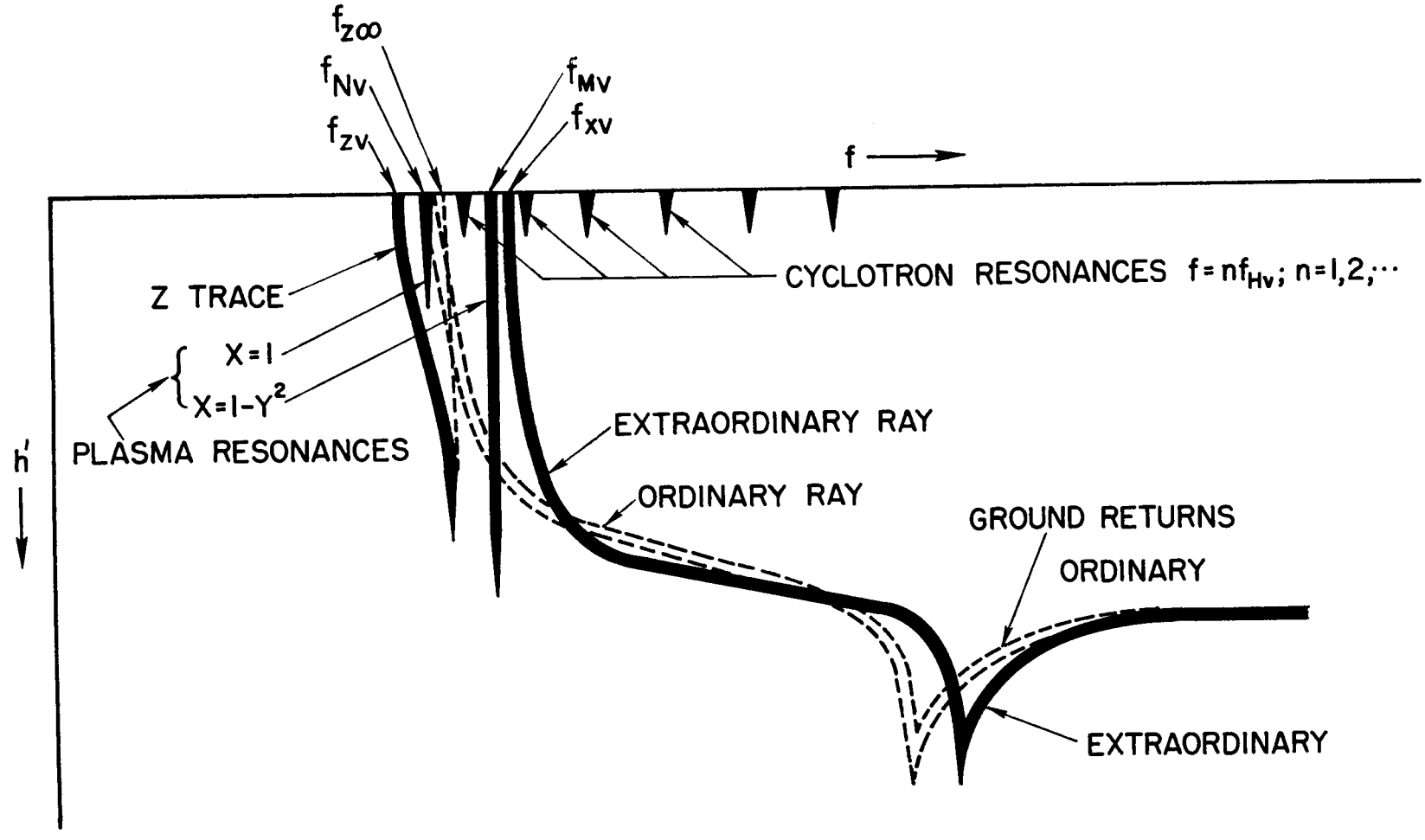

7 Schematic diagram to illustrate the nomenclature used to describe features observed on topside ionograms.

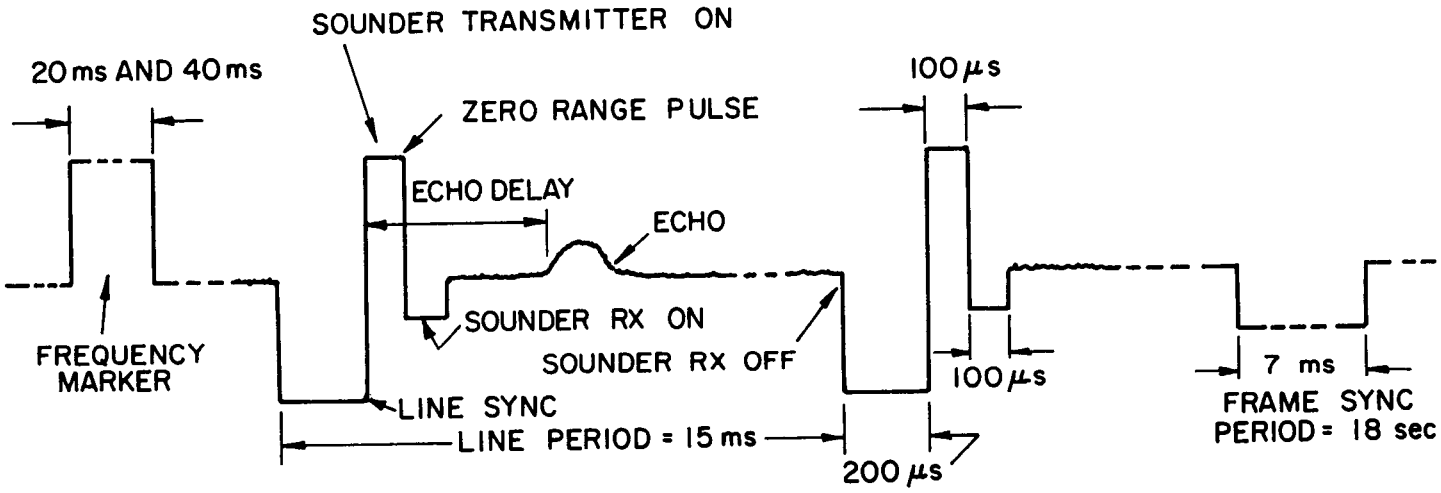

8 Alouette video format. (Courtesy NASA).

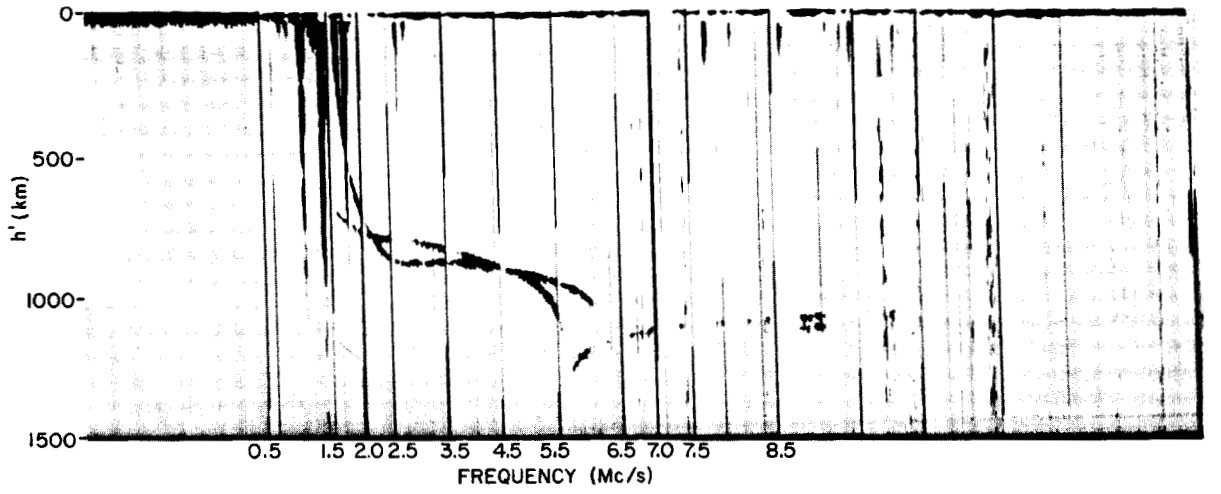

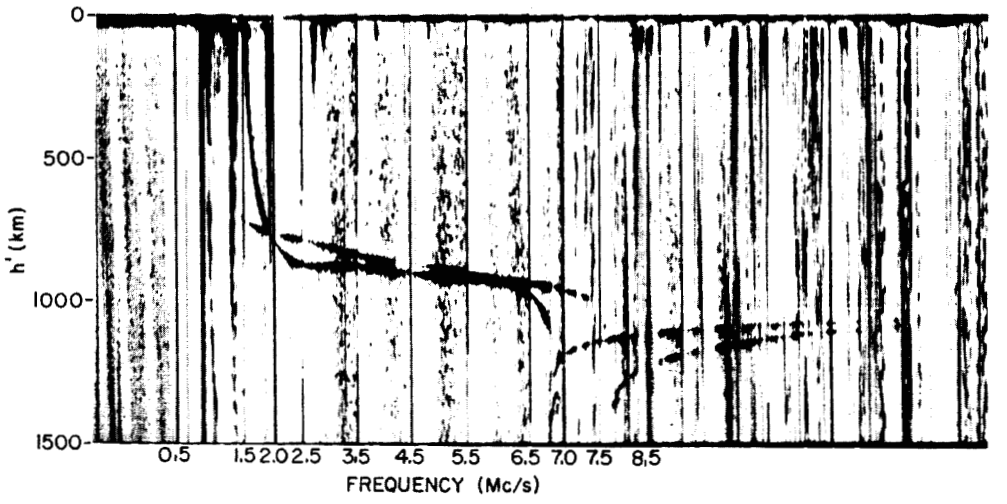

9
10 Daytime topside ionograms. Note topside reflected rays and ground returns. The plasma resonances (or spikes) are also clearly visible, as are the cyclotron harmonics.

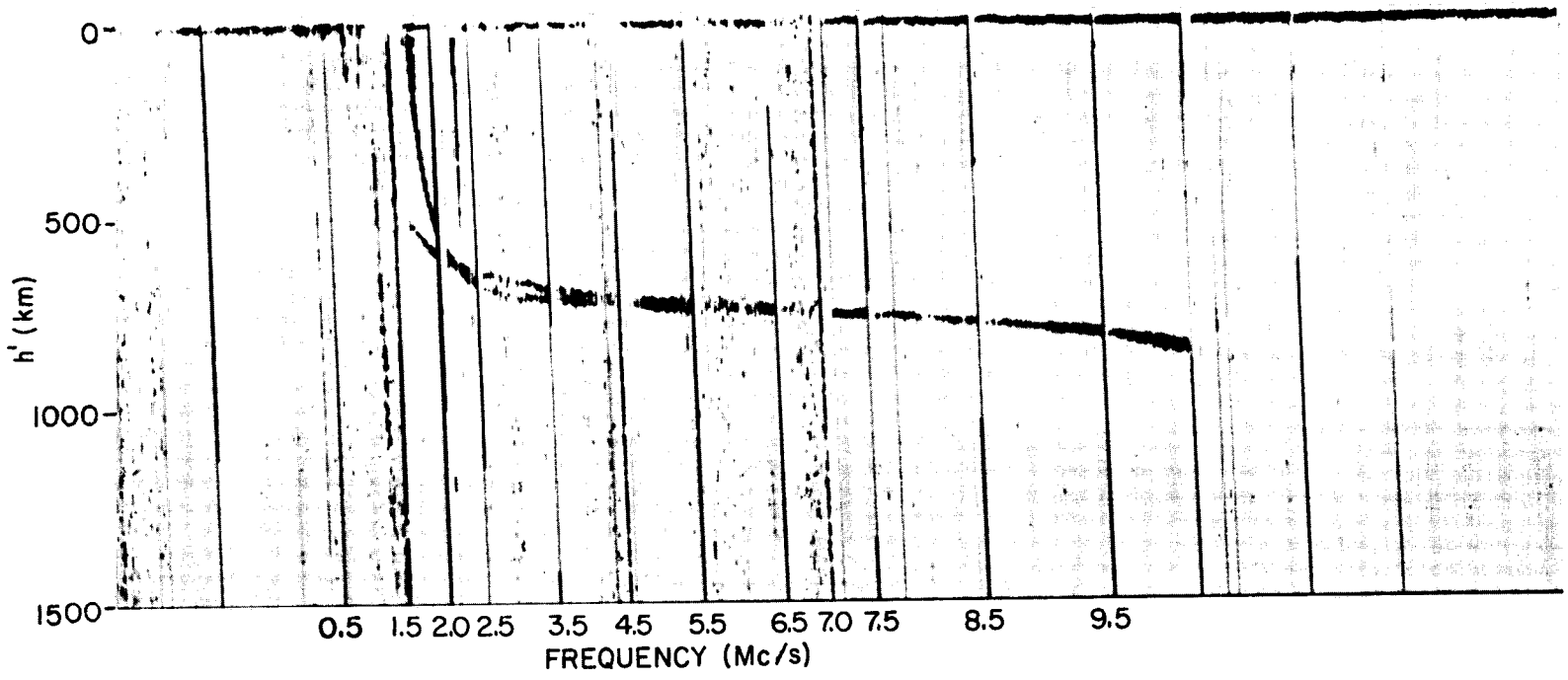

11 Daytime topside ionogram. F2 layer critical frequency not observed (> 10.5 Mc/s).

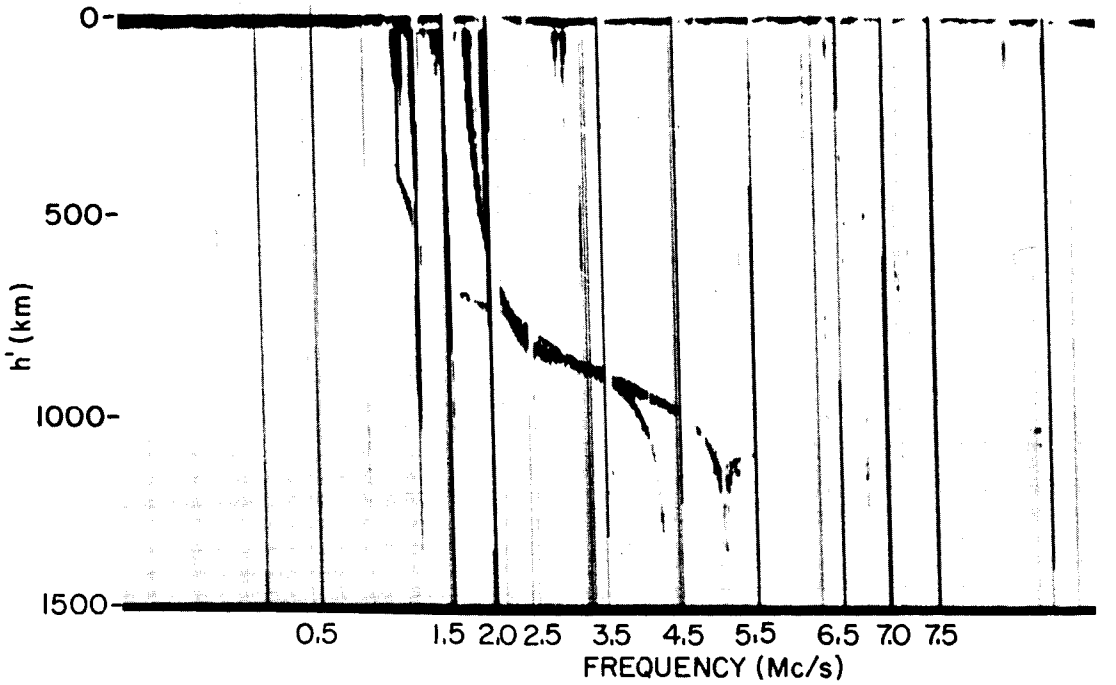

12 Day-night transition type ionogram. Note clear Z trace.

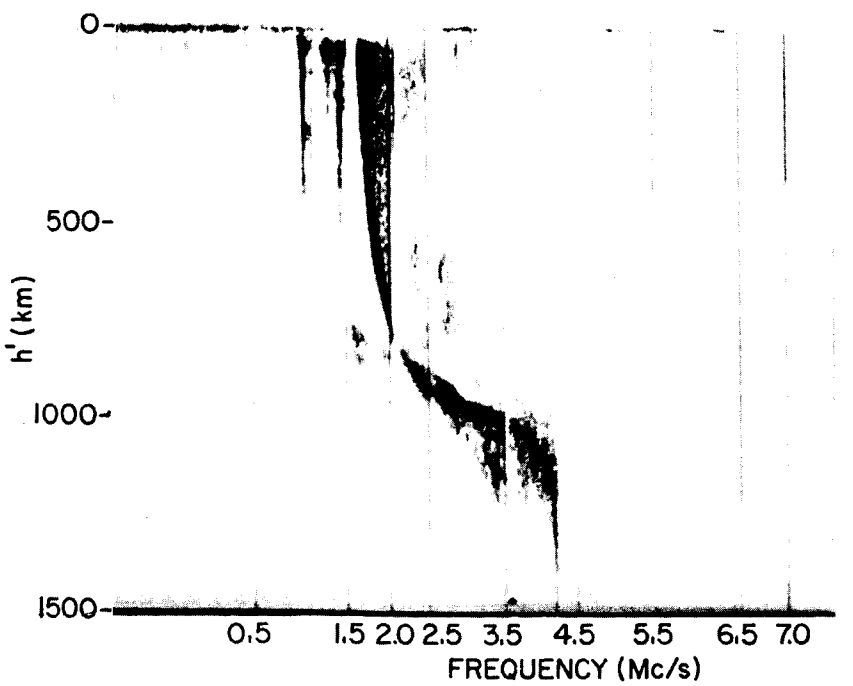

13 Day-night transition type ionogram. Note spread F echoes.

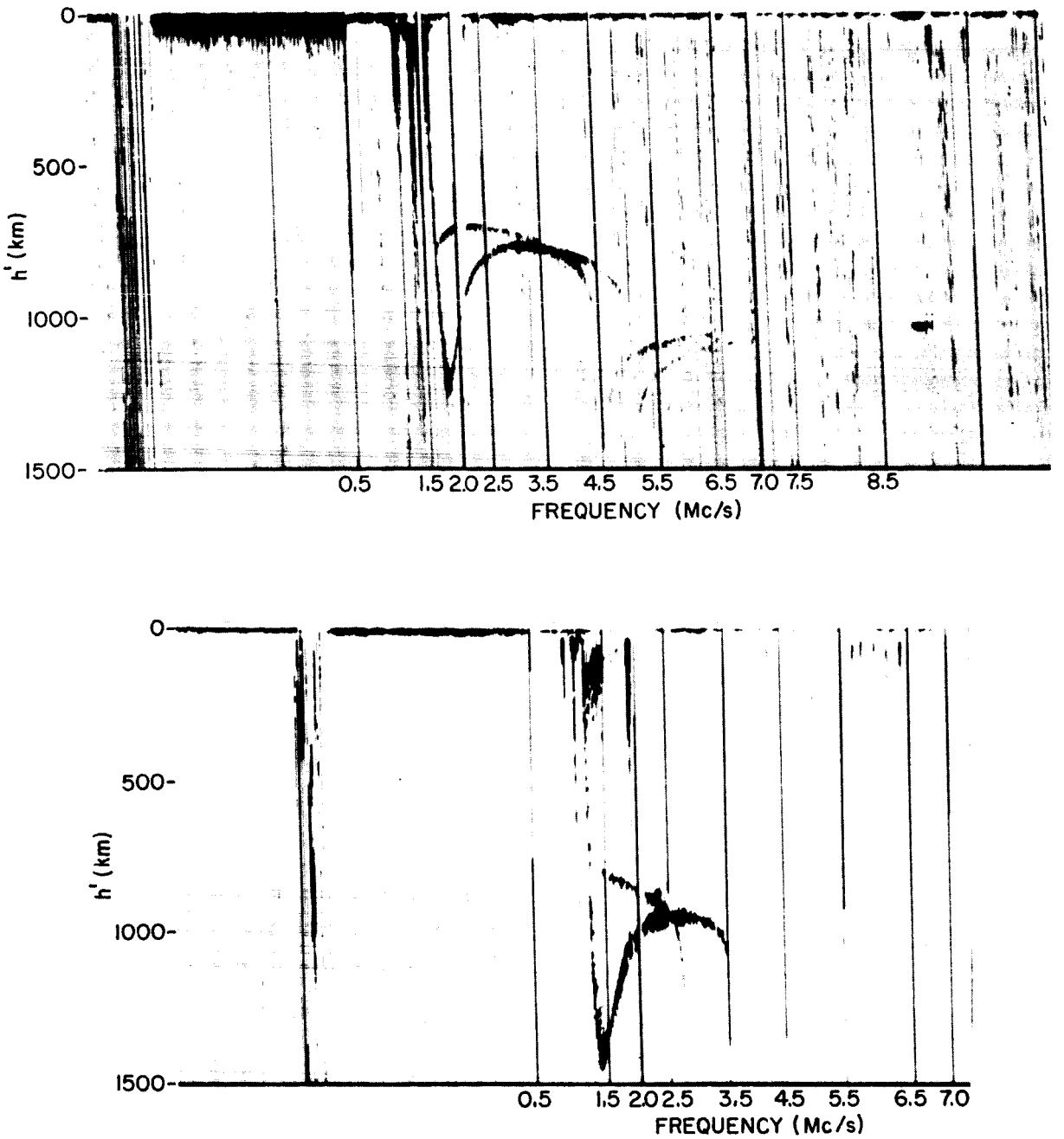

14
15 Examples of nighttime ionograms.

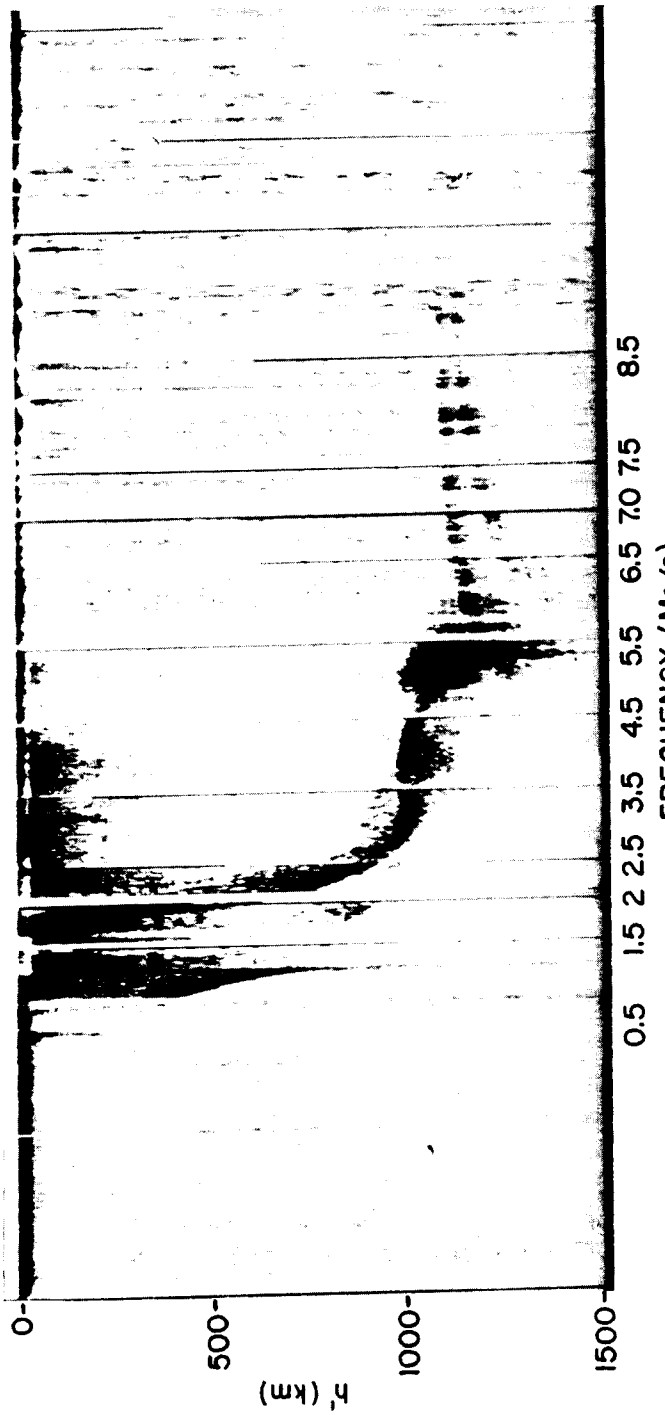

16 Topside ionogram showing spread F.

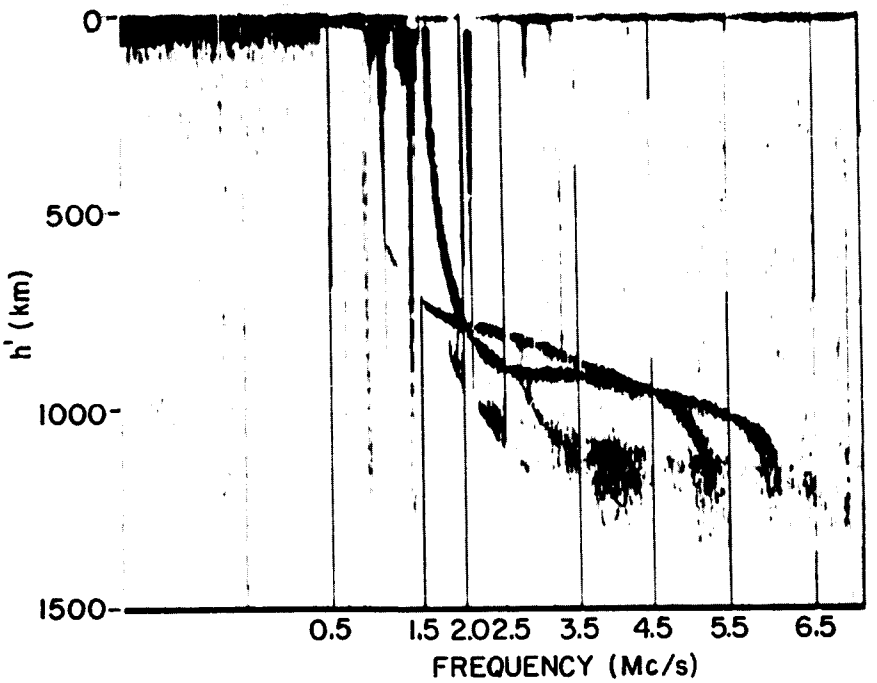

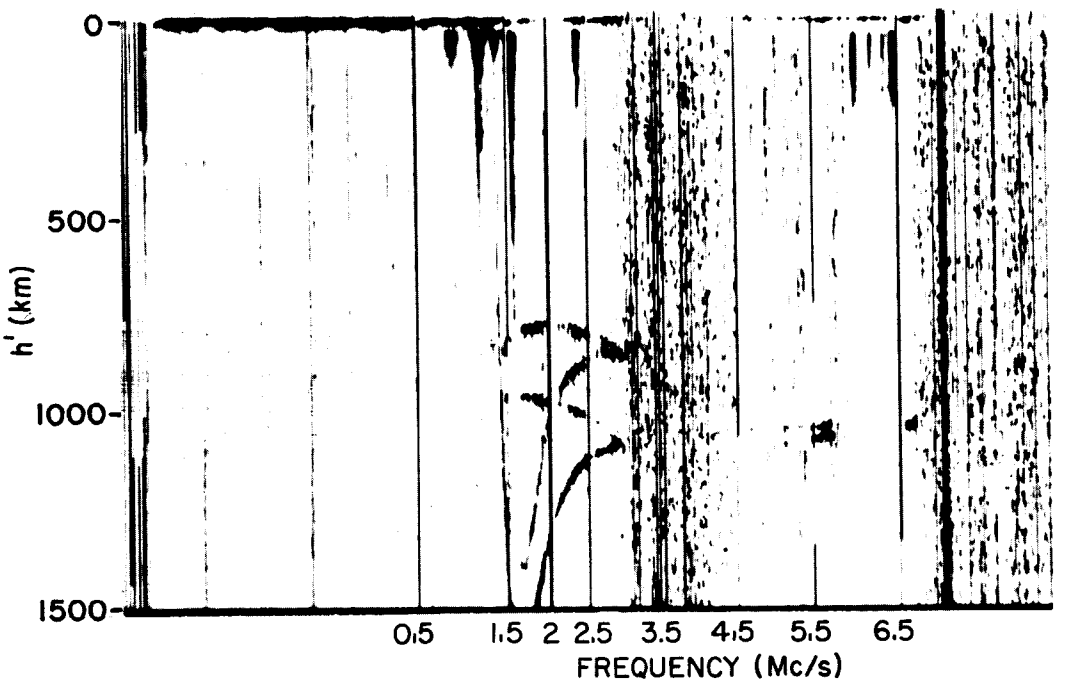

17
18 Topside ionograms showing multiple traces.

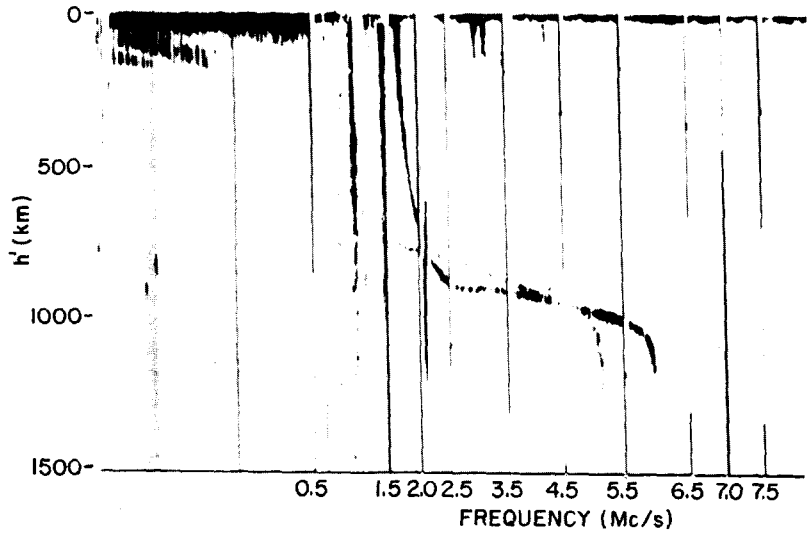

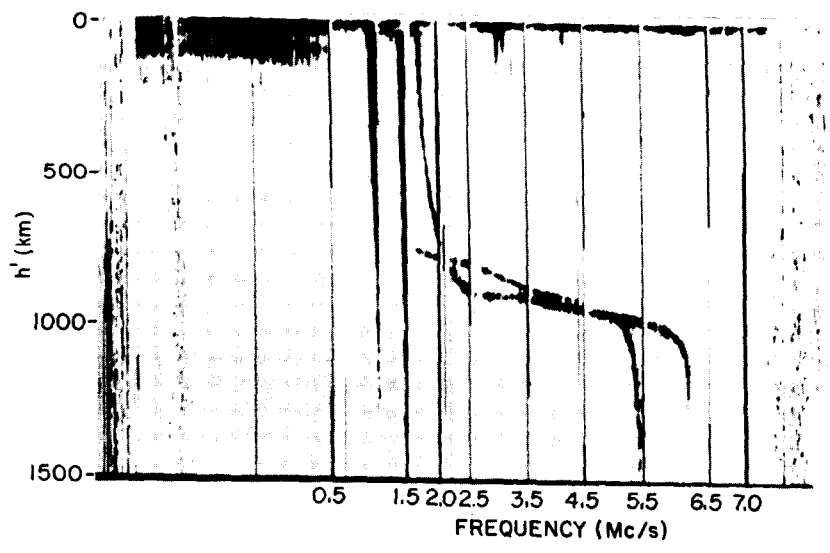

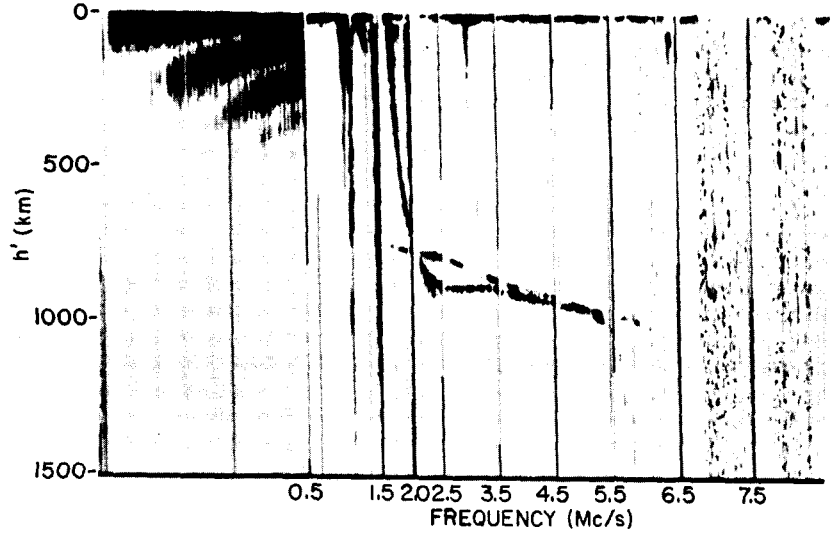

19 Topside ionograms taken approximately two minutes
20 apart on the same pass. Note serrated appearance
21 of resonances and the apparent reception of signals at low frequencies.

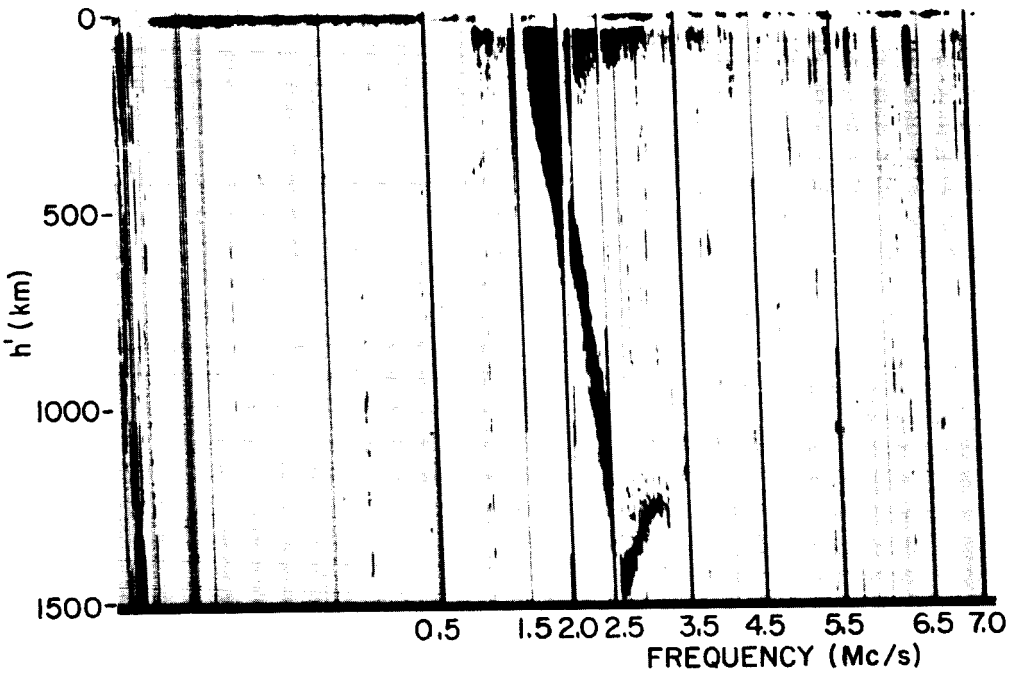

22 On this nighttime record, the curvature of the Extraordinary trace just below the cusp is in the opposite direction to that usually observed.

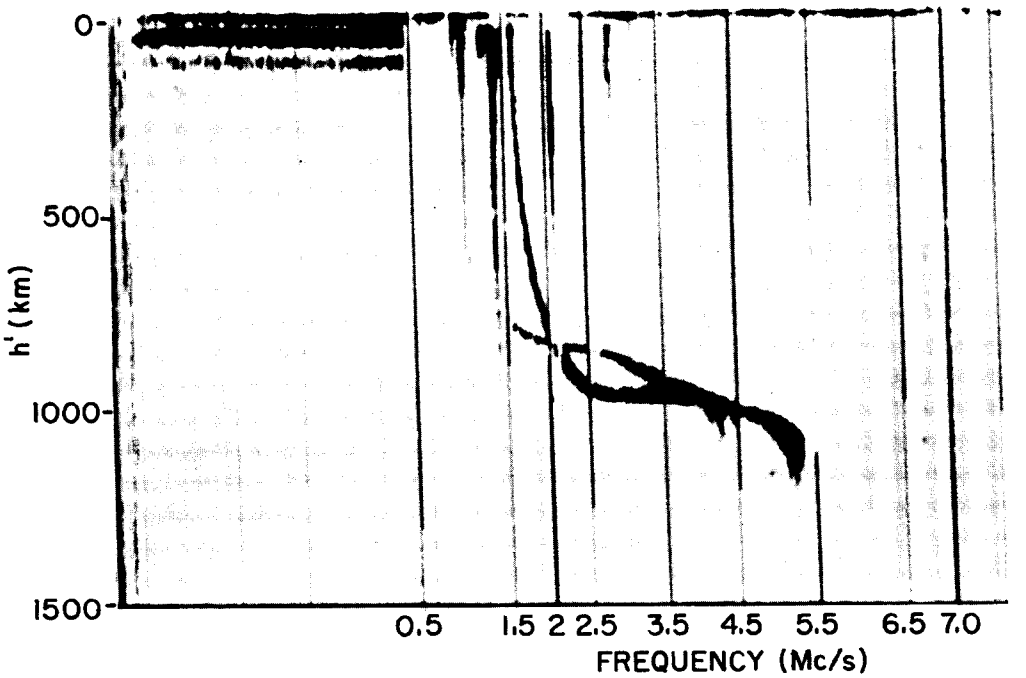

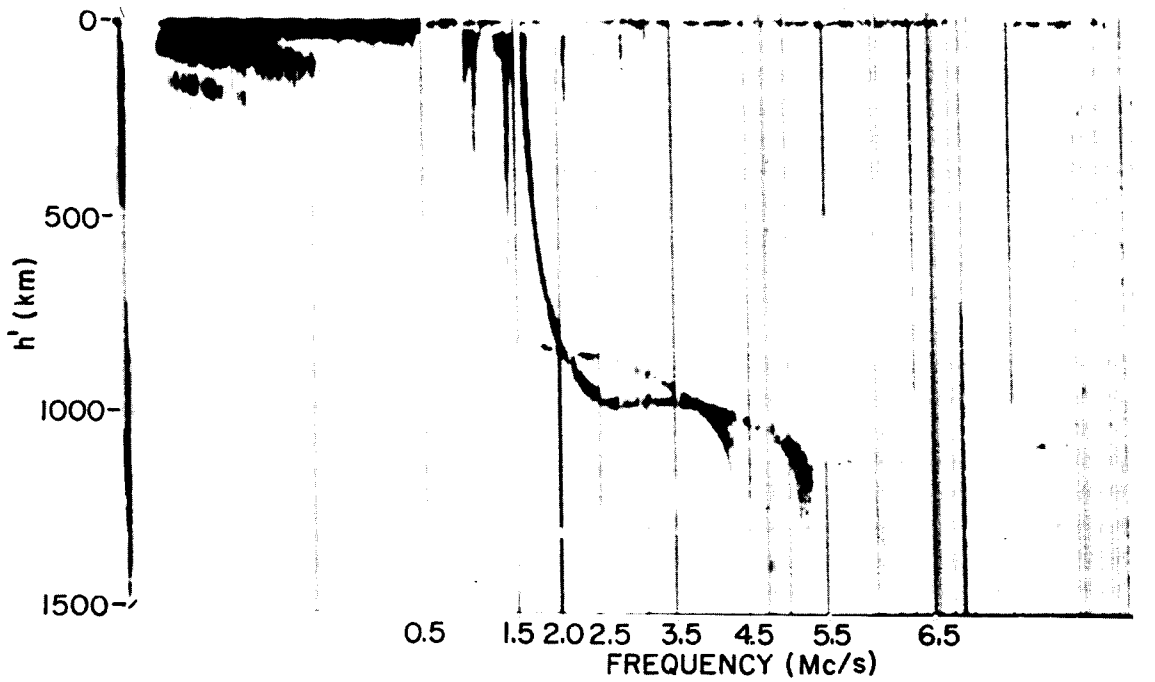

23
24 Further examples of records showing the apparent reception of signals at low frequencies.

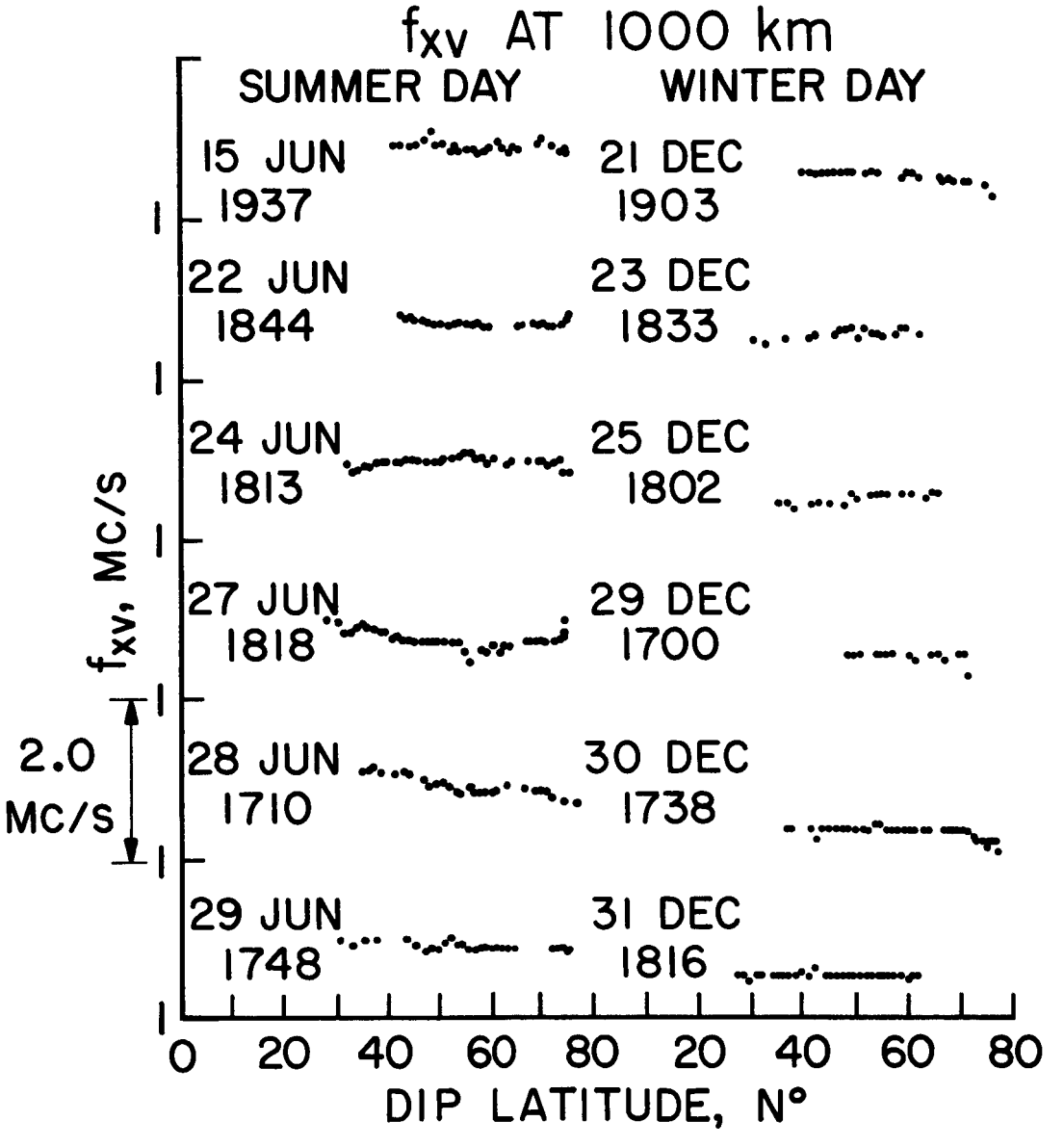

25a The variation with dip latitude of the frequency, f_{xv}, at which the Extraordinary trace has zero range, for a series of days in summer and in winter near local noon at the vehicle (June 1963 and December 1962). The numbers following the month shown on the diagram give the Greenwich Mean Time at the point of closest approach of the Alouette satellite to Stanford.

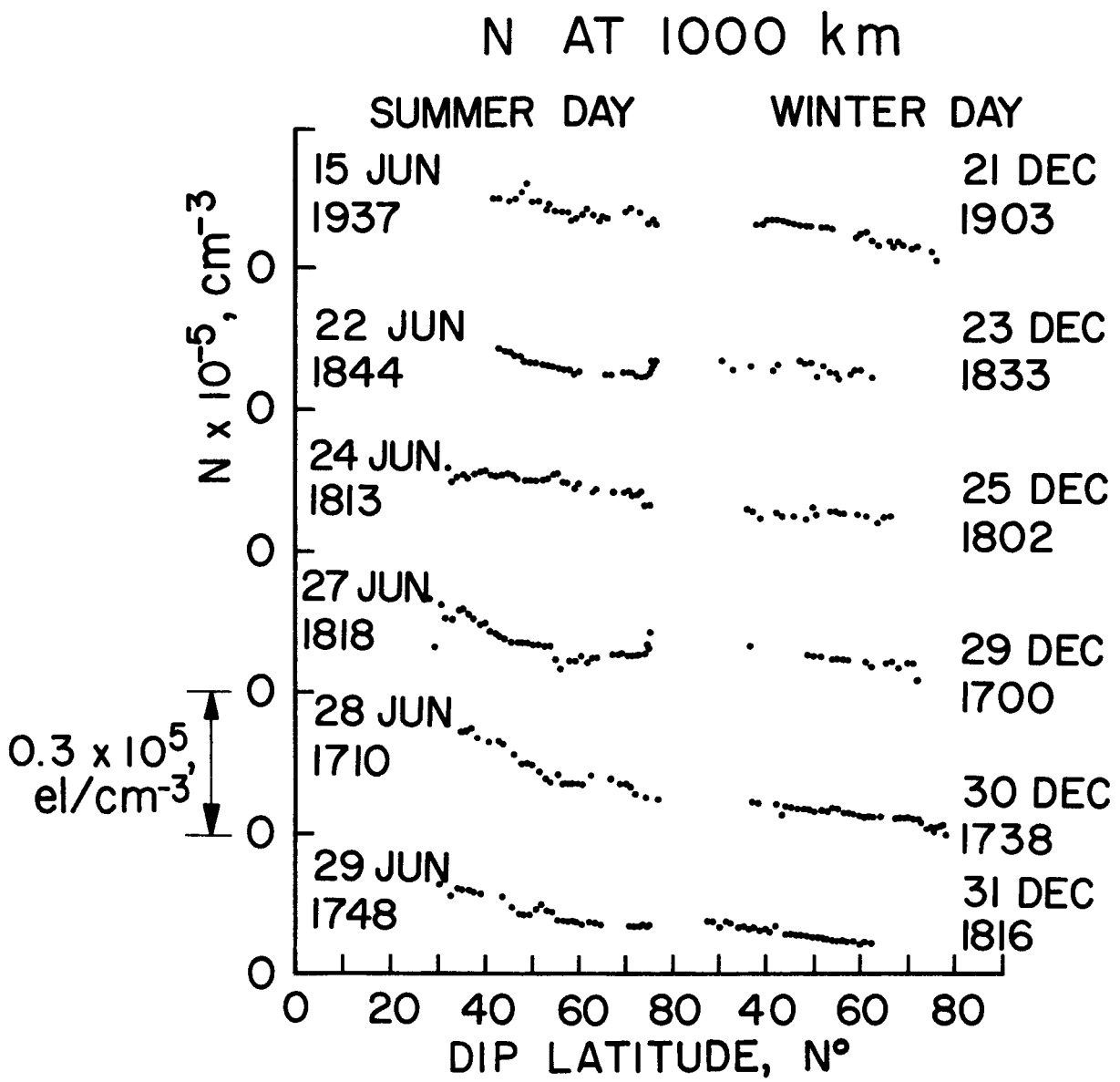

25b The variation with dip latitude of the mid-day electron density at 1000 kilometers deduced from the observational data plotted in the previous diagram (Fig. 25a) for a series of days in summer and in winter. The dates for each pass are shown together with the Greenwich Mean Time of the closest point of approach to Stanford of the Alouette satellite.

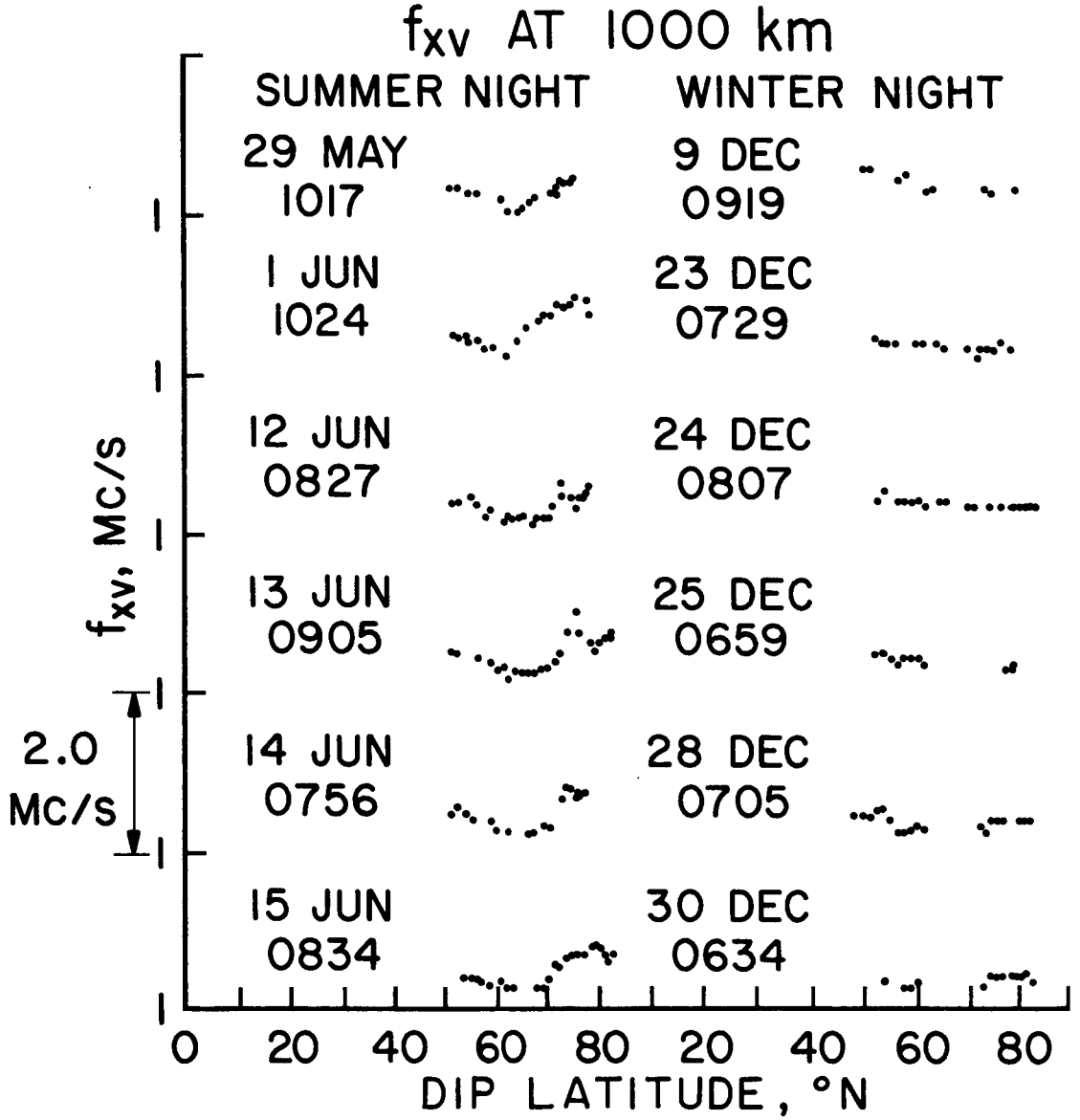

26a The variation with dip latitude of the frequency, f_{xv}, at which the Extraordinary trace has zero range, for a series of nights in summer and in winter near local midnight at the vehicle. The numbers following the month as shown on the diagram correspond to the Greenwich Mean Time at the point of closest approach of the Alouette satellite to Stanford. The results are for May and June 1963 and December 1962.

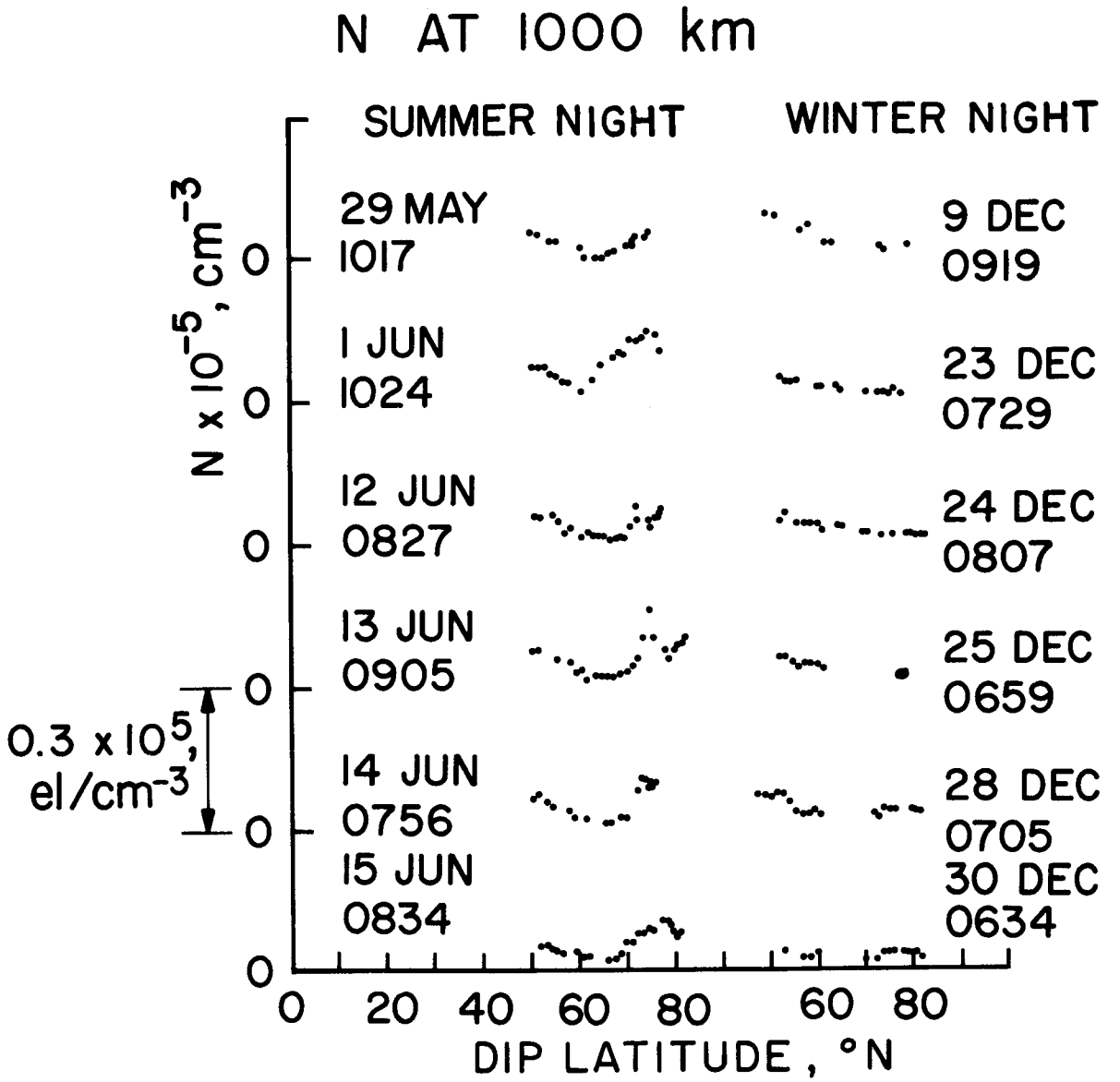

26b The variation with dip latitude of the midnight electron density at 1000 kilometers deduced from the observational data plotted in the previous diagram (Fig. 26a) for a series of nights in summer and in winter. The dates for each pass are shown together with the Greenwich Mean Time of the point of closest approach to Stanford of the Alouette satellite.

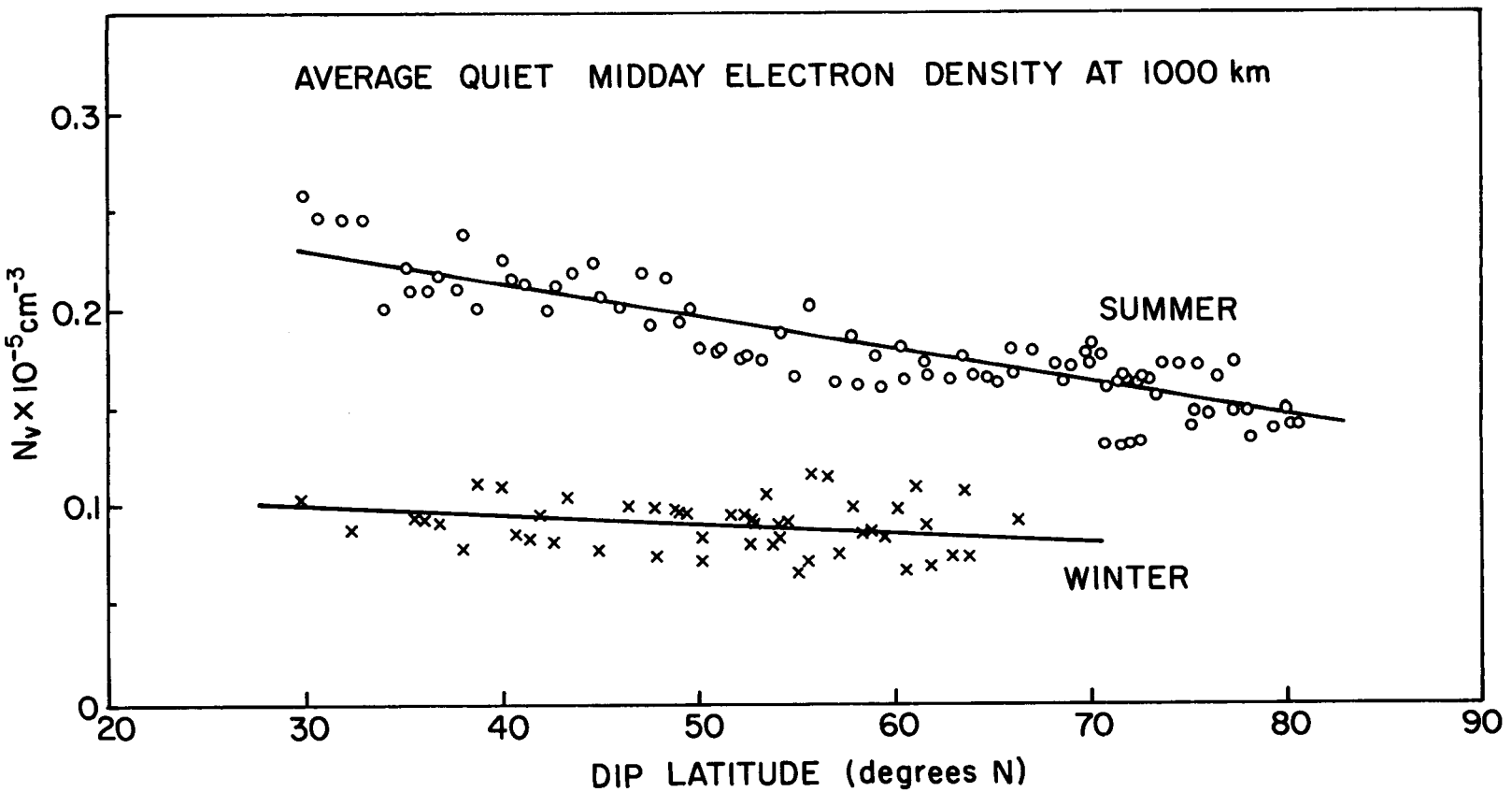

27 The average variation with dip latitude of the electron density near noon at 1000 kilometers for International Quiet Days in summer and winter. The results are for quiet days in January, May, June and July 1963, and for December 1962.

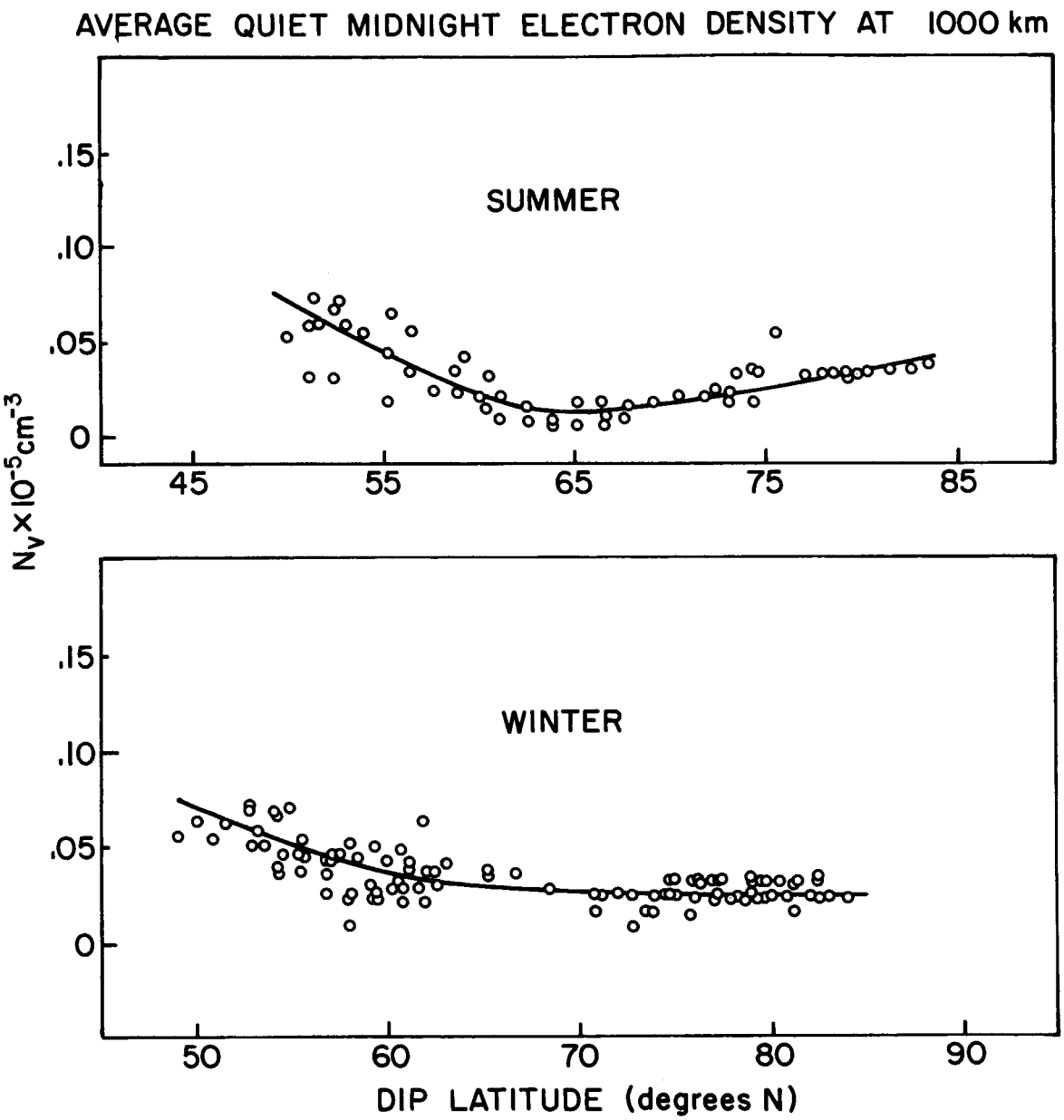

28 The average variation with dip latitude of the electron density near midnight at 1000 kilometers for International Quiet Days in summer and winter. The results are for quiet days in January, May, June and July 1963, and December 1962.

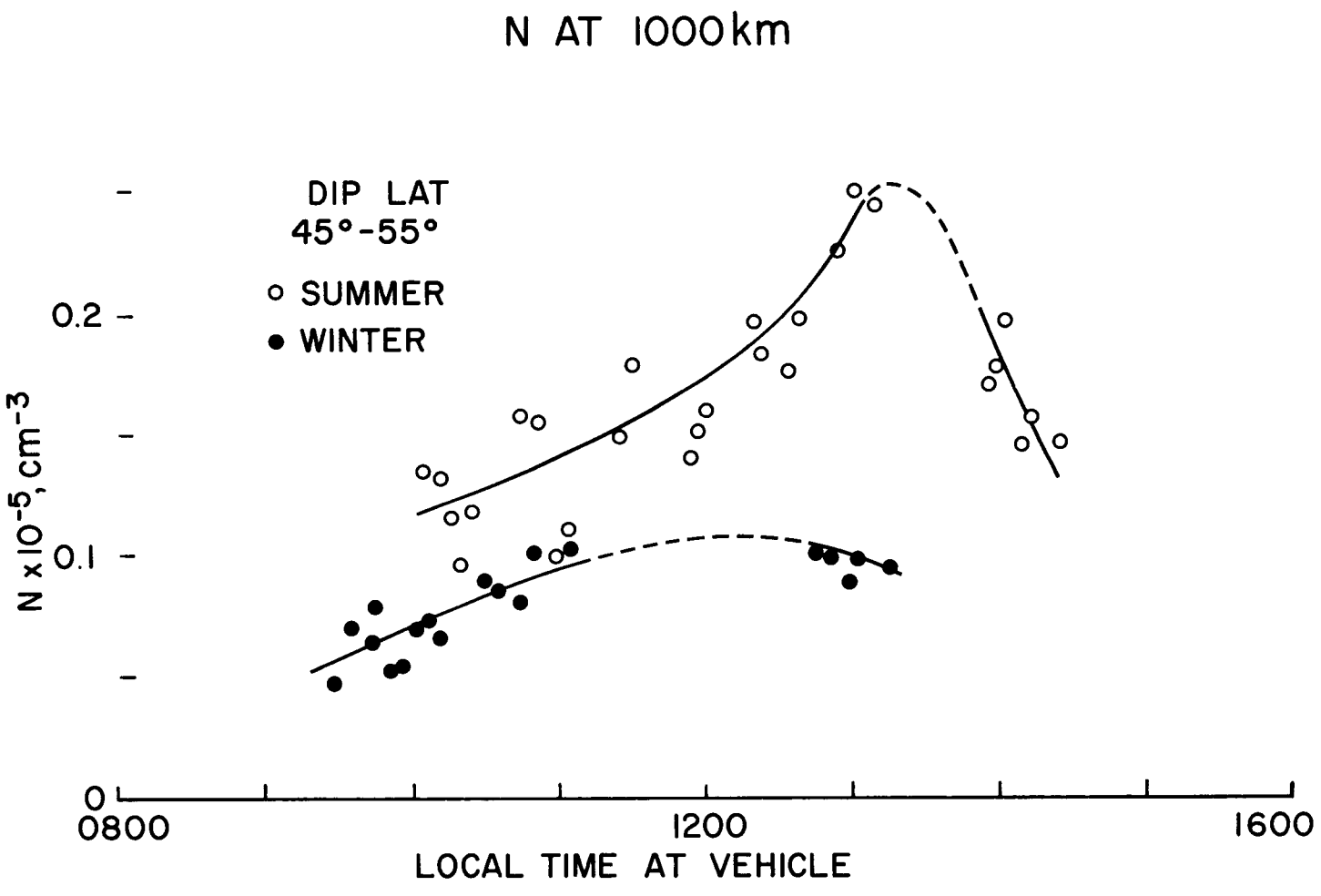

29 The variation with local time at the vehicle near noon of the electron density at 1000 kilometers over the range of dip latitudes, 45° to 55° North for a series of days in summer (circles) and in winter (dots).

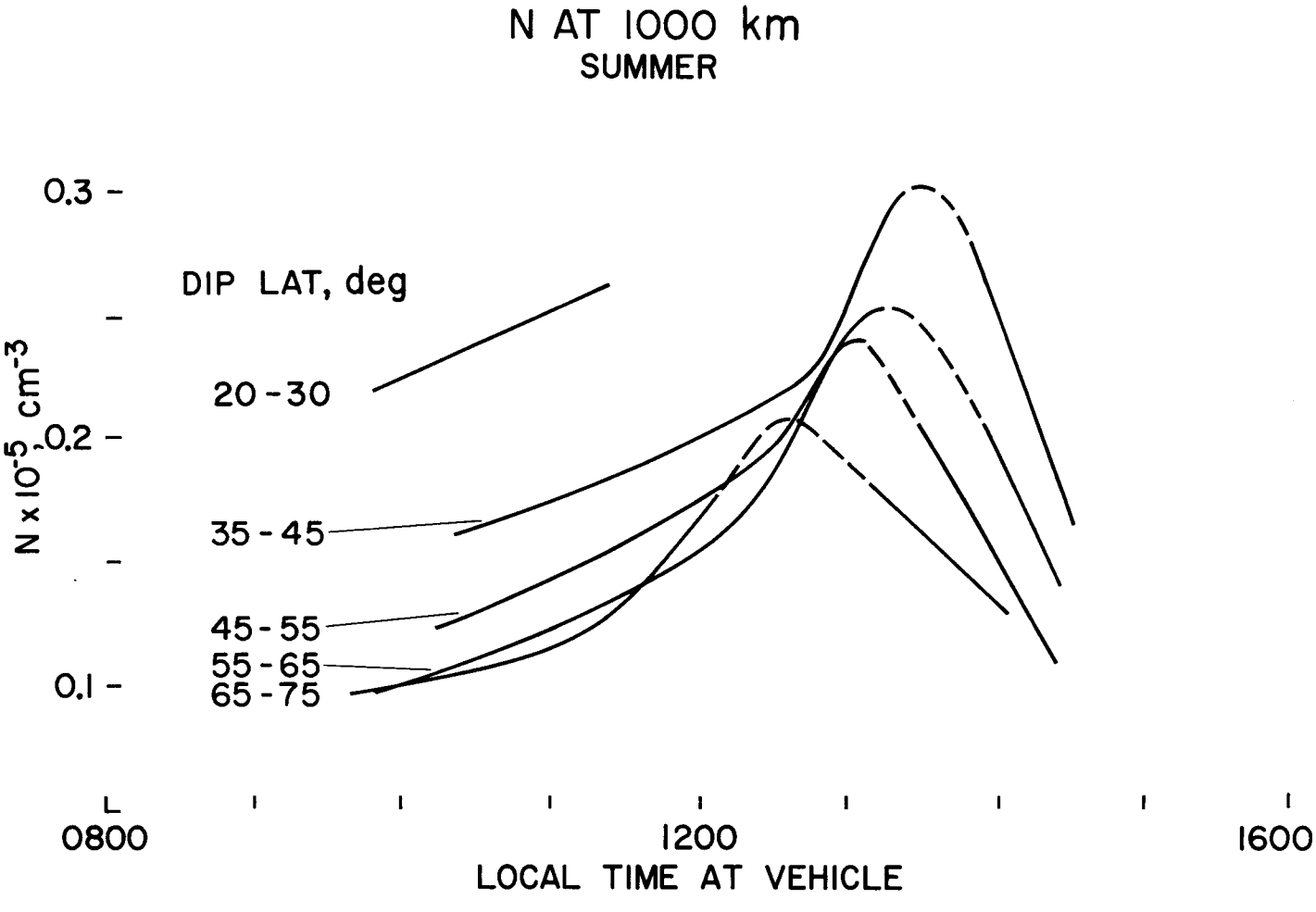

30 The variation with local time at the vehicle during the day of electron density at 1000 kilometers for a series of latitude ranges in summer (1963).

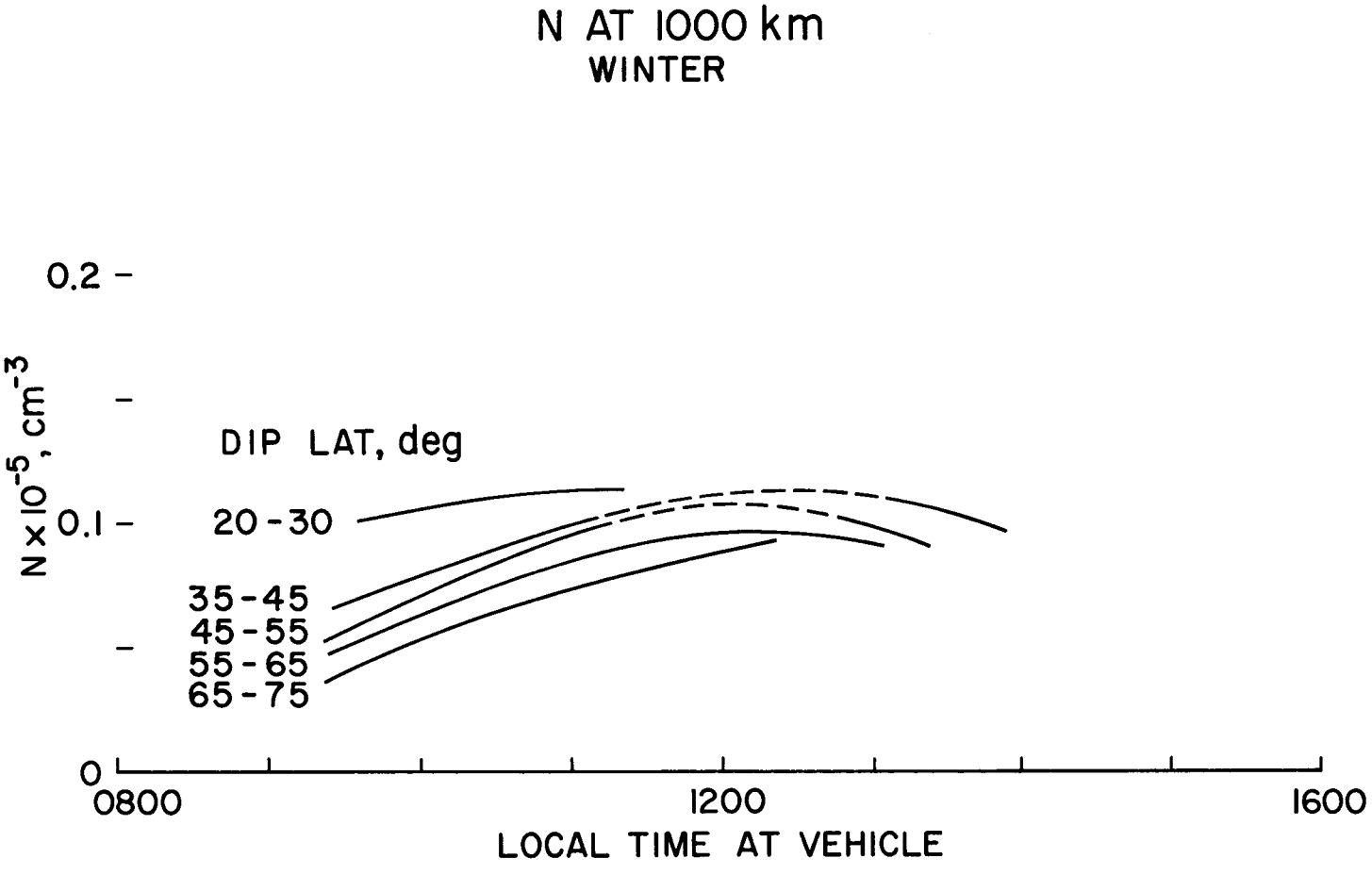

31 The variation with local time at the vehicle during the day of electron density at 1000 kilometers for a series of latitude ranges in winter (1962-3).

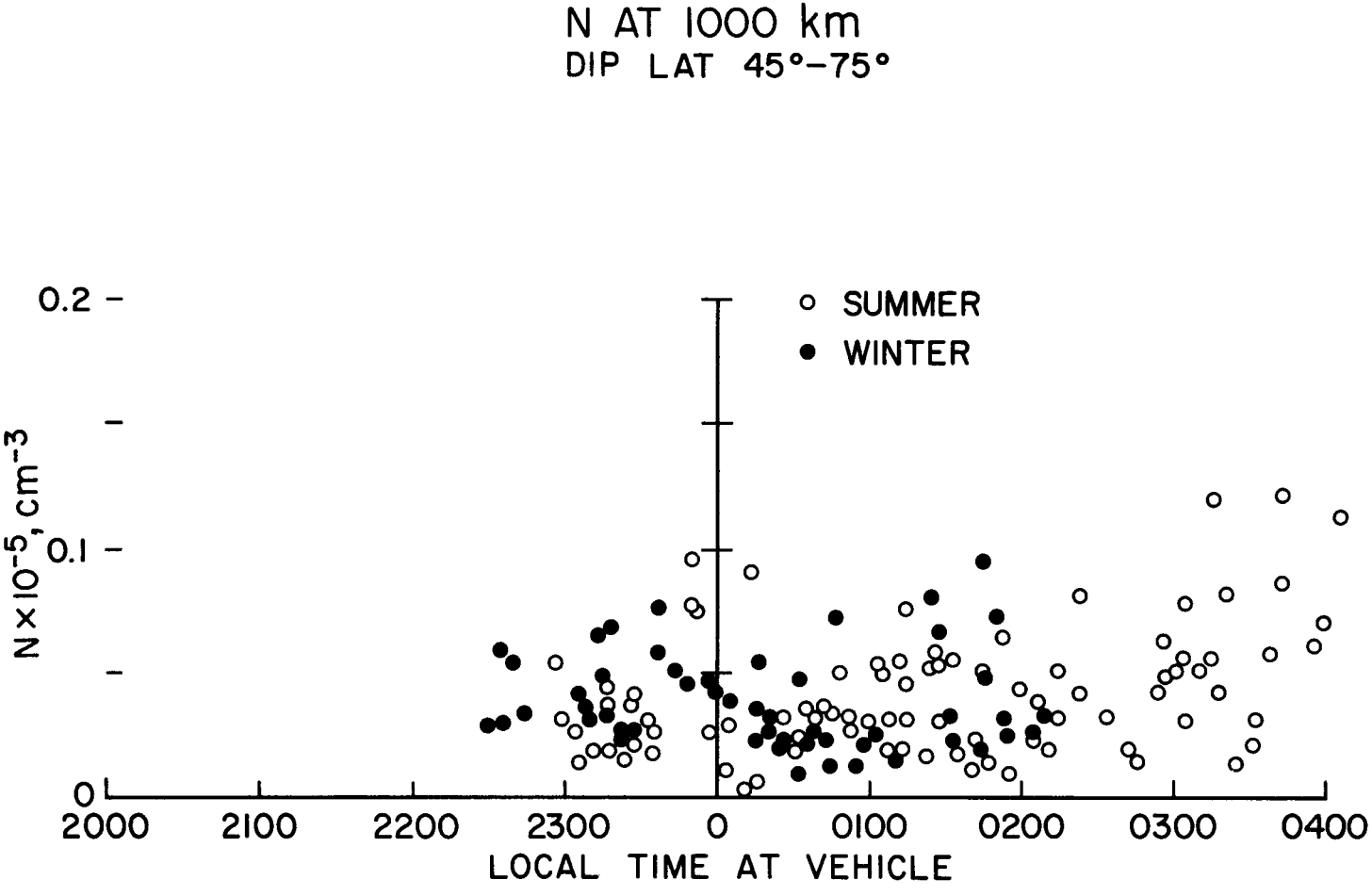

32 The nighttime electron density at 1000 kilometers over the range 45° to 75° North geomagnetic latitude in summer (circles) and in winter (dots). The electron density is shown as a function of local time at the vehicle. The results are for 1962-3.

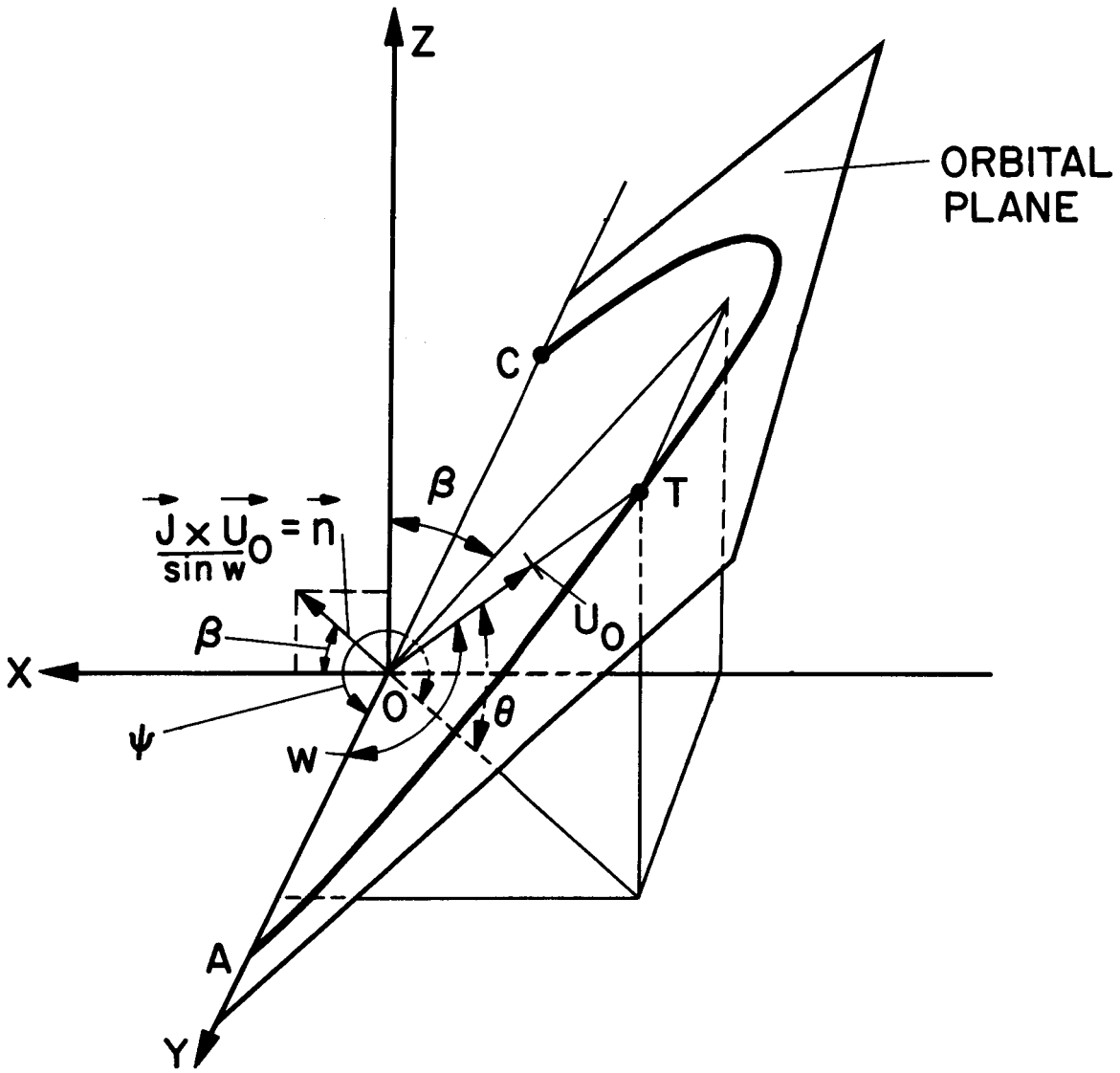

A.1 The trajectory of the Alouette satellite over a latitude range of 10° is assumed to be in the plane ATC.

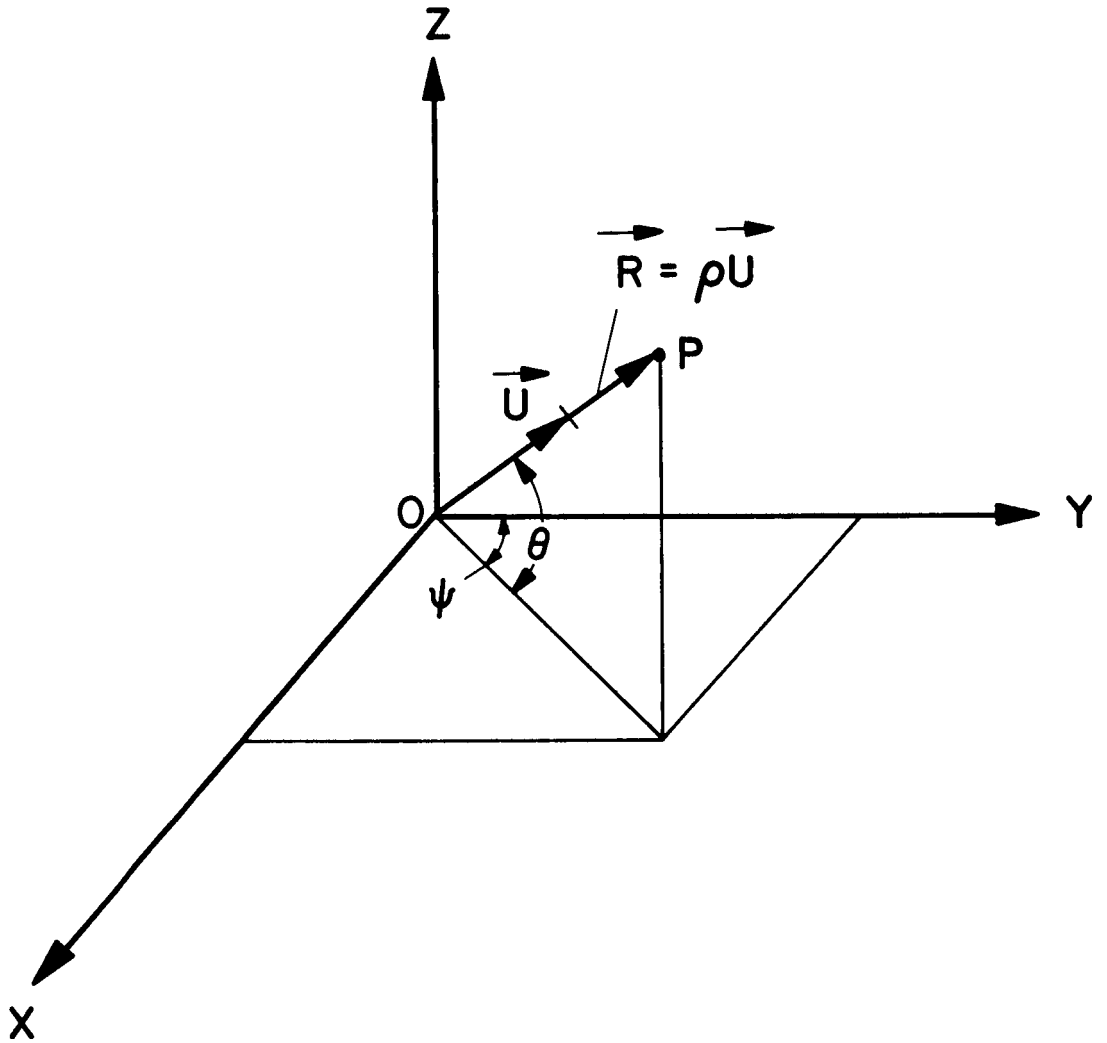

A.2 Coordinate system for the calculation of the latitude and longitude of the sub-satellite point.

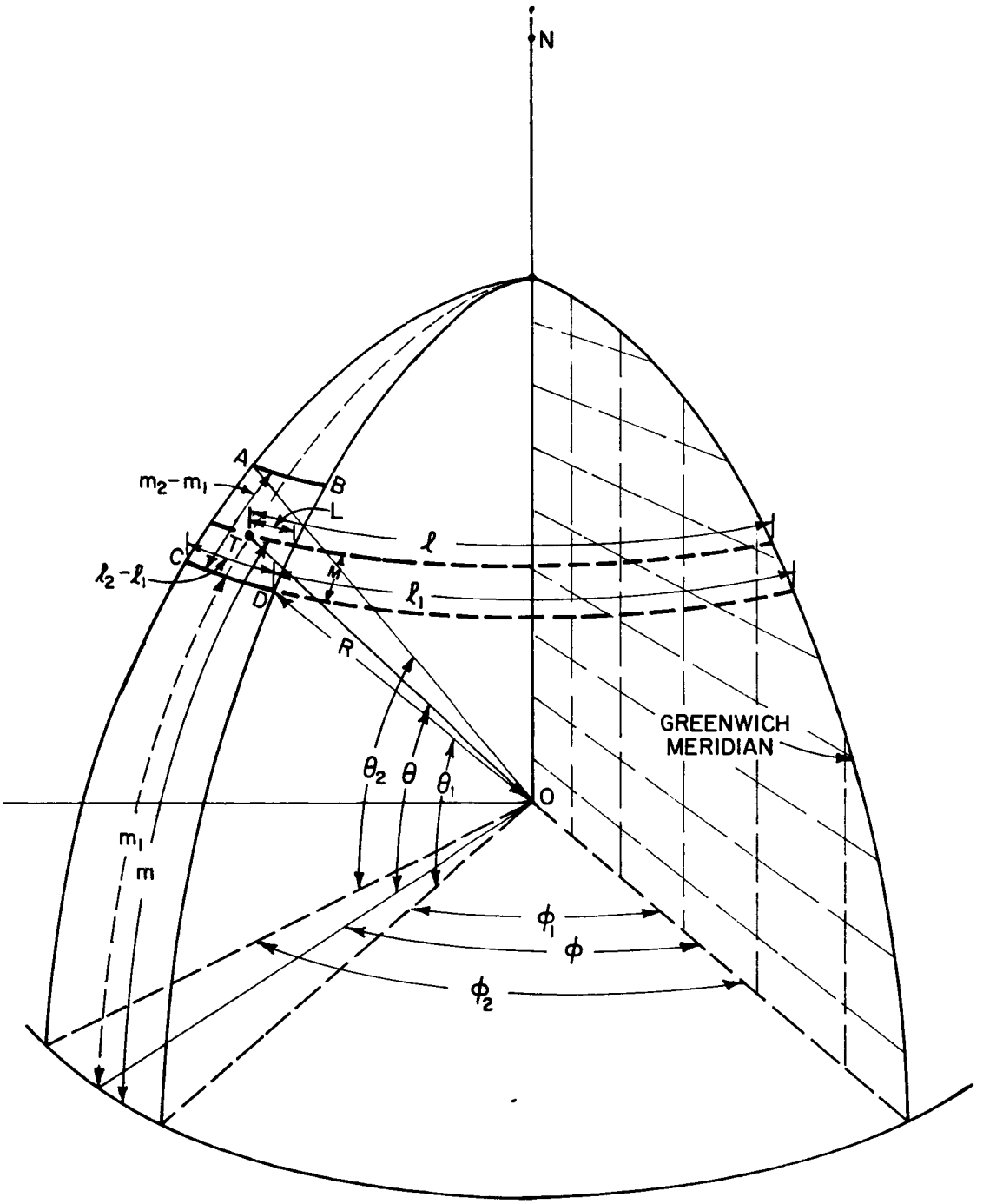

C.1 To illustrate the curvilinear coordinate system used in the derivation of equation (6).

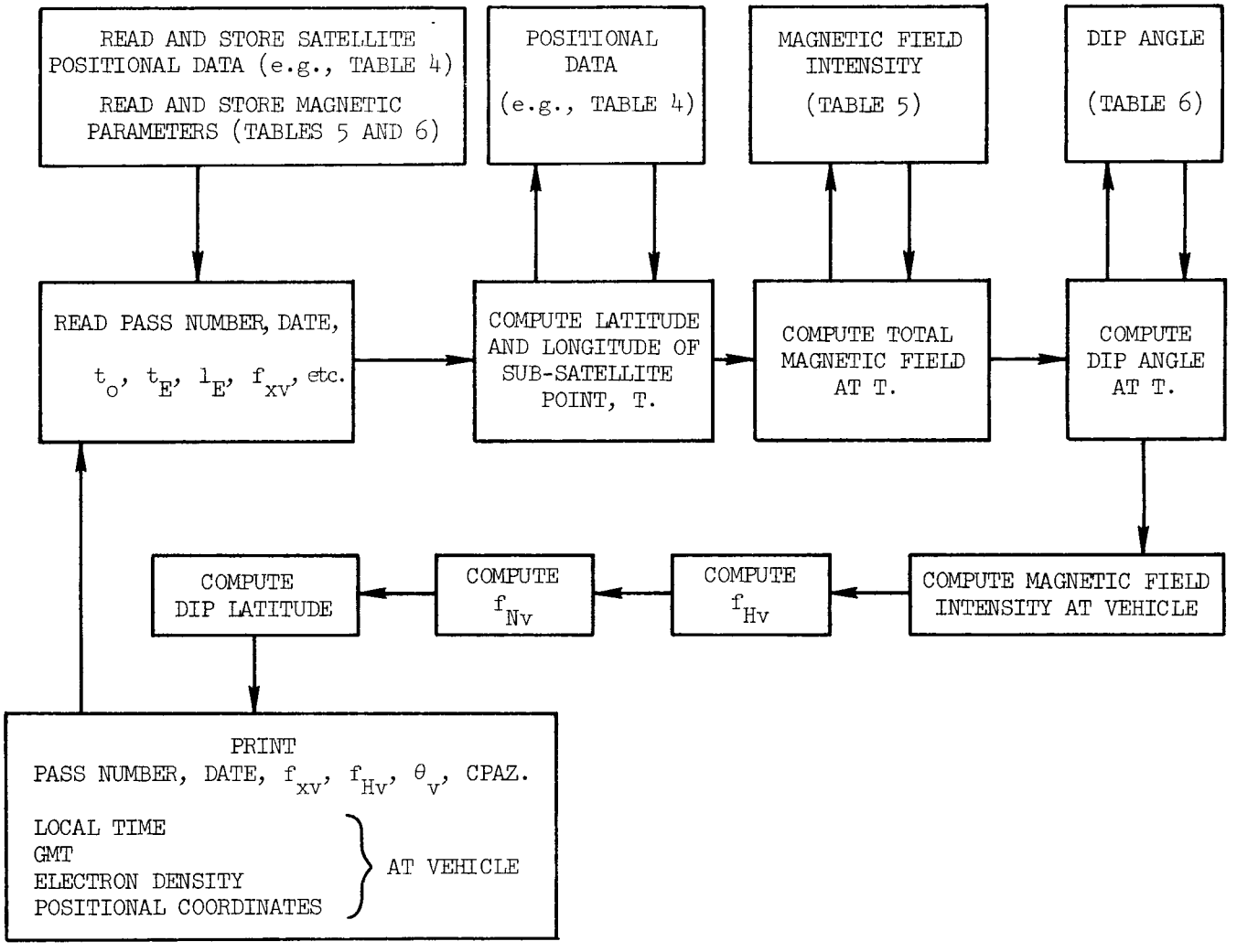

D.1 Flow diagram to illustrate the arrangement of the digital computer program for the calculation of electron density at the Alouette orbit.